Università di Pisa

Dipartimento di Fisica

Curriculum in
Fisica Teorica

Applications of Random Matrix models to the QCD phase diagram

Candidato:
Andrea Vilasi

Relatore:
Massimo D'Elia
Co-Relatore:
Philippe de Forcrand

Maggio 2016

Contents

Chapter 1

Introduction

1.1 An introduction to Quantum Chromodynamics

Quantum Chromodynamics (QCD) is the theory supposed to regulate the strong interactions.
Studies on hadrons in the last fifty years suggested that they were made of *quarks*, the fundamental particles of the theory. An important discovery that eventually led to the advent of QCD was the ability of non-Abelian gauge field theories to describe the *asymptotic freedom*, the property that ensures that two close enough (or sufficiently high energy) quarks stop interacting and approximatively behaves like free particles. Non-Abelian gauge theories are characterized by symmetries generated by a non-commutative algebra, so that it was believed that quark dynamics should be described by these further symmetries.
From the experimental point of view, quarks have never been observed in nature as isolated states. This feature, together with some other problem, like the discrepancy between theoretical prediction and experimental results on the total cross sections of the process $e^+e^- \to$ hadrons or the decay $\pi_0 \to \gamma\gamma$, have strongly suggested that quarks should have a new degree of freedom, the *color*. It was predicted and experimentally confirmed that the number of colors carried by the quarks is $N_c = 3$.
Summarizing QCD can be seen as a gauge theory based on the non-abelian SU(3)-color group that mediates the color interaction between quarks. Since the generators of SU(3) are eight, such interactions are regulated by eight massless non-Abelian gauge fields, the *gluons*, characterized by a nontrivial color charge (differently from the QED mediator, the *photon*, that is electrically neutral).

The experimental non-evidence in nature of a nonzero color charge lead to the so-called *confinement hypothesis*, which postulates that all the hadrons in nature have to be completely neutral with respect to color (or to have a "zero color charge") and consequently quarks cannot be observed as isolated states. The non-Abelian structure of QCD makes gluons able to couple to themselves and it can believed that such self-couplings can be responsible for the confinement. Perturbatively one sees that the coupling strength weakens for small separation quarks. One could speculate that it become strong for large separations and this could be an explanation for the

confinement. However for large separations the perturbative approach is no more applicable and one has to use non-perturbative QCD. The breakthrough in the study of the non-perturbative regime came with the Lattice formulation (LQCD). Thanks to this formulation one can regularize the path integral integration over fields and compute numerically the integrals through Monte Carlo sampling methods.

Summarizing it seems that at low energies quarks and gluons are confined into bound states, the hadrons. However the asymptotic freedom of QCD predicts a high energy region in which quarks and gluons are deconfined and they weakly interact: such phase is called *Quark-Gluon Plasma* (QGP) phase.
The thermodynamics of QCD predicts a phase transition between these two phases. It seems that deconfinement can be reached in a high temperature T or high baryon density ρ regime. The characteristic temperatures and densities transition are of order $T \approx 10^{12} K$ and $\rho \approx 10^{1}5 g/cm^3$. Temperatures of this level were present in the early universe, just after the Big Bang. On the other hand densities like these are predicted to exist inside compact objects like neutron stars. Furthermore, the quark-gluon plasma phase is conjectured to be observed in heavy-ion colliders, like the Relativistic Heavy Ion Collider (RHIC) at Brookeven and the Large Hadron Collider (LHC) at CERN.

1.2 Random Matrix Theory in physics: an overview

Physics has discovered the importance of the Random Matrix approach almost in the last century. With Wigner [62] and Dyson [15] as first pioneers, at the beginning the random matrices were used for describing statistics of excited levels in nuclei.
Although the historical favorite application was the nuclear physics, today the RMT extends its domain over several fields in physics and mathematics. Just to cite some examples: disordered and quantum chaotic systems, problems of non-equilibrium dynamics, dynamical phase transition in glasses, integrable systems, quantum gravity, supersymmetric gauge theories [9]. Interesting reviews of all these and other applications can be found in Ref.s [9], [3],[34].
More generally one can be interested in spectral properties of some operator or in matrices that describe some kind of correlations. Because they are too complicated to be analyzed explicitly, RMT allows to substitute deterministic operators with finite-dimensional matrices whose elements are random. Hence the problem becomes to establish connections (maybe through universality arguments) between the spectral properties of the original model and the randomized one.
Universality is one of the most recurring words in RMT. Usually one appeals to universality to intend that in certain conditions the specific probability distribution of the matrix elements is not important, but the averages of operators only depend on few universal parameters. Another frequent feature of RMT is that in the limit of big matrix size ($N \to \infty$) the theory becomes equivalent to some other effective theory with physical sense with which it shares the same global symmetries.

Although not yet discussed until now, since the work of 't Hooft [52] on a two-dimensional model for mesons, the RMT even provided a useful tool for studying

important properties of QCD. In a later stage, a RM model was elaborated for describing the fluctuations of the small eigenvalues of the Dirac operator [12][58]. The eigenvalues of the Dirac operator can be seen to fluctuate non trivially because of the QCD dynamics. However, if we restrict to eigenvalues near zero, universal behaviors that avoid the complications of a dynamical QCD partition function can be seen.
This thesis is in particular devoted to the study of the chiral phase transition of QCD, that is affected only by such small eigenvalues. For this purpose we will show in the following chapters that we are able to use a random matrix ensemble to reproduce the global symmetries of the Dirac operator for studying the important mechanism of the chiral symmetry breaking.

1.3 General background and scheme of the thesis

Random Matrix Theory (RMT) have proven to be a useful tool to study the phase diagram of Quantum Chromodynamics (QCD). The thermodynamics of QCD predicts a phase transition from the confined hadron matter to a state of deconfined weakly interacting quark and gluons, the so-called *Quark Gluon Plasma* (QGP). Such transition can be studied in the plane parametrized by the temperature T and the baryon chemical potential μ_B. The formulation of QCD on the Lattice (LQCD), which relies on Monte Carlo techniques of numerical integration, fails to investigate directly the phase diagram at nonzero chemical potential because of the notorious *sign problem*. On the other hand, effective theories are able to provide useful information about the existence and the nature of such transition. Chiral Random Matrix Theory (χRMT) is one of them. In particular one of the main challenges is to determine theoretically and experimentally the position of the *critical endpoint* of QCD, a second order point (T_E, μ_E) which represents the endpoint of a supposed first order line that continues at lower T and higher μ.

Born to investigate the spectral properties of the Euclidean Dirac operator, χRMT reproduces some of the main features of the QCD phase structure at nonzero T and μ with *two flavors*. Using a Landau-Ginzburg-like effective potential, in this work we are going to study the properties of *a* RM model introduced in the final form in a paper of Halasz, Jackson, Stephanov and Verbaarschot [30]. The virtue of such model is the opportunity to study in an analytical way the chiral transition, especially analyzing how the zeros of the partition function in the complex μ plane (and the singularities of the potential) behave in thermodynamic limit ($V \to \infty$) according to the Yang-Mills theory. In RM theories the volume is replaced by the dimension of the matrices, N. The advantage to have an explicit expression of the partition function both in the finite and infinite size case allows to study finite size effects.

The first two months of this thesis work have been spent at the Institute for Theoretical Physics of the ETH Zurich. Here the candidate started to study the theoretical background of the model and to set up the computational part with the program *Wolfram Mathematica*. The central part of the thesis is focused on the extrapolation of the radius of convergence of a Taylor series of the effective potential

(i.e. the free energy of the system) at fixed temperature in the baryon chemical potential centered around $\mu_B = 0$. This is one of the techniques even used in LQCD, because of the chance to perform simulations at $\mu_B = 0$ and reconstruct partially the power series with the available coefficients. The knowledge of the radius of convergence would allow to estimate the position of the critical endpoint of the QCD phase diagram and the spinodal lines of the first order transition.
In principle such Taylor expansion is not essential for the RM model because we are exactly able to determine through other ways the location of the critical point and the phase boundary. However this toy model can be interesting to test the advantages and the limits of some mathematical methods of power series analysis and decide what is the best to be used even in LQCD.
The second part of the work consists of a modification of the model including *all* (or at least a great number of) the Matsubara frequencies, indeed the initial model describes successfully a mean-field transition using only the lowest one. The third part analyzes the potentialities and the limits of the model to reproduce the phase structure of QCD at *imaginary* chemical potential, already known from LQCD simulations. The final part of the work represents the effort to use the previous techniques of power series analysis with real LQCD data, in particular to detect the Roberge-Weiss singularity at imaginary μ for $N_f = 2$.

Chapter 2

QCD and the Dirac Spectrum

2.1 The QCD partition function

The full QCD partition function in Minkowskian coordinates can be expressed as a functional integral in the gauge fields A_μ, in the fermion fields $\psi, \bar{\psi} = \psi^\dagger \gamma_0$ and the ghost fields $c, \bar{c}$:

$$Z_{QCD} = \int [dA][d\psi d\bar{\psi}][dcd\bar{c}] exp\left[i \int d^4x \{\mathcal{L}_G + \mathcal{L}_{GF} + \mathcal{L}_{FP} + \mathcal{L}_F + \mathcal{L}_\theta\} \right]. \quad (2.1)$$

The first term in the exponential is the so-called *pure gauge* (or Yang-Mills) term:

$$\mathcal{L}_G = -\frac{1}{4g^2} F^{a\ 2}_{\mu\nu}, \qquad with \qquad F^a_{\mu\nu} = \partial_\mu A^a_\nu - \partial_\nu A^a_\mu + f_{abc} A^b_\mu A^c_\nu \quad (2.2)$$

Here f_{abc} are the structure constants of the gauge group $SU(N_c)$, whereas $A_\mu = A^a_\mu T_a/2$ where T_a are the generators of the gauge group. The second term is the *gauge fixing* term:

$$\mathcal{L}_{GF} = -\frac{1}{2\alpha} (\partial^\mu A^a_\mu)^2. \quad (2.3)$$

The third is the *Faddeev-Popov* term:

$$\mathcal{L}_{FP} = -\partial^\mu \bar{c}_a D^{ab}_\mu c^b \quad (2.4)$$

The fourth is the fermionic term:

$$\mathcal{L}_F = \sum_{f=1}^{N_f} \bar{\psi}_f (i\gamma^\mu D_\mu - m)\psi_f \quad (2.5)$$

The last is the so-called θ term:

$$\mathcal{L}_\theta = \frac{\theta}{32\pi^2} F^a_{\mu\nu} \tilde{F}^a_{\mu\nu}, \qquad \text{with} \qquad \tilde{F}_{\mu\nu} = \frac{1}{2} \epsilon_{\mu\nu\alpha\beta} F^{\alpha\beta}. \quad (2.6)$$

The integral $\nu = 1/32\pi^2 \int d^4x F^a_{\mu\nu} \tilde{F}^a_{\mu\nu}$ is a topological invariant (called *topological charge*) i.e. it does not change under continuous transformations of the gauge fields.

The terms $\mathcal{L}_{GF}$ and $\mathcal{L}_{PF}$ come out from the quantization of the gauge fields. Because of the gauge invariance of the action, in order to eliminate redundant

integrations over the gauge fields and have a well-defined gluon propagator, Faddeev and Popov proposed a procedure that leads to the appearance of this two terms. Since we are not interested in performing a perturbative approach, we will omit from now on to write explicitly the Faddev-Popov and the gauge-fixing terms.
Going into euclidean coordinates ($x_\mu^M \equiv (x_0^M, \mathbf{x}^M) \to x_\mu^E \equiv (-ix_4^E, \mathbf{x}^E)$) and using the same notation as before for the euclidean fields, the full QCD partition function can be written as:

$$Z_{QCD} = \int dA\, d\psi\, d\bar{\psi}\, e^{-S_E[A,\psi,\bar{\psi}]}, \tag{2.7}$$

where:

$$S_E[A,\psi,\bar{\psi}] = \int d^4x \left[\frac{1}{4g^2} F^{a\ 2}_{\mu\nu} - i\frac{\theta}{32\pi^2} F^a_{\mu\nu}\tilde{F}^a_{\mu\nu} + \sum_{f=1}^{N_f} \bar{\psi}_f(\gamma_\mu D_\mu + m_f)\psi_f \right] \tag{2.8}$$

Integrating in the fermionic variables one can write the fermionic term as:

$$\int d\psi\, d\bar{\psi}\, exp\left[\sum_{f=1}^{N_f} \bar{\psi}_f(\gamma_\mu D_\mu + m_f)\psi_f \right] = \prod_{f=1}^{N_f} det(\gamma_\mu D_\mu + m_f) \tag{2.9}$$

The anti-Hermitian Dirac operator in Eqn.(2.7) is given by:

$$D \equiv \gamma_\mu D_\mu = \gamma_\mu(\partial_\mu + iA_\mu) \tag{2.10}$$

where the γ_μ are the euclidean Dirac matrices which satisfy the relation $\{\gamma_\mu, \gamma_\nu\} = 2\delta_{\mu\nu}$. In the chiral representation they can be written as:

$$\gamma_0 \equiv \gamma_4 = \begin{pmatrix} 0 & 1 \\ 1 & 0 \end{pmatrix}, \quad \gamma_k = \begin{pmatrix} 0 & i\sigma_k \\ -i\sigma_k & 0 \end{pmatrix}, \quad \gamma_5 = \begin{pmatrix} 1 & 0 \\ 0 & -1 \end{pmatrix}, \tag{2.11}$$

We can define the eigenvalues and the eigenstates of D as:

$$D\phi_k = \xi_k \phi_k \tag{2.12}$$

Being D an anti-hermitian matrix, its eigenvalues have to be purely imaginary[1], therefore $\xi_k = i\lambda_k$, where $\lambda_k \in \mathbb{R}$.

2.2 Global symmetries of the Dirac operator

As we know the QCD action is constrained by gauge symmetry, Poincaré invariance and renormalizability, which determine the structure of the Dirac operator. In this section we will discuss the global symmetries of the euclidean Dirac operator.

Chiral Symmetry. Let us consider the the fermionic action:

[1] An anti-hermitian (or *skew-hermitian* matrix) matrix A is always a *normal* matrix ($A^\dagger A = AA^\dagger$) and therefore it can always been diagonalized through a matrix U such that $UAU^\dagger = \Lambda$. This and the anti-hermitianity imply $UA^\dagger U^\dagger = -UAU^\dagger = -\Lambda = \Lambda^\dagger$, that is A has purely imaginary eigenvalues.

$$S_F = \int d^4x \sum_{f=1}^{N_f} \bar{\psi}_f (D + m_f)\psi_f \tag{2.13}$$

The integrand can be rewritten using the left-right handed decomposition as:

$$\sum_{f=1}^{N_f} \bar{\psi}_f (D + m_f)\psi_f = \bar{\Psi}_R D \Psi_R + \bar{\Psi}_L D \Psi_L + \bar{\Psi}_R M_{RL} \Psi_L + \bar{\Psi}_L M_{LR} \Psi_R, \tag{2.14}$$

where $\Psi = (\psi_1, \ldots, \psi_{N_f})$, $M_{RL} = M_{LR} = diag(\{m_f\})$, $\psi_{L(R)} = P_{L(R)}\psi$ and $\bar{\psi}_{L(R)} = \psi^\dagger_{L(R)}\gamma_0$ (with $P_L = (1 - \gamma_5)/2$ and $P_R = (1 + \gamma_5)/2$). In the chiral limit $m_f \to 0$ the fermionic action results to be invariant under the transformations:

$$\begin{aligned} &\Psi_L \to U_L \Psi_L \qquad &&\bar{\Psi}_L \to \bar{\Psi}_L U_L^\dagger \\ &\Psi_R \to U_R \Psi_R \qquad &&\bar{\Psi}_R \to \bar{\Psi}_R U_R^\dagger, \end{aligned} \tag{2.15}$$

where $U_L \in U_L(N_f)$ and $U_R \in U_R(N_f)$. The product $U_L(N_f) \times U_R(N_f)$ can always be decomposed into:

$$U_L(N_f) \times U_R(N_f) = SU_L(N_f) \times SU_R(N_f) \times U_V(1) \times U_A(1) \tag{2.16}$$

However, because of the so-called *axial anomaly*, the axial symmetry group $U_A(1)$ is explicitly broken. The second group $U_V(1)$ represents the conservation of the baryon number.
Therefore the full chiral symmetry in the massless limit is given by $G = SU_L(N_f) \times SU_R(N_f)$. This tensor product can usually be indicated with the product $SU_A(N_f) \times SU_V(N_f)$. The symmetry $SU_A(N_f)$ is obtained taking $U_L = U_R^{-1}$ and it is explicitly broken if we introduce nonzero quark masses. The $SU_V(N_f)$ vector symmetry is given choosing with $U_L = U_R$ and is good for degenerate quark masses ($m_f = m$ for all f) but it is explicitly broken for different quark masses. In truth here there is a little abuse of notations, because although $SU_V(N_f)$ is a subgroup, $SU_A(N_f)$ is not. However with this notation we mean that every element of G can be always seen like a composition of a vectorial and an axial transformation.

A remarkable phenomenon is the *spontaneous symmetry breaking* that takes place in the chiral limit with the symmetry pattern

$$G = SU_L(N_f) \times SU_R(N_f) \to H = SU_V(N_f). \tag{2.17}$$

This mechanism is related to the fact that the axial transformations cannot be implemented á la Wigner-Weyl[2] and they do not leave the QCD vacuum invariant. All the generators of the transformations that do not leave the vacuum invariant are called *broken generators*. Following the Goldstone theorem, if the symmetry is spontaneously broken, for each broken generator it has to exist a (pseudo)scalar massless particle with the same quantum numbers of the broken generator. Such

[2]A symmetry is realized á la Wigner-Weil if it can be implemented by an operator $U = e^{i\epsilon_a Q_a}$ that acts in the Hilbert space of the theory (where Q_a are the generators of the transformation) that leaves the vacuum of the theory invariant: $U|0> = |0>$.

particles are called the Goldstone bosons. For instance in the $N_f = 2$ QCD these Goldstone bosons *would* coincide with the massless pions. However for nonzero masses of the u and d quarks, the chiral symmetry is explicitly broken and the pions result to be not massless, but with a mass near $140MeV$.
The spontaneous breaking of the chiral symmetry in the massless case can be related to the nonzero expectation value known as *chiral condensate* $\left\langle \bar{\psi}\psi \right\rangle = \left\langle \bar{\psi}_R\psi_R + \bar{\psi}_L\psi_L \right\rangle \approx -(240MeV)^3$. If the axial transformations were exactly implemented then this expectation value would be zero. The non vanishing of the chiral condensate can be verified through lattice simulations.

Axial symmetry
The axial $U_1(A)$ symmetry implies the following relation for the Dirac operator:

$$\{\gamma_5, D\} = 0 \tag{2.18}$$

As result all the possible couples of eigenvalues and eigenfunctions of the anti-hermitian operator D are:

$$\begin{cases} i\lambda_k & & \phi_k, \\ -i\lambda_k & \text{with eigenfunctions} & \gamma_5\phi_k, \\ 0 & & \phi_k = \pm\gamma_5\phi_k \end{cases} \tag{2.19}$$

with $\lambda_k \in \mathbb{R}$. Therefore we have either complex conjugated or zero eigenvalues. The zero modes ($\lambda_k = 0$) of the Dirac operator appear in the case of an (anti) instanton gauge field. The zero-mode eigenfunctions have definite chirality, because $\gamma_5\phi_k = \pm\phi_k$. We now denote with N_+ and N_- the number of zero modes with positive and negative chirality, respectively. The Atiyah-Singer theorem states that the number of zero modes with positive (negative) chirality is related to the topological charge by:

$$\nu = \frac{1}{32\pi^2}\int d^4x F^a_{\mu\nu}\tilde{F}^a_{\mu\nu} = N_+ - N_- \tag{2.20}$$

We know that it is possible to write the partition function (2.7) as a sum of terms defined on different topological sectors with topological charge ν:[3]

$$Z^{QCD}(M,\theta) = \sum_\nu e^{i\nu\theta} Z^{QCD}_\nu(M) \tag{2.21}$$

If we use a chiral basis $\psi = (\psi^1_R, \dots \psi^{N_+}_R, \psi^1_L, \dots \psi^{N_-}_L)$ s.t. $\gamma_5\psi^j_{R(L)} = \pm\psi^j_{R(L)}$ with $N_+ = N_- + \nu$ right handed states and N_- left-handed states, in the chiral representation of the gamma matrices (2.11) the Dirac operator assumes the structure:

$$D = \begin{pmatrix} 0 & iW \\ iW^\dagger & 0 \end{pmatrix}, \tag{2.22}$$

where W is a matrix of dimension $N_+ \times N_-$. Indeed it is simple to prove that $\left\langle \bar{\psi}^R_i | D | \psi^L_j \right\rangle = 0 = \left\langle \bar{\psi}^L_i | D | \psi^R_j \right\rangle$ for all i and j and that D has exactly ν eigenvalues

[3]Viceversa we can write $Z_\nu(M)$ using the Fourier inversion $Z_\nu(M) = \frac{1}{2\pi}\int_0^{2\pi} d\theta e^{-i\nu\theta} Z^{QCD}(M,\theta)$

equal to zero. The form of Eq.(2.22) explicits the fact that the euclidean Dirac operator is anti-hermitian. Given the decomposition of the partition function in different topological sectors, one can write the partition function $Z_\nu(M)$ as a function of the Dirac eigenvalues:

$$Z_\nu(M) = \int_\nu dA \prod_f \prod_k m_f^{|\nu|}(\lambda_k^2 + m_f^2) e^{-\int d^4x \frac{1}{4g^2} F^a_{\mu\nu}{}^2} \tag{2.23}$$

2.3 The Banks-Casher relation

One of the most relevant aspects of the chiral symmetry breaking is the relation between the chiral condensate and the eigenvalue density of the Dirac operator near zero. For this purpose let us introduce the Banks-Casher relation [7]. We define the average spectral density for eigenvalues $\{\lambda_k\}$ as

$$\rho(\lambda) = \left\langle \sum_k \delta(\lambda - \lambda_k) \right\rangle, \tag{2.24}$$

where the average is over the full QCD action. If we take V as the four-volume, the Banks-Casher relation states that the absolute value of the chiral condensate $\left\langle \bar{\psi}\psi \right\rangle$ is given by:

$$\Sigma \equiv |\left\langle \bar{\psi}\psi \right\rangle| = \lim_{\lambda\to 0} \lim_{m\to 0} \lim_{V\to\infty} \frac{\pi\rho(\lambda)}{V}, \tag{2.25}$$

where the limits have to be taken in the order indicated. This is important since eigenvalues accumulate near $\lambda = 0$ as the volume goes to infinity. In particular, it can be seen that reversing the $\lambda \to 0$ and $V \to \infty$ limits one obtains zero, since for any finite volume one has $\rho(0) = 0$ as a consequence of the of the $\pm i\lambda$ symmetry of the eigenvalues. We are going now to show two different proofs of Eq.(2.25).

Proof (1). To demonstrate Eq.(2.25) it is useful to introduce the average resolvent of the Dirac operator[4]:

$$G(z) = \left\langle \sum_k \frac{1}{z + i\lambda_k} \right\rangle \tag{2.26}$$

This can be interpreted as the electric field at the position z of the two dimensional complex plane generated by the charges located at $(i\lambda_k)$ (as we know the two dimensional spatial dependence of the electric field is $|\vec{E}(r)| \sim 1/r$). Using this analogy we have a set of charges that lie on the imaginary axis, as shown in Fig.2.1. Due to the symmetric distribution with respect to the real axis, the sign of the resolvent changes if we cross the imaginary axis. To obtain the desired relation it is sufficient to use the Gauss theorem ($\oint \vec{E}(\vec{r})d\vec{r} \propto Q$) choosing a contour centered on

[4]The resolvent of an operator A is defined as $G(z;A) = (A - z\mathbb{I})^{-1}$. The resolvent can be useful to obtain information about the spectral decomposition of A. For instance it can be demonstrated that given an isolated eigenvalue λ of A, if is possible to define a curve C_λ such that the residue $-\frac{1}{2\pi i}\int_{C_\lambda} G(z;A)dz$ defines a projection operator onto the λ eigenspace of A.

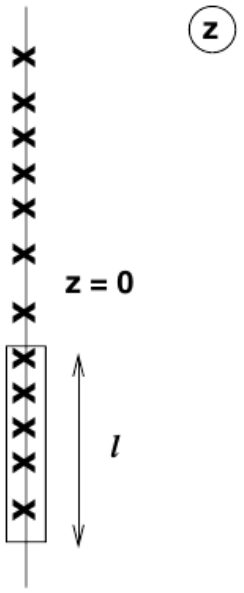

Figure 2.1: Distribution of the Dirac operator eigenvalues in the complex z plane. The eigenvalues are a set of "charges" that lie symmetrically on the imaginary axis. Figure taken from Ref.[57].

$i\lambda$ whose extension is $-m \leq Re(z) \leq m$ and $-l/2 + \lambda \leq Im(z) \leq +l/2 + \lambda$. If we assume that inside the contour the density is almost constant, the total charge is a $\rho(\lambda)l$.

$$\int_{C_\lambda} G(z) = il(G(i\lambda + m) - G(i\lambda - m)) = 2\pi i\rho(\lambda)l. \tag{2.27}$$

The first identity follows from the fact that the integration along the real segments gives a zero contribution and the second follows from the integral Cauchy formula [5]. Since $G(i\lambda - m) - G(i\lambda + m) = 2ReG(i\lambda + m)$, we have:

$$ReG(i\lambda + m) = \pi\rho(\lambda). \tag{2.28}$$

Near the center of the spectrum ($\lambda \to 0$) we can approximate $ReG(i\lambda + m) \approx G(i\lambda + m)$ because the imaginary part of the resolvent is negligible. Since we know that the chiral condensate is related to the resolvent by:

$$\left\langle \bar{\psi}\psi \right\rangle = \lim_{m\to 0} \lim_{V\to\infty} \frac{G(m)}{V} \tag{2.29}$$

Then using (2.28) and sending $\lambda \to 0$, we obtain immediately the Banks-Casher relation.

Proof (2) The second proof of the Banks-Casher relation follows directly from the relation (2.29). Using (2.26) and splitting the contribution of the zero and

[5]The integral over a closed curve γ in a simply connected domain $A \in \mathbb{C}$ of an holomorphic function f is given by $f(z) = \frac{1}{2\pi i} \oint_\gamma \frac{f(\xi)}{\xi - z} d\xi$

nonzero eigenvalues, we have:

$$\left\langle \bar{\psi}\psi \right\rangle = \lim_{m\to 0}\lim_{V\to\infty}\left\langle \frac{1}{V}\sum_{\lambda_n>0}\frac{2m}{\lambda_n^2+m^2} + \frac{1}{V}\frac{|\nu|}{m}\right\rangle \tag{2.30}$$

where $|\nu|$ is the number of zero modes and the absolute topological charge. With the assumption for the topological susceptibility to scale with the volume $\langle\nu^2\rangle/V = const$, in the $V\to\infty$ limit the second term vanishes. Using the identity:

$$\lim_{m\to 0}\frac{2m}{\lambda_n^2+m^2} = \pi\delta(\lambda_n) \tag{2.31}$$

we have

$$\left\langle \bar{\psi}\psi \right\rangle = \lim_{m\to 0}\lim_{V\to\infty}\left\langle \frac{1}{V}\sum_{\lambda_n>0}\pi\delta(\lambda_n)\right\rangle = \lim_{\lambda\to 0}\lim_{m\to 0}\lim_{V\to\infty}\frac{\pi\rho(\lambda)}{V} \quad \blacksquare \tag{2.32}$$

Since in such a case the average distance between the eigenvalues is given by the inverse of the spectral density, an important consequence of the Banks-Casher formula is that the small eigenvalues of the Dirac operator are spaced as:

$$\Delta\lambda = \frac{1}{\rho(0)} = \frac{\pi}{V\Sigma} \equiv \lambda_{min}. \tag{2.33}$$

It is possible to see that the spectrum of the free Dirac operator goes as $\rho^{free}(\lambda)\sim V\lambda^3$ from which we have that $\Delta\lambda^{free}\sim 1/V^{1/4}$. This difference with respect to (2.33) shows how the presence of the gauge fields causes a modification of the spectrum near zero. Strong interactions result in a correlation of the eigenvalues and consequently in a breaking of the chiral symmetry. Indeed it is possible to see that for uncorrelated eigenvalues (as in the free case), the distribution near zero goes as $\rho(\lambda)\sim\lambda^{2N_f+1}$ in the chiral limit, that is no breaking of the chiral symmetry [59].

Eq.(2.33) naturally leads to define a scale

$$z = \lambda V\Sigma \tag{2.34}$$

for the study of the distribution of the eigenvalues. For this purpose it is convenient to introduce a *microscopic spectral density* [57] as:

$$\rho_s(z) = \lim_{V\to\infty}\frac{1}{V\Sigma}\rho\left(\frac{z}{V\Sigma}\right) \tag{2.35}$$

Notice that this limit exists if the chiral symmetry is broken. important to describe the infrared properties of the Dirac spectrum. One conjectures [57] that $\rho_s(z)$ is completely determined by the global symmetries of the Dirac operator and by the chiral breaking pattern. If this is true, how anticipated in the introduction, it can be deduced through a simpler theory (like the RMT) with the same global symmetries and with a same breaking pattern. It can be demonstrated [57] that the computation of the microscopic spectral through a RMT and through the low energy chiral effective QCD lead to the same results. This point will be better clarified in the following sections.

The mechanism of the chiral symmetry breaking becomes non trivial if we consider a *nonzero baryon chemical potential*. Indeed in such case the Banks-Casher relation no longer holds. At $\mu \neq 0$ the euclidean Dirac operator is no longer anti-hermitian due to the modification $D \to D + \mu\gamma_0$: its spectrum is now spread onto the 2 dimensional complex plane and the symmetry breaking is no more related to an accumulation of the eigenvalues on the imaginary axis near zero. However new interesting mechanisms related to oscillation of the microscopic spectral density in a bounded region of the complex plane arise. This process can be found for instance in Ref.[39]. Such an oscillating behavior of the density affects in a relevant way the computation of the chiral condensate, that turns out to be discontinuous.

2.4 Low energy limit of QCD at zero chemical potential

The low energy limit of QCD for light quarks at zero quark chemical potential is well reproduced by a *chiral lagrangian* with the same global symmetries of QCD. The chiral lagrangian describes the interaction of pseudoscalar mesons, the *pions*, that are the Goldstone bosons related to the chiral symmetry breaking. The pions are described by fields $U \in SU(N_f)$ that can be parametrized as $U = exp(i\sqrt{2}\pi_a T_a/F)$ where T_a are the generators of $SU(N_f)$ and F the pion decay constant. The Goldstone fields transform under the chiral group $U_L(N_f) \times U_R(N_f)$ like the chiral condensate $U \to U_R U U_L^{-1}$. The mass term explicitly breaks the chiral symmetry. However it can be restored imposing for the mass term to transform as:

$$M_{RL} \to U_R M_{RL} U_L^{-1}, \qquad M_{LR} \to U_L M_{LR} U_R^{-1} \tag{2.36}$$

It is possible to prove that the effective lagrangian that respects the chiral and the Lorentz invariance at the second order in the momenta and the first order in quark masses is given by:

$$L_{eff}(U) = \frac{F^2}{4} Tr(\partial_\mu U \partial_\mu U^\dagger) - \frac{\Sigma}{2} Tr(M_{RL} U^\dagger + M_{LR} U) \tag{2.37}$$

Here Σ is the chiral condensate. Developing to lowest order in the pion fields we obtain a lagrangian with a pion mass equal to $m_\pi^2 = 2m\Sigma/F^2$.

2.5 Low energy limit of QCD at nonzero chemical potential

We now want to find the low energy expression of the QCD partition function in presence of a nonzero quark chemical potential and define the extension of the microscopic regime in this case. The QCD partition function can be written as:

$$Z_{QCD} = \int DA\, e^{-S_{YM}} \prod_{f=1}^{N_f} det(D + m_f + \mu_f \gamma_0), \tag{2.38}$$

Let us consider for the moment the most general case of all different $\{\mu_f\}$. In such case we should have an explicit breaking of chiral symmetry through a term:

$$\sum_{f=1}^{N_f} [\bar{\psi}_L^f \mu_f \psi_L^f + \bar{\psi}_R^f \mu_f \psi_R^f] = \bar{\Psi}_L B_1 \Psi_L + \bar{\Psi}_R B_2 \Psi_R \tag{2.39}$$

that is not invariant under $U_L(N_f) \times U_R(N_f)$, but this does not happen if $\mu_f = \mu$ for all f. Here $\Psi = (\psi_1, \ldots, \psi_{N_F})$ and $B_1 = B_2 = diag(\{\mu_f\})$. However invariance is recovered by transforming the mass term as in $\mu_f = 0$ case (Eq.(2.36)) and the chemical potential term in this way:

$$B_1 \to U_L B_1 U_L^{-1} \qquad B_2 \to U_R B_2 U_R^{-1} \tag{2.40}$$

Kogut et al. [32] proved that the low energy theory with a small chemical potential is also a theory that predict a spontaneous symmetry breaking $U_L(N_f) \times U_R(N_f) \to U_V(N_f)$ through a Goldstone bosons mechanism. The effect of the chemical potential is to modify the derivative term of the Goldstone field U:

$$\partial_\mu U \to \nabla_\mu \equiv \partial_\mu U - [B_\mu, U], \qquad \text{with} \quad B_\mu = diag(\{\mu_k\})\delta_\mu, 0. \tag{2.41}$$

Therefore the final expression of the low energy effective chiral lagrangian at the order p^2 in the momenta is:

$$L = \frac{F^2}{4} \nabla_\mu U \nabla_\mu U^\dagger - \frac{\Sigma}{2} Tr(MU + MU^\dagger) \tag{2.42}$$

2.5.1 Microscopic domain and applicability of RM theories

It is interesting to make clearer the connections between QCD, effective low-energy theories and the chiral RMT, that we will introduce in the following chapter. We showed that the low energy chiral lagrangian describes the interaction of pseudo-scalar mesons, the pions. It is possible to see that taking a four-volume $V = L^4$, the range in which the pions dominate is[6]:

$$L \gg \frac{1}{\Lambda_{QCD}} \tag{2.43}$$

The Goldstone bosons of chiral effective theory can be factorized in a zero momentum and a nonzero momentum part:

$$U = U_0 e^{i\psi(x)} \tag{2.44}$$

[6]To see this, it is sufficient to compare in that regime the pion contribution in the partition function $exp(-m_\pi L)$ with that of a heavier particle (whose typical mass is $\sim \Lambda_{QCD}$), $exp(-\Lambda_{QCD} L)$.

Gasser and Leutwyler [23] demonstrated that there is a kinematic range inside which the fluctuations of the zero modes dominate the fluctuations of the nonzero modes:

$$m_\pi^2 \equiv \frac{2\Sigma m}{F^2} \ll \frac{1}{L^2} \tag{2.45}$$

Intuitively this relation states that the wavelength of the pions is much larger than the size of the box L so that the field variations inside the box are negligible and the derivative terms are small. In the case of a nonzero chemical potential the further condition to impose is that:

$$\mu \ll \frac{1}{L} \tag{2.46}$$

Therefore we can define the so-called *microscopic domain* (also called ϵ *domain*), given by

$$\frac{1}{\Lambda_{QCD}} \ll L \ll \frac{1}{m_\pi}, \qquad \mu \ll \frac{1}{L} \tag{2.47}$$

The problem is that the physical values of the parameters *are not* in this domain (to see this it is sufficient to take for instance physical value of the pion mass $m_\pi \sim 140MeV$ and $\Lambda_{QCD} \sim 200MeV$). Hence it is impossible to approximate the QCD partition function with physical parameters through a integral over the zero modes of Goldstone fields (that could be well reproduced with a RMT). However in we are interested in the spectral properties of the Dirac operator, it is possible to obtain the resolvent $G(z)$ using the random matrix approximation in the microscopic range to perform the computation. This is well explained in the Appendix **??**.

2.5.2 Leutwyler-Smilga sum rules

Our claim at the end of Sec.2.3 was that the microscopic spectral density (2.35) was only a function of the global symmetries of QCD and hence that every theory able to replicate them would give the same spectral density. Let us show how this can happen through the *Leutwyler-Smilga sum rules*.

Leutwyler-Smilga [33] proved that in the microscopic range the mass and the θ dependence of the QCD partition function is completely determined by the global symmetries and it has form:

$$Z^{eff}(M,\theta) = \int_{U\in SU(N_f)} DU\, e^{V\Sigma\, Re\, Tr(MU)e^{i\theta N_f}} \tag{2.48}$$

Taking only the sector of topological charge ν we can derive from Eq.(2.48):

$$Z_\nu^{eff}(M) = \int_{U\in U(N_f)} DU\, det^\nu U\, e^{V\Sigma Tr(MU)} \tag{2.49}$$

Expanding the Z_ν of (2.23) and the Z_ν^{eff} in terms of the masses (for simplicity we can consider equal masses $M = m\mathbb{I}$) and equating the coefficients of the $O(m^k)$ terms we obtain a set of relations that put constraints on the eigenvalues of the Dirac operator. For instance, equating the $O(m^2)$ coefficients we have:

$$\left\langle \frac{1}{V^2} \sum_{\lambda_k>0} \frac{1}{\lambda_k^2} \right\rangle = \frac{\Sigma^2}{4N_f} \tag{2.50}$$

From Eq.(2.50) it is possible to deduce how the chiral condensate is related to the correlation of the Dirac operator eigenvalues. It is interesting to rewrite Eq.(2.50) replacing the sum with an integral over the spectral density (2.24):

$$\frac{1}{V^2\Sigma^2} \int \frac{\langle \rho(\lambda) \rangle \, d\lambda}{\lambda^2} = \frac{1}{4N_f}. \tag{2.51}$$

Introducing again the microscopic scale $z = \lambda V \Sigma$ this integral can be expressed in the limit $V \to \infty$ as a function of the microscopic spectral density $\rho_s(z)$ of Eq.(2.35).

$$\frac{1}{4N_f} \xrightarrow[V\to\infty]{} \int \rho_s(z) \frac{dz}{z^2} \tag{2.52}$$

One of the most important things of these sum rules is that we have obtained them only taking into account the chiral symmetry of the partition function and its spontaneous symmetry breaking. In particular the distribution of the small eigenvalues (i.e the microscopic spectral density) is totally determined by the global symmetries of QCD and its chiral symmetry breaking. Therefore if we use a different theory with the same global symmetries which respects the same pattern of symmetry breaking we exactly obtain the same density and more generally the same sum rules. The simplest theory we can choose is the Chiral Random Matrix Theory that we will introduce in the next chapters.

Chapter 3

Phase transitions and QCD phase diagram

3.1 Yang-Lee theorems

Yang and Lee approached the analysis of the phase transitions through the study of the analyticity properties of the grand partition function of thermodynamic systems. In particular they dealt with systems of interacting atoms and characterized quite generally the condensation phenomena [63]. Furthermore, they extended the approach to other phase transition problems such as ferromagnetism, order-disorder transitions, etc. in a second paper [64].

The formalism we use is the one of a system of interacting atoms in a volume V, with temperature T and chemical potential μ. The hamiltonian of a system with N interacting atoms can be written as:

$$H(N) = \sum_{i=1}^{N} \frac{\mathbf{p}_i^2}{2m} + \sum_{i>j} W(|x_i - x_j|) \tag{3.1}$$

where $W(|x_i - x_j|)$ is an interaction term between the atoms i and j. We suppose that the interaction causes the existence of a distance of minimum approach r_0. The partition function $Q_N(T, V)$ of such a system is given by:

$$Q_N(T, V) = \frac{1}{h^{3N} N!} \int (dp\, dq)^{3N} e^{-H(N)/KT}. \tag{3.2}$$

Since we have a distance of minimum approach r_0, inside a finite volume V we can have only a finite number of atoms, $\bar{N}$. This implies that $Q_N(T, V) = 0$ for $N > \bar{N}$. The grand partition function hence is given by:

$$Q(T, V, z) = \sum_{N=0}^{\bar{N}} z^N Q_N(T, V) \tag{3.3}$$

where $z = exp(\mu/KT)$ is the *fugacity*. As we know all the thermodynamic quantities are defined in the *thermodynamic limit* ($V \to \infty$). For instance the *pressure* and the *density* of the system can be expressed as:

$$\frac{P}{T} = \lim_{V\to\infty} \frac{logQ(T,V,z)}{V} \tag{3.4}$$

$$\rho = \lim_{V\to\infty} \frac{\partial}{\partial logz} \frac{logQ(T,V,z)}{V} \tag{3.5}$$

Do these two limits always exist? It was believed that Eqs. (3.4) and (3.5) were valid in the gas phase (the second indeed gives us the correct equation of state), but it was not so clear whether they continued to be valid at the condensation point and in the liquid phase. The two following theorems give a clear answer to this problem.

Theorem 3.1.1. ***(Yang-Lee 1.)*** *For all positive real values of z, the limit*

$$\lim_{V\to\infty} \frac{logQ(T,V,z)}{V} \tag{3.6}$$

exists and it defines a continuous, monotonically increasing function of z.

Theorem 3.1.2. ***(Yang-Lee 2.)*** *If in the complex z plane there is a region R containing a segment of the positive real axis that is always free of roots of Q, then in this region all the limits:*

$$\lim_{V\to\infty} \frac{\partial^k}{\partial (logz)^k} \frac{1}{V} logQ, \qquad k = 0, 1 \ldots \tag{3.7}$$

are analytic with respect to z.
Furthermore the operations $(\partial/\partial logz)$ *and* $\lim_{V\to\infty}$ *commute in R, so that e.g:*

$$\lim_{V\to\infty} \frac{\partial}{\partial logz} \frac{1}{V} logQ = \frac{\partial}{\partial logz} \lim_{V\to\infty} \frac{1}{V} logQ \tag{3.8}$$

and this gives us the known equation of state:

$$\rho = \frac{\partial}{\partial logz} \frac{P}{T} \tag{3.9}$$

The proofs of these two important theorems can be found in the original article of Ref.[63].

Let us analyze [26] the important consequences of these theorems. As we have seen above, for finite volume V the grand partition function $Q(T,V,z)$ is a polynomial of degree $\bar{N}$ in the variable z. Therefore, Q has exactly $\bar{N}$ roots in the complex z plane, which are complex conjugated for $z > 0$ or even real numbers for $z < 0$. In this case, we can always find a contour of the non-negative real z axis which does not contain roots of the polynomial. From this follows that $logQ(V,T,z)$ is analytic inside this contour and therefore the *pressure* and the *density* at finite volume:

$$P_V = \frac{T}{V} logQ(T,V,z), \qquad \rho_V = \frac{N}{V} = \frac{1}{V} \frac{\partial}{\partial logz} logQ(T,V,z) \tag{3.10}$$

are analytic functions of z.
In the thermodynamic limit ($V \to \infty$, $N \to \infty$, N/V fixed) the degree of the

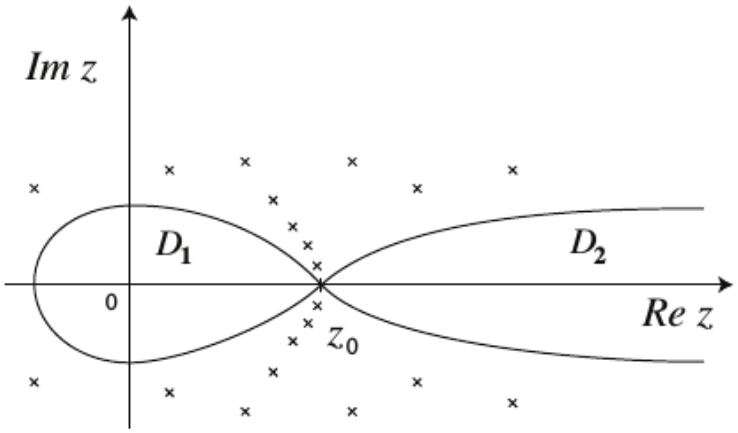

Figure 3.1: Analyticity regions D_1 and D_2 for the pressure in the thermodynamic limit in the complex z plane. The points are the zeros of $Q(T, V, z)$ and $z = z_0$ it the phase transition point. Figure taken from Ref.[26].

polynomial $Q(T, V, z)$ increases, therefore the number of the roots in the complex z plane increases. It could happen in the limit the appearance of a real positive accumulation point z_0 for the roots. In this case one could have a "splitting" of the analyticity region in two regions D_1 and D_2 (see Fig.3.1) that do not contain roots of Q. The second theorem of Yang-Lee (taking $k = 0$) ensures the limit (3.6) to be uniformly convergent to an analytic function in the region D_1 (or in D_2).

Separately in these two regions, the properties discussed at finite V continue to be valid, that is the system is in a well defined thermodynamic phase. However these two phases can not coincide, otherwise the limit (the pressure, for instance) should be an analytic function *even* in the point z_0. Therefore the point $z = z_0$ is a point of coexistence of two different phases for the system, and the crossing from D_1 to D_2 through z_0 represents a *phase transition.*

3.2 The QCD phase diagram

3.2.1 Thermodynamics of QCD

The *asymptotic freedom* of QCD (the decreasing of the coupling constant increasing the energy scale) suggests us that QCD matter undergoes a phase transition from a state with confined hadrons into a new state, a *gas* with deconfined weakly-interacting quark and gluons, the so-called *Quark Gluon Plasma* (QGP). To explore the possibility of such a transition one has to study the thermodynamics of QCD at equilibrium. In general we know that thermodynamic properties of a system can be expressed through a phase diagram in the space of some parameters in which each point corresponds to a stable thermodynamic state characterized by various thermodynamic functions (i.e. pressure, density etc). As we have already seen, the QCD partition function in the presence of a nonzero baryon chemical potential, can

be expressed as a path integral in the Euclidean space:

$$Z_{QCD}(T,\mu_B) = \sum_{\alpha} exp\Big\{ - \frac{E_\alpha - \mu_B N_{B,\alpha}}{T} \Big\} = \int DA\, D[\bar{\psi}\psi] \exp[-S_E] \tag{3.11}$$

This can be interpreted as the partition function of a statistical system with temperature T and chemical potential μ_B. The nature of the QCD phase transition and the phase structure is strictly connected to the processes of *deconfinement* and *chiral restoration*.

3.2.2 $Z(N_c)$ symmetry and deconfinement

Let us consider the *pure gauge* QCD, that is the case in which we send the quark masses $m_q \to \infty$. The resultant action is the pure Yang-Mills action S_{YM} (it is equivalent to replace the fermionic determinant with 1). We are interested in showing a particular symmetry that leaves this action invariant and how it can be related to the *deconfinement* phenomenon.
Going for a moment into lattice formulation without entering into details, we start defining a quantity called the *Polyakov loop*:

$$\ell(\mathbf{m}) = tr \prod_{j=0}^{N_T-1} U_4(\mathbf{m}, j) \tag{3.12}$$

that is the trace of the product of all link variables $U_4(\mathbf{m}, j)$ in the spatial direction at fixed spatial position $\mathbf{m}$. The *center* of the gauge group $SU(N_c)$ is $\mathbb{Z}(N_c)$. It can be seen as the set of the form $z_k = exp(2i\pi k/N_c)\mathbb{I}$ that commutes with every element of $SU(N_c)$. A *center transformation* consists of multiplying all the temporal links at a given time slice $n_4 = t_0$ with the same element z_k of the center:

$$U_4(\mathbf{m}, t_0) \to z_k U_4(\mathbf{m}, t_0) \tag{3.13}$$

The symmetry (3.13) represents a symmetry of the lattice gauge action. The reason is that the pure gauge action is made of products of link variables along closed loops, and since every closed loop has as many elements in one direction as in the opposite. Center symmetry elements commute with all group elements and hence in a closed loop cancel each other. The Polyakov loop can be considered as "closed" along the compact time direction. Since in the center transformation only a fixed time slice is multiplied by an element of the center, the Polyakov loop transforms as:

$$\ell \to z_k \ell \tag{3.14}$$

If we now consider the correlator of Polyakov loops in a pure gauge theory, it is related to the free energy of a static quark-antiquark pair $f_{q\bar{q}}$ [43]:

$$\langle \ell(\mathbf{m})\ell(\mathbf{n}) \rangle = e^{-\beta f_{q\bar{q}}(\mathbf{m}-\mathbf{n})} \tag{3.15}$$

For large distances we expect decorrelation and hence:

$$\langle \ell(\mathbf{m})\ell(\mathbf{n}) \rangle \xrightarrow[|\mathbf{m}-\mathbf{n}|\to\infty]{} |\, \langle \ell \rangle \,|^2, \tag{3.16}$$

where $\langle \ell \rangle = 1/N_S^3 \sum_{\mathbf{n}} \langle \ell(\mathbf{n}) \rangle$

In the confined phase of the pure gluonic theory the free energy of the quark-antiquark pair increases linearly with the distance ($f_{q\bar{q}}^{con}(r \to \infty) \sim \sigma r$, where $r = |\mathbf{m} - \mathbf{n}|$), whereas in the deconfined phase it is finite ($f_{q\bar{q}}^{dec}(r \to \infty) \sim const + exp(-mr)/r$). This implies:

$$\begin{cases} \langle \ell \rangle = 0 & \text{confinement} \\ \langle \ell \rangle \neq 0 & \text{deconfinement} \end{cases} \tag{3.17}$$

How can we connect the vanishing of the Polyakov loop with the center symmetry? Known that the Polyakov loop transforms under the center symmetry via Eqn.(3.14), if the pure QCD gluonic action is invariant under the center symmetry transformation we could write, for $N_c = 3$:

$$\langle \ell \rangle = \frac{1}{3} \left\langle \ell + z_k \ell + z_k^2 \ell \right\rangle = \frac{1}{3}(1 + e^{2ik\pi/3} + e^{4ik\pi/3}) \langle \ell \rangle = 0 \tag{3.18}$$

This follows from the fact that the sum inside the brakets vanishes. Being the action invariant under $Z(3)$, the center-transformed gauge configurations have the same weight in the partition function and hence are "equiprobable".
However Eq.(3.18) can not hold if the center symmetry is broken or *spontaneously* broken. Hence we expect that the center symmetry is realized in the low temperature (confined) phase. Instead in the high temperature (deconfined) phase the center symmetry is spontaneously broken and the average Polyakov loop clusters around one of the $Z(3)$ roots. This process is called the *deconfining transition* and it is related to the spontaneous breaking of the center symmetry, for which the Polyakov loop represents an order parameter.

The insertion of dynamical fermions in the theory explicitly breaks the center symmetry (the center symmetry transformation breaks the temporal anti-periodic boundary conditions of the fermions). Thus the center symmetry is exactly realized only in the pure gauge theory with no dynamical quarks. With dynamical quarks the polarization effects make the free energy of a quark-antiquark pair in the confined phase *finite* for infinite distances, hence the Polyakov loop does not vanish. As a result, the Polyakov loop is no more an order parameter for the process.

3.2.3 Chiral Symmetry

The chiral symmetry of the QCD action was already introduced in the previous chapter.
We only remark again that in the massless quark case the lagrangian of QCD acquires chiral symmetry $SU(N_f)_L \times SU(N_f)_R$, corresponding to $SU(N_f)$ flavor rotations of the left-handed (right-handed) quark multiplets independently. The ground state of QCD breaks the chiral symmetry spontaneously $G = SU_L(N_f) \times SU_R(N_f) \to H = SU_V(N_f)$ and $N_f^2 - 1$ Goldstone pseudoscalar bosons come out. The breaking of the chiral symmetry is a non-perturbative phenomenon. At sufficiently high temperature $T \gg \Lambda_{QCD}$, (in the QGP phase with weakly interacting quark and gluons) due to the asymptotic freedom of QCD, the perturbation theory should become applicable.

In this regime chiral symmetry is not broken. Thus we must expect a transition from a broken chiral symmetry vacuum state to a chirally symmetric equilibrium state at some temperature $T_c \sim \Lambda_{QCD}$. Such phase transition, known as *chiral phase transition*, is regulated by an order parameter, the so-called *chiral condensate*:

$$\left\langle \bar{\psi}\psi \right\rangle = \sum_{f=1}^{Nf} \frac{1}{V} \frac{\partial \, logZ}{\partial m_f} \tag{3.19}$$

The introduction of nonzero quark masses explicitly breaks the symmetry. The nature of "transition" as a function of the number of flavor N_f and of the quark masses will be analyzed in the following sections.

3.2.4 The transition at $\mu_B = 0$

The transition at zero baryon chemical potential has been studied extensively in the numerical simulations on the lattice. The results of the simulations at $\mu_B = 0$ depend on the number of flavors and colors considered in the theory. For instance from a finite size scaling analysis on the lattice [21] it has been established that a first order transition takes place in the pure $SU(3)$ gauge theory ($N_c = 3$, $N_f = 0$) and the critical temperature is found near $T_c \simeq 270MeV$. For $N_f > 0$ using realistic values of u, d, s quark masses, it was found from a staggered fermion and Wilson fermion analysis [5] that there is a passage from the hadronic to the quark-gluon plasma phase through an analytic crossover. The value of the pseudo-critical temperature at zero chemical potential is not unique, but it depends on the variables used for its definition. For example a possible choice is to look and the chiral susceptibility $\chi = \partial^2 logZ/\partial m^2$ that exhibits a peak near the crossover region. Lattice simulations for the position of this peak has given $T_{pc} \approx 155Mev$ [17]. We will see in the following sections that another interesting study of the transition order can be made varying the *quark masses* as an external parameter, obtaining the so called *Columbia plot*.

3.2.5 Introduction of a baryon chemical potential: the sign problem

Although the net number of baryons or quarks in the vacuum is zero, in some situation one has to consider the effect of nonvanishing baryon number density n_B, like in heavy ion collisions or ultra-dense matter in neutron stars. This leads to the introduction of a nonzero baryon chemical potential μ_B and to use the grand canonical partition function Eqn.(3.11). The introduction in the theory of a nonzero chemical potential brings many drawbacks in the use of Monte Carlo techniques.
Without making explicit the details, let us consider the full QCD action in Lattice formulation at nonzero chemical potential [24]:

$$Z(T,\mu) = \int [dU] det\, M(U, m_q, \mu_q) e^{-S_{YM}[U]} \tag{3.20}$$

where U are the link variables, S_{YM} is the pure gauge action and $M = D(U,\mu_q) + m_q$, where $D(U,\mu_q)$ is the discretized Dirac operator. In the case of $\mu_q = 0$, let us define the measure $\rho[U] = exp\left[-S_{YM}[U]\right] detM[U]$ and let us suppose that it is a *positive*

definite function of its variables (the link variables for each site). This is true because for $\mu_q = 0$, $D(0)$ is anti-hermitian and it has complex conjugated eigenvalues λ_i. Hence:

$$det[D(0) + m_q] = \prod_i (\lambda_i + m_q)(\lambda_i^* + m_q) > 0 \tag{3.21}$$

If one wants to compute the average of an observable:

$$\langle O \rangle = \frac{\int DU\, O[U]\rho[U]}{\int DU\, \rho[U]}, \tag{3.22}$$

one can use standard Monte Carlo techniques to approximate the integral with a sum over a small set of field configurations picked with a probability $\propto \rho[U]$. Indeed the suppression of most configurations allows to avoid using the total number of possible configurations, that increases exponentially in the volume V. These are called Monte-Carlo *importance sampling* techniques. For $\mu_q \neq 0$ the Dirac operator $D(\mu_q)$ is no more antihermitian and the determinant in no longer real (unless μ_q is purely imaginary). We have that now $\rho[U]$ is complex and therefore we can no more use Monte Carlo importance sampling techniques to evaluate the integral. This problem is known as the *sign problem*.

3.2.6 Conjectured QCD phase diagram

Before describing some methods to extrapolate the phase structure at nonzero chemical potential, let us now look at the conjectured phase diagram in the (T, μ_B) plane for $N_f = 2$. We will focus at first to the study of the chiral phase transition in the massless u and d case and then successively in the physical case.
As we told in the previous chapter if the mass of the quarks is zero we have a *true* chiral phase transition with the chiral condensate as an order parameter. Fig.3.2 shows a phase transition of the second order which starts from the point $(T = T_c, \mu = 0)$ where T_c is estimated to be near $160MeV$. Moving in the (T, μ) plane it is expected the existence of a tricritical point (T_3, μ_3) which connects the second order line with a first order line.
Increasing the quark masses towards the real ones, the second order transition weakens and eventually becomes a smooth crossover. Therefore the first order line should end at a second order endpoint labeled with (T_E, μ_E) and the crossover line reaches the $\mu = 0$ axis at a temperature $T^* > T_c$.

Let us now show the conjectured QCD phase diagram in the whole (T, μ_B) plane at $N_f = 2$ with physical quark u and d masses in Fig.3.3. As we can notice the situation here is richer. Because of the impossibility to use lattice simulations at nonzero μ_B, the following structure is mostly derived from effective models (like the *Chiral Random Matrix* model that we are going to explain in this thesis). To know more about this look at the following section. We start remarking some points.

- The existence of a first order transition at low T is expected from effective theories predictions.

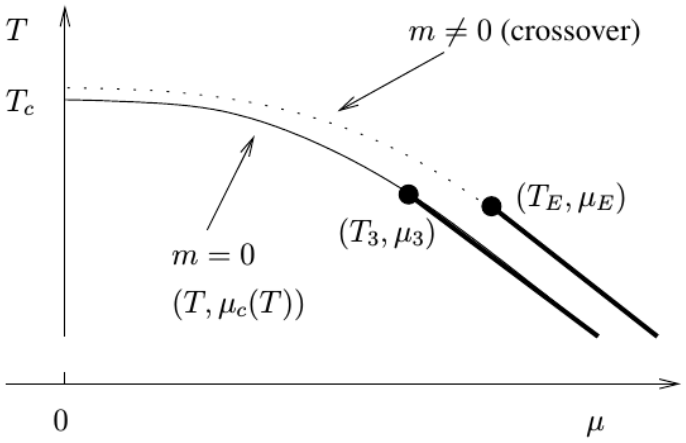

Figure 3.2: Conjectured phase diagram of $N_f = 2$ QCD in the massless and nonzero mass case. Figure taken from Ref.[49].

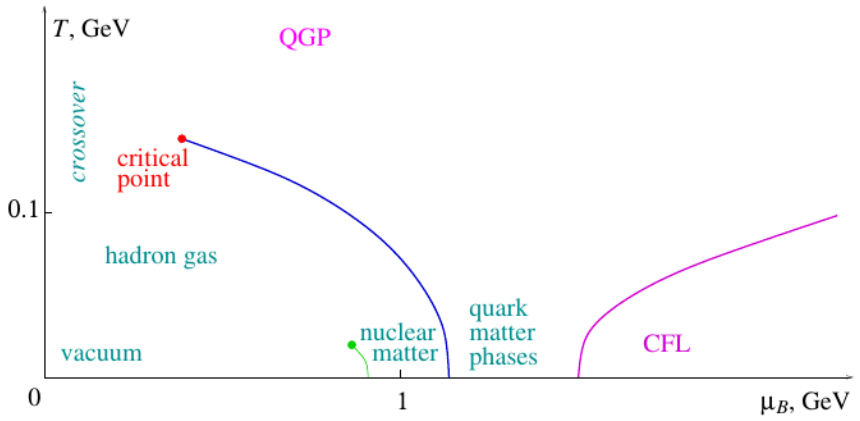

Figure 3.3: A qualitative plot of the QCD phase diagram at $N_f = 2$ in the whole (T, μ_B) plane with real quark u,d masses.

- In the low temperature region it can be supposed the existence of another first order line which start from the $T = 0$ axis and should end with a second order endpoint (T_G, μ_G). It is related to the phase transition of the nuclear matter. Indeed, given a nucleon mass of $m_N \approx 939MeV$ and a binding energy of $16MeV$, a non vanishing density of nuclear matter should arise at $T = 0$ and $\mu_{NM} \approx 923MeV$. At $\mu_B = \mu_{NM}$ the baryon density should jump from zero to the normal nuclear density of $n_0 = 0.17fm^{-3}$. Low energy experiments predict $\mu_G \approx \mu_{NM}$ and $T_G = 15 - 20MeV$ [11].

- In the low-T and high-μ_B region ($\mu_B \gg \Lambda_{QCD}$) the ground state of QCD should form "Cooper pairs" leading to *color superconductivity*. The theoretical background of this process will not be treated in this thesis, for an interesting review see Ref.[4].

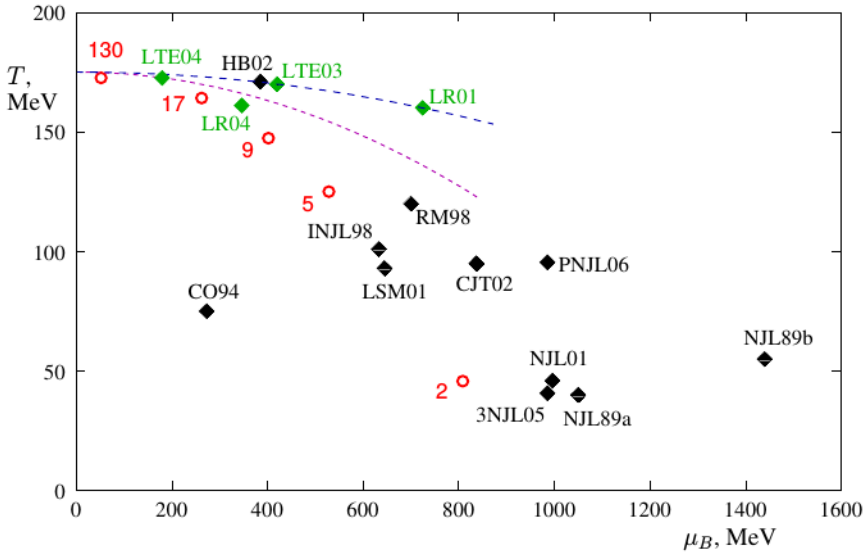

Figure 3.4: Comparison of predictions for the location of the QCD critical point on the phase diagram. Black points are model predictions, green points are lattice predictions. The two dashed lines are parabolas with slopes corresponding to lattice predictions of the slope $dT/d\mu_B^2$ of the transition line at $\mu_B = 0$. The red circles are locations of the freezeout points for heavy ion collisions at corresponding center of mass energies per nucleon (in GeV).

3.2.7 Finding the critical point: models and lattice extrapolations

As we told in the previous sections for physical masses the first order transition line is supposed to end at second order a point which is called the *QCD critical point*. Even the first order transition line of the boiling water has such a point at $p = 218atm$ and $T = 374K$: approaching it the two distinct phases of water and vapor become less and less distinct. This mechanism maybe could happen even in QCD between the gas of hadrons and the quark-gluon plasma.
In absence of some reliable method to simulate QCD at nonzero chemical potential, one can try to detect this critical point using model calculations and effective theories (like *Nambu-Jona-Lasinio* (NJL) model, *Random Matrix* (RM) model, *Linear Sigma* (LS) model, *Cornwall-Jackiw-Tomboulis* (CJT) model and others). An interesting review of such predictions, together with lattice extrapolations, is reported in Fig.3.4 [50], where it can be noticed that the locations vary very widely.

Let us now summarize two lattice methods to extrapolate the position of the critical point from an analysis at μ_B (or μ_q)$= 0$. Some interesting reviews about this are Ref.[50], [46], [22].

1. **Taylor expansion**. If one wants to compute the average of an operator at nonzero chemical potential $\langle O \rangle_{\mu_q}$ a way to avoid the sign problem is to perform

a Taylor expansion in μ_q/T around $\mu_q = 0$:

$$\langle O \rangle_{\mu_q} = \sum_{n=0}^{\infty} c_n(T) \left(\frac{\mu_q}{T} \right)^n, \tag{3.23}$$

where:

$$c_n(T) = \frac{T^n}{n!} \frac{\partial^n}{\partial \mu_q^n} \langle O \rangle_{\mu_q=0} \tag{3.24}$$

The coefficients can be simulated at $\mu_q = 0$. The Taylor expansion makes sense only inside a radius of convergence that can be limited by the closest singularity from the origin in the complex μ_q/T plane. Paradoxically, the end of the effectiveness of the Taylor expansion could be a signal for the detection of a critical point at nonzero density, in relation with the divergent behavior of some observable near the criticality. Hence one of the goal of this thesis is to detect properly the *radius of convergence* of a Taylor expansion like Eq.(3.23) with the knowledge of only few coefficients and using different methods. We will deal properly with this problem with the Random Matrix model in Chap.6 and later on with other lattice extrapolations.

2. **Imaginary chemical potential.** Another approach consists of introducing an *imaginary chemical potential* $\mu_{I,q}$ [19]. It is easy to see that an imaginary chemical potential preserves the anti-hermiticity of the Dirac operator, the probability density is positive and no sign problem arises. Hence lattice simulations can be implemented usefully in the $\mu_{q,I} \neq 0$ region. We are able to estimate the average value of an observable at imaginary chemical potential using Monte Carlo methods, to compute the coefficients c_n of the Taylor expansion and then analytically continuing at real μ_q with the substitution $\mu_q \to -i\mu_q$:

$$\langle O \rangle_{\mu_{I,q}} = \sum_{n=0}^{\infty} c_n(T) \left(\frac{\mu_{I,q}}{T} \right)^n \longrightarrow \langle O \rangle_{\mu_q} = \sum_{n=0}^{\infty} c_n(T) \left(\frac{-i\mu_q}{T} \right)^n \tag{3.25}$$

The opportunity to extend the average backward to real μ_q is obviously limited by the presence of singularities in the complex plane. For instance we will see in the following section how the presence of the Roberge-Weiss transition lines limits the applicability of the method at μ_I not so far from the origin.

3.2.8 Phase structure at imaginary chemical potential: the Roberge-Weiss transition

We anticipated in the previous section the potentiality to extend our theory to imaginary chemical potentials in the research of the critical point. If we define as $\theta = \mu_{q,I}/T$, the QCD partition function in presence of an imaginary chemical potential can be written as:

$$Z(\theta) = Tr \left[e^{i\theta N_q} e^{-H_{QCD}/T} \right] \tag{3.26}$$

The partition function has a periodicity of 2π in θ and furthermore a periodicity of $2\pi/3$ is plausible to appear in the confined phase in which N_q can appear only in

multiple of 3. However Roberge and Weiss [42] confirmed that the periodicity in θ is always of $2\pi/3$ with an analytic behavior of $Z(\theta)$ at high temperature and non analytic at low temperature.

Such periodicity can be automatically deduced from the fact that the introduction of an imaginary chemical potential can be seen as a shift in the fermionic temporal boundary conditions of an angle θ_q. A transformation $\theta_q \to \theta_q + 2\pi k/N_c$ can be directly absorbed by a center transformation of the gauge links (3.13) that leaves the action and the measure invariant. This implies a periodicity in θ_q of $2\pi/N_c$.

Let us analyze in detail the behavior of the *Polyakov loop* (3.12) as a function of the temperature. In general it assumes complex values and it can always been written as $\ell(\mathbf{n}) = |\ell(\mathbf{n})|e^{i\phi}$. As we have seen in Sec.3.2.2, in the deconfined phase of the pure gauge theory the center symmetry is spontaneously broken and the Polyakov loop clusterizes along one of the three $Z(3)$ roots, hence the average phase $\langle\phi\rangle = 2k\pi/3$, with $k = 0, 1, 2$. In such phase each of these three roots is equally probable and degenerate in energy. Conversely in the confined phase the average phase is always zero $\langle\phi\rangle = 0$.
Introducing the dynamical fermions, the center symmetry is explicitly broken, the quark masses act like a magnetic field variable that makes the Polyakov loop purely real aligning the phase along $\langle\phi\rangle = 0$ both in the confining and deconfining phase. When we introduce a $\mu_I \neq 0$, the phase of the Polyakov loop is further shifted $\ell(\mathbf{x}) \to \ell(\mathbf{x})e^{i\theta}$, hence this time the quark masses act to align $\theta + \langle\phi\rangle \to 0$. Therefore in the low temperature (confining) region we expect to have $\langle\phi\rangle = -\theta$, whereas in the high temperature (deconfining) region the $Z(3)$ degeneracy is explicitly broken by the mass term but now the chemical potential term θ regulates the particular $Z(3)$ sector to occupy. In detail, for high T:

$$\theta \in \left[\frac{(2k-1)\pi}{3}, \frac{(2k+1)\pi}{3}\right] \Rightarrow \langle\phi\rangle = \frac{2k\pi}{3}, \quad k = 0, 1, 2 \tag{3.27}$$

Hence every time that $\theta = (2k+1)\pi/3$, one expects a transition from one $Z(3)$ sector to another (see Fig.3.5). Summarizing we can say that the periodicity of the partition function of $2\pi/3$ is smoothly realized at low temperature, while at high T phase transitions occur for $\theta = (2k+1)\pi/3$, ($k \in \mathbb{Z}$). The phase structure is the one of Fig.3.6, with a periodic repetition of first order lines in the high T regime, the so called *Roberge-Weiss lines.* The endpoint temperature of the first order RW lines is labeled with T_{RW}. It is important to highlight [13] that the RW lines correspond to point where a $Z(2)$ symmetry is spontaneously broken, indeed we should have two equivalent center sectors but only one of them is selected. In particular the $\theta = \pi$ line is such that at high temperature the *charge symmetry* is explicitly broken independently of the quark masses.

From the RW endpoint some critical line could originate and maybe it could reach the $\mu_I = 0$ axis conditioning the phase transition at real chemical potential. Studies for the deconfinement [20] and the chiral [8] transition have been made. nature of such lines and of the RW endpoint will be analyzed in the following section.

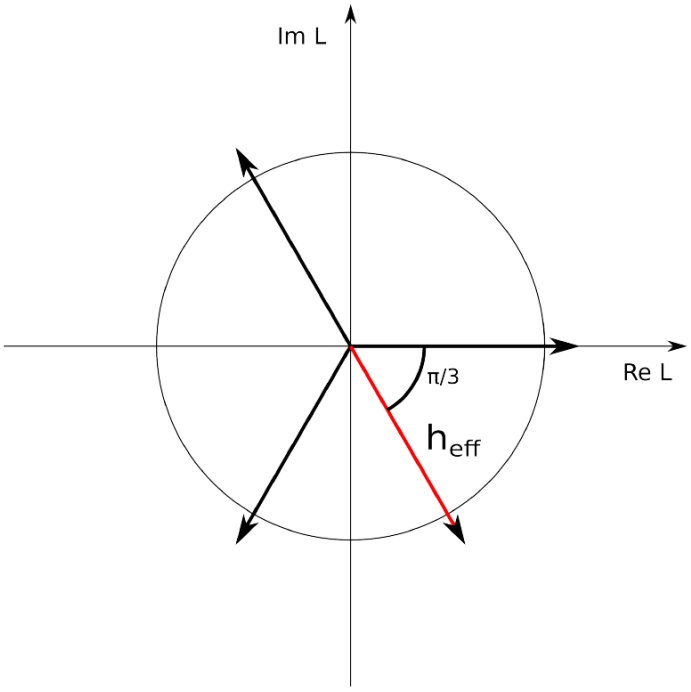

Figure 3.5: Polyakov loop (L) plane at the RW transition $\theta = \pi/3$

.

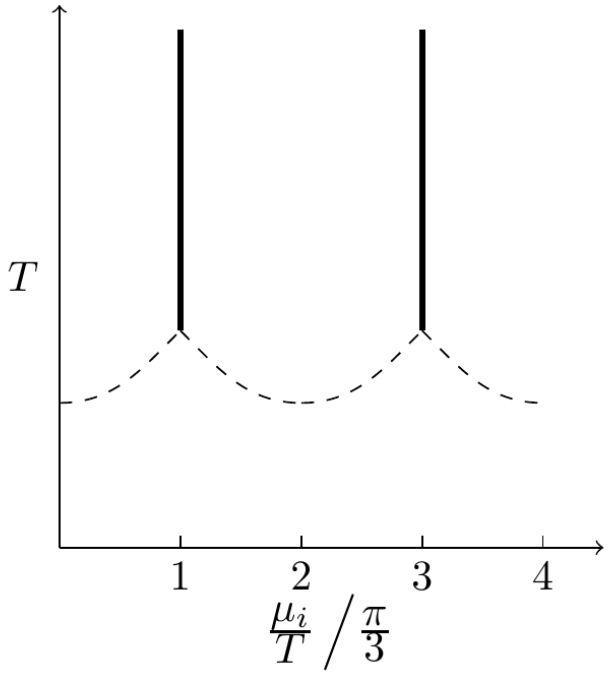

Figure 3.6: Phase structure at imaginary quark chemical potential. The thick lines are the RW transition lines. The nature ot the dashed lines (and possible endpoints) depends on the quark masses.

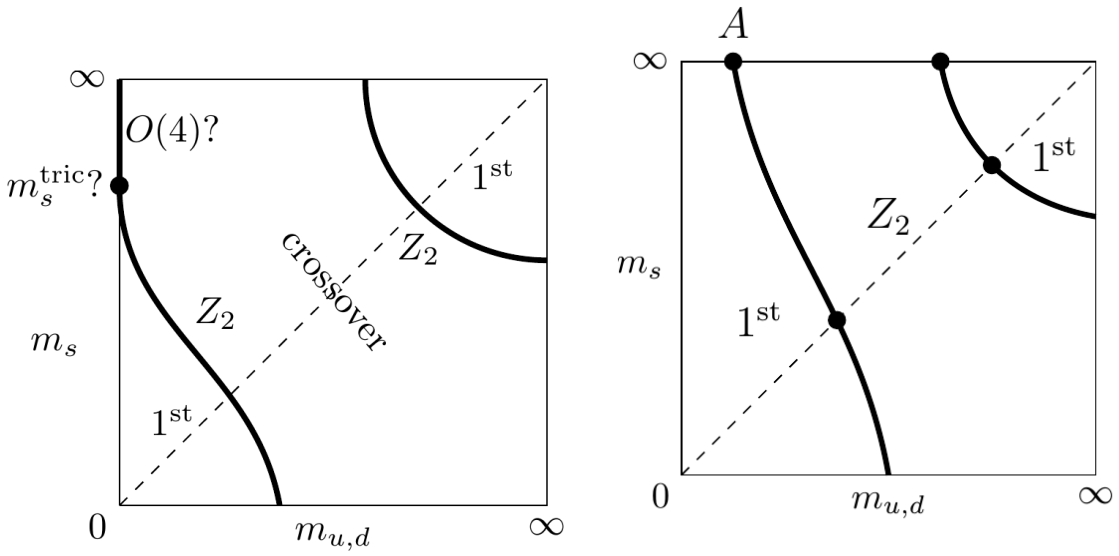

(a) $\mu_q = 0$ (b) $\mu_q/T = i\pi/3$

Figure 3.7: Columbia plots at **(a)** $\mu_q = 0$ and **(b)** at the RW transition $\mu_q/T = i\pi/3$.

3.2.9 Tuning the masses: the Columbia plot

It is interesting to perform a study about the nature of the transitions (at real and imaginary chemical potential) varying the quark masses like external parameters. In this way we obtain the so-called *Columbia plot*.
The Columbia plot of the current knowledge of the QCD phase transition at zero baryon chemical potential for $N_f = 2 + 1$ quarks is reported in Fig.(3.7.a) (taken from Ref.[8]). We have a first order phase transition inside the two regions around $m_u = m_d = m_s = 0$ (three massless quarks) and $m_u = m_d = m_s \sim \infty$ (pure gauge or infinitively massive quarks). Both regions are bounded with second order lines. The labels "$Z(2)$" and "$O(4)$" refer respectively to the 3d Ising and the 3d $O(4)$ model universalities. In the middle region (the physical values of the quark masses are here) we do not have a true transition but an analytic crossover. The limit of two massless flavors is still an open topic, in which the $U_A(1)$ axial anomaly could play a relevant role (see Ref. [8], [40], [41]).

How does the situation vary switching on an imaginary chemical potential $\mu_{q,I}$? In correspondence of the Roberge-Weiss point $\mu_{q,I}/T = \pi/3$ lattice simulations suggest us a scenario like the one in Fig.(3.7.b). Still the massless quarks and the pure gauge cases are predicted to be inside a first order transition region. This time these regions are bounded by lines of tricritical points and the middle region is now replaced by a second order region of the $Z(2)$ 3d Ising universality.

Let us now try to summarize the results we have just read. As we told before at the Roberge-Weiss point $\mu_{q,I}/T = \pi/3$ we have a first order transition line above a temperature T_{RW}. The nature of the endpoint and the possible continuation of this line can be properly governed tuning the values of the masses. The endpoint can be of the second order (in the "middle" mass region) or it can be of the first order (as what happens in the *chiral* and in the *deconfinement* case). It the latter situation

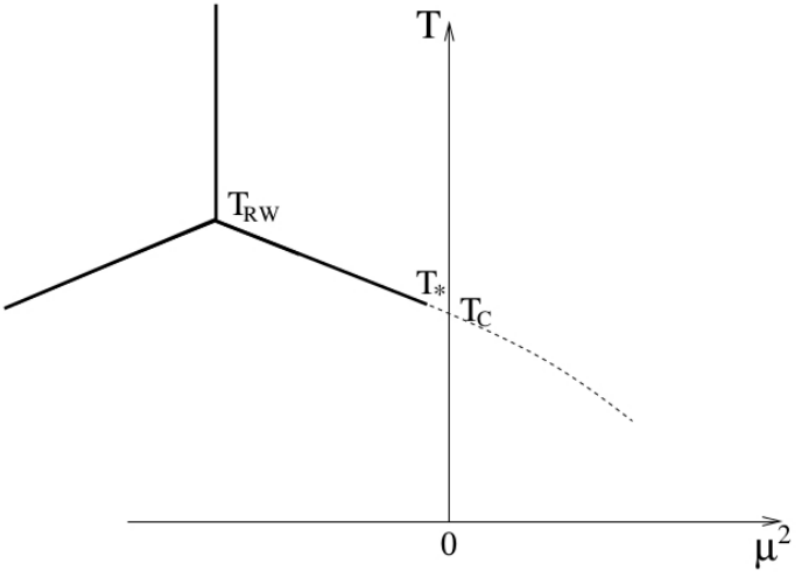

Figure 3.8: At low masses the RW endpoint is a *triple* point and two first order lines branch off from it. One of them could reach an endpoint at temperature T^* before reaching the $\mu^2 = 0$ axis.

we should have two first order lines that branch out from this point: one of them could reach the $\mu_q = 0$ axis or stopping before, as shown in Fig.3.8. In the physical quark masses case one should plausibly plot a crossover line that joins the points $(T_{pc}, \mu_q = 0)$ and $(T_{RW}, \mu_{I,q} = \pi/3)$.

3.2.10 Experiments to explore the phase diagram

High energy ion collisions are actually the only way that could confirm in laboratory the existence of the new state of matter predicted by QCD, the *Quark Gluon Plasma*. Since 2000 the collider RICH at Brookhaven started to perform Cu-Cu and Au-Au collisions at $\sqrt{s_{NN}} \backsimeq 130GeV$ and $\sqrt{s_{NN}} \backsimeq 200GeV$ [35].
As the current state of research we have to remark that since November 2015 the LHC at CERN started providing collisions of stable beams of Pb at a centre of mass energy $\sqrt{s_{NN}} \backsimeq 5TeV$ per colliding nucleon pair. Also, RHIC has recently started to perform U-U collision at $\sqrt{s_{NN}} \backsimeq 193MeV$ and Au-Cu collisions at$\sqrt{s_{NN}} \backsimeq 200MeV$[35].

The experimental search of the QCD critical point consists of sweeping the (T, μ_B) plane varying the energy of the beams through the so-called *beam energy scans* (BES). The QCD system in heavy ion collisions goes through various stages. The description of such stages and the mechanisms involved in the time evolution after the collision are still to be well understood. The backward reconstruction of the trajectories are strongly model dependent. However, keeping this in mind, it can be useful to try to briefly summarize the possible time evolution of the system after such collisions following Ref.[35] (from which we took Fig.3.10).

- At first the colliding nuclei are accelerated to near-light speed. At those energies, the life-time of gluons emitted from the valence quarks or other gluons

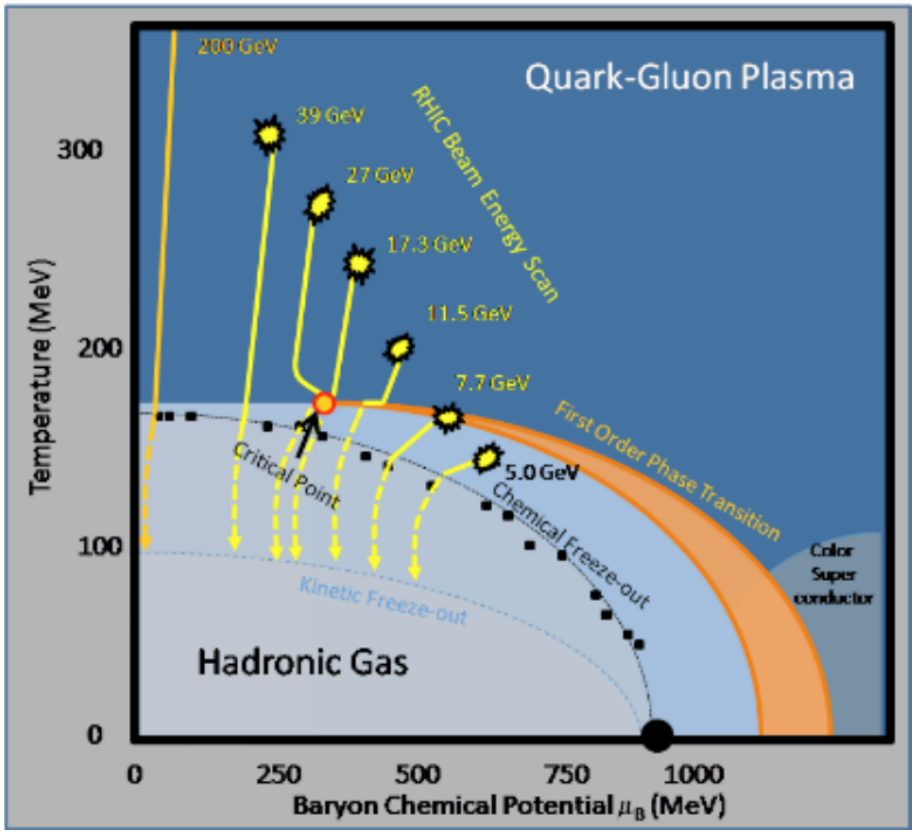

Figure 3.9: A schematic of the phase diagram of QCD. The black closed circles are current heavy-ion experimental calculations of the chemical freeze-out temperature, T^f_{chem} , and $\mu^f_{chem,B}$. The yellow curves show the estimated trajectories of the possible collision energies at RHIC. Figure taken from Ref.[1].

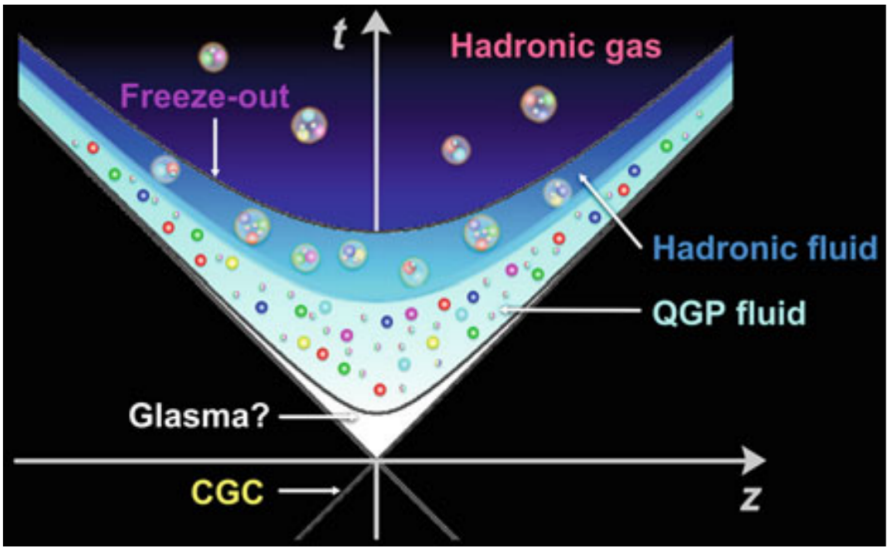

Figure 3.10: Spacetime evolution of a heavy ion collision process. Figure taken from Ref.[35].

become long enough to allow additional emissions of soft gluon themselves, in a cascading process that increases the number of gluons. This state of matter is called *color glass condensate* (CGC).

- After the collisions the system locally thermalizes in a really short time ($\sim 10^{-23}s$). In this phase color tube structures appear between the colliding nuclei: this state is called *glasma* (word to indicate a mixture between color glass condensate and quark-gluon plasma).

- In the following stage the state of the system is called the *Quark Gluon Plasma* (QGP). It has been verified that especially because of the azimuthal anisotropy of the spatial and momentum distribution, in a certain period of its lifetime the QGP can be treated through hydrodynamic models with viscosity. The first behavior as a hot fluid medium was observed in the analysis of Au-Au collisions at RHIC.

- Because of the difference in pressure with respect to the external environment, the hot bubble of QGP expands and cools down, reaching a point where the hydrodynamic description is no more applicable. This process is called the *freeze out*. Decreasing in temperature, the hot bubble overpass the critical deconfining point making possible the *hadronization*. One usually says that the system has reached the freeze out when the temperature reach values near $T_f \sim 130 \div 160 MeV$, (just below the pseudocritical temperature of $T_{pc} \simeq 170 MeV$), but one can use even other hydrodynamic criteria. One has to distinguish two different kinds of freeze out: the chemical and the thermal freeze out. *Chemical* freeze out describes the point where hadron abundances stop changing. *Thermal* (or *kinetic*) freeze out instead defines the point where the momenta of the particles stop changing, i.e. where all type of momentum-changing collisions cease. A criterium predicted by Zimànyi says that in a dynamically evolving fireball these two freeze-out points do not coincide [53]. As one can observe from Fig.3.9, typically the chemical freeze-out happens earlier (and therefore at higher temperature) than the thermal one: $T^f_{chem} > T^f_{therm}$. [1]

- After the freeze out the hadronic matter is considered as *weakly* interacting and it is detected. This important assumption makes possible to reconstruct the trajectories from the detection backward to the freeze-out moment. Furthermore, if this is true, it is possible to study the properties of the hadronic matter just below the deconfining temperature, hoping to detect experimental evidences of a critical behavior.

The experimental deductions about the QCD phase diagram are reported in Fig. 3.9, taken from Ref.[1].

[1] Another thing to observe is that usually the scattering rate is particle specific, hence the thermal freeze out should depend on the different hadrons we are considering. Hence it is difficult to implement the thermal freeze out for a hydrodynamic model. Fortunately, usually there is one species that dominates the scattering cross section triggering the other freeze-outs.

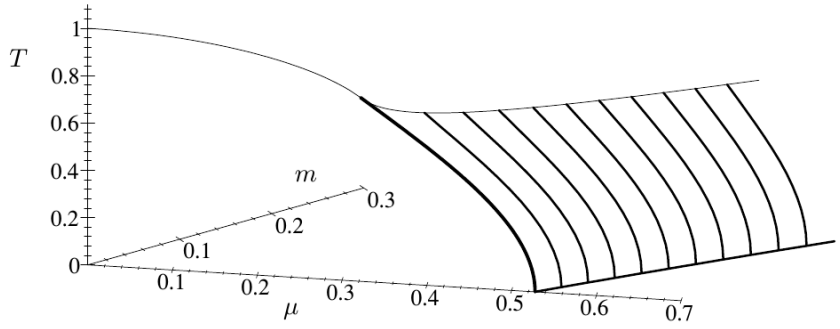

Figure 3.11: The phase diagram of a RM model of QCD at $N_f = 2$ in the (T, μ_B, m) space. The almost parallel lines are the first order lines varying the mass. The line of the endpoints that originates from the tricritical point is called the *wing line*.

3.2.11 The tricritical point

It is interesting to focus on the *tricritical* nature of the point (T_3, μ_3) of the QCD phase diagram at $m = 0$. One could thing that the adjective "tricritical" can refer to a coexistence of three different states. Actually, to see this is useful to consider a third dimension of the phase diagram, the *mass*. It is possible to see that there are two first order surfaces (symmetric with respect to the inversion $m \to -m$) that originate from the first order line in the plane $m = 0$ (see Fig.3.11). On these surfaces there is a coexistence of a low-density and a high-density state, but no order parameter is present, because chiral symmetry is explicitly broken at nonzero mass. The edge of this surface may be directly connected with a line of critical points.
The only plane where the low-density and the high-density phase are separated by a real phase transition is the $m = 0$ plane. Hence the first order line in this plane can be recognized to be a triple line because it represents the coexistence of a high temperature density phase and two low temperature density phases with opposite signs of the mass (or of the chiral condensate $\left\langle \bar{\psi}\psi \right\rangle$ that now is an order parameter and is discontinuous crossing this line for each of the three directions).

As Ref.[30] suggests, one can now study the behavior near the tricritical point from universality. Indeed, because the upper critical dimension for this point is 3 and the fluctuations for the second order phase transition are 3 dimensional, one can describe this point with mean-field exponents apart from logarithmic corrections. The long-wave oscillations or the order parameter $\phi \sim \left\langle \bar{\psi}\psi \right\rangle$ can be described with an effective Landau-Ginzburg potential of the form:

$$\Omega_{eff} = \Omega_0(T, \mu) + a(T, \mu)\phi^2 + b(T, \mu)\phi^4 + c(T, \mu)\phi^6 \tag{3.28}$$

with $c > 0$. The sixth power is essential to reproduce the three coexisting phases. Let us now take a look to the T,μ-behavior of the coefficients and how they can affect the order of the transition. The value of the order parameter varying T and μ is given by the absolute (real valued) minimum of the effective potential. If $c(T, \mu) > 0$ $\forall\, T$, μ we can have:

- **b>0**, **a=0**. The equation $\partial\Omega/\partial\phi = 4b\,\phi^3 + 6c\,\phi^5 = 0$ has $\bar{\phi} = 0$ as only real

solution. Near this point we see that even the second derivative $\partial^2\Omega/\partial\phi^2|_{\bar{\phi}=0} = 0$. This corresponds to a point in which a minimum is turning into a maximum. Slightly varying T and μ from these "critical" values, an absolute minimum in zero (restored phase) or two symmetric minima (broken phase) can appear. This is the second order line.

- **b<0**, **a>0**. The vanishing of the first derivative leads to $\bar{\phi} = 0$ (that is a minimum) and to the four solutions $\bar{\phi} = \pm\sqrt{-b/3c}\sqrt{1 \pm \sqrt{1 - 3ac/2b^2}}$ (two minima and two maxima). Properly tuning T and μ one can vary the coefficients in order to have the minimum in zero and the two symmetric minima equally deep. In such a case we have three coexisting phases and a first order transition.

- **b=0**, **a=0**. We can notice at first that this interesting point can be in particular reached both from the $(b_F < 0, a_F > 0)$ of the first order line and from the $(b_S > 0, a_S = 0)$ of the second order line. Hence it should be intuitive to deduce that this corresponds to the tricritical point. We have that $\phi = 0$ is the only solution of $\partial\Omega/\partial\phi = 0$ and here the potential behaves like $\sim \phi^6$, hence all the derivatives up to the fifth vanish.

3.2.12 Complex chemical potential study of the chiral phase transition

The generic case

It is interesting to perform a study of the chiral phase transition using the tools of Yang-Lee analysis in Sec.3.1. In their paper they showed a strict correlation between the zeros of the partition function and the thermodynamic singularities in the complex $z = exp(\mu/T)$ plane. The partition function of QCD can be considered a polynomial of the variable z, (where we take for μ the *baryon* chemical potential), due to the quantization of the baryon charge. One can make an interesting analogy with electrostatics [49]. Writing the partition function as:

$$Q(z) = \prod_k (z - z_k), \tag{3.29}$$

the free energy is:

$$\Omega(z) = -TlogQ = -T\sum_k log(z - z_k). \tag{3.30}$$

If we move in the complex z plane, the real part $Re\Omega = -T\sum_k log|z - z_k|$ can be considered as the electrostatic potential created by the charges z_k in the complex plane. In the thermodynamic limit, we can suppose for the zeros line to coalesce into a 1-dimensional line. The electrostatic potential $Re\Omega$ is continuous along this line, whereas the analog electric field

$$E = -\nabla(Re\Omega) = -\left(\frac{\partial Re\Omega}{\partial Rez}, \frac{\partial Re\Omega}{\partial Imz}\right) \tag{3.31}$$

is discontinuous due to a density ρ of zeros. We can interpret this line as the location of a Riemann sheet of the analytic function $\Omega(z)$. It is now important to analyze the

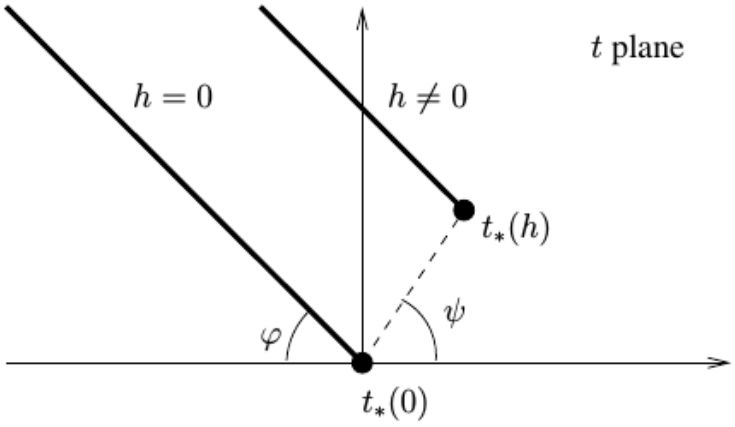

Figure 3.12: Stokes boundary and branching points in the complex $t = (z - z_c)/z_c$ plane with a zero and nonzero magnetic variable h. Figure taken from Ref.[49].

behavior of the partition function near the critical point, z_c.

Let us start with the case of $h = 0$, where h is the *magnetic field variable*, a role played by the quark mass for the chiral phase transition in QCD. For this purpose, if we define the variable $t = (z - z_c)/z_c$ the singular part of the free energy near the criticality has the form:

$$\Omega_{sing}(t) = \begin{cases} A_+ t^{2-\alpha}, & t > 0; \\ A_-(-t)^{2-\alpha}, & t < 0; \end{cases} \tag{3.32}$$

where α is the specific heat exponent and $A_\pm$ are two constants whose ratio is known. Due to the parity with respect to conjugation $\Omega(t) = \Omega(t^*)$, such potential has two cuts (the so-called *Stokes boundaries*) whose position is obtained using the electrostatic analogy that wants "potential" $Re\Omega$ to be continuous along the cut and whose slope φ is fixed from the A_+/A_- ratio [49]. The end of the Stokes boundary is called the *branching point*. In the $h = 0$ the branching points lie on the real t axis. If we now turn on the magnetic field h, (read: introduce a nonzero quark mass m), then we have another relevant variable near the critical point. In QCD the presence of a quark mass explicitly breaks the chiral symmetry. In the scaling region the singular part of the free energy scales with t and h to hold the scaling variable $x \equiv th^{-1/(\beta\delta)}$ fixed. Therefore it results that the two symmetric branching points are shifted in the complex z plane by an amount $t_* = x_* h^{1/(\beta\delta)}$ and the phase of t_* results to be equal to $\psi = \pi/2\beta\delta$ [49], where β and δ are the critical exponents. An interesting picture that explain the general $h = 0$ and $h \neq 0$ cases is reported in Fig.3.12.

The QCD chiral transition case

To look in particular at what happens in the chiral phase transition of QCD, let us start from the phase diagram of Fig.3.2.

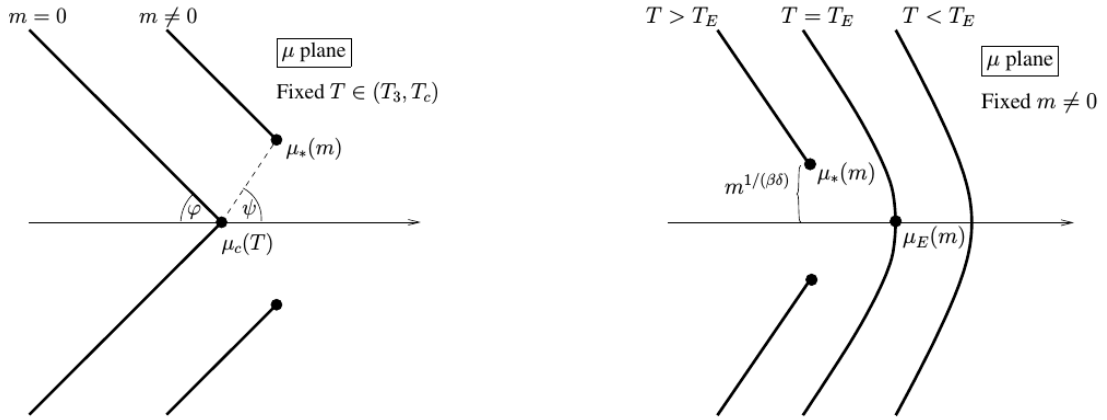

Figure 3.13: Stokes boundaries and branching points of the free energy in the massless and nonzero mass case for a temperature $T \in (T_3, T_C)$ (left) and for T near T_E (right). Figure taken from Ref.[49].

In the massless case, the only relevant parameter in the vicinity of the transition is the so called *thermal variable* $t \sim \mu^2 - \mu_c^2$: the perturbation in this case is represented by a variation of the chemical potential. Since near the criticality $z - z_c = exp(\mu/T) - exp(\mu_c/T) \approx \mu - \mu_c$, we could perform the study in the complex μ plane using the results of the previous section. Because the transformation $\mu \to \mu^2$ is *conformal* [2] we can obtain the same results looking at the analyticity properties in the complex μ^2 (or t) plane.
When we turn on the mass of the quarks we include in our model a *magnetic-field* variable that becomes relevant near the $O(4)$ critical point and breaks explicitly $O(4)$ down to $O(3)$. As shown in the previous section, the effect in the complex μ^2 plane is to introduce a shift of the branching points toward complex values, at least for those temperatures slightly lower than T_c (we have no more a second order transition but now a smooth crossover). Decreasing the temperature the branching point approaches the real axis at a value $\mu = \mu_E$ in correspondence of a temperature $T = T_E$. The couple (T_E, μ_E) represents the ending point of the first order transition line for nonzero masses. A clear explanation of this mechanism is reported in Fig.3.13.

[2] Being a conformal transformation, it preserves the angles, that is it does not affect the inclination of the Stokes boundary or the phase of the branching points.

Chapter 4

Mathematical methods for power series analysis

4.1 Introduction

We start this chapter introducing some remarks about power series. Most of the material is taken from Ref.[27]. Let us define a power series $f(z)$ as

$$f(z) = \sum_{n=0}^{\infty} c_n z^n \tag{4.1}$$

where z is complex variable, c_n is the n^{th} coefficient. In the following section we will define the *radius of convergence* R of the power series, an important tool that ensures us the convergence of the series for $|z| < R$ and its divergence for $|z| > R$. In many critical phenomena the critical behavior of a function near a transition point can be represented through a behavior of the form $f(z) \sim A(1 - z/z_c)^{-\lambda}$. If z_c is the closest singularity to the origin, then $R = |z_c|$. The knowledge of R in principle can be obtained knowing the behavior of the coefficients for $n \to \infty$. However in practice we can know only a little number of coefficients of the Taylor series: what is in such case the best method to estimate R? The power and the drawbacks of the application of the power series expansion theory in the research of the QCD critical point and other criticalities in the phase diagram will be explored in the following chapters.

4.2 Radius of convergence: definition

Theorem 4.2.1. ***(Radius of convergence)*** *Given the series* (4.1) *centered around zero* ($z_0 = 0$)*, then* $\exists!$ r *s.t.*

1. $\forall z \in \mathbb{C}$ *such that* $|z| < r$ *the series converges absolutely;*

2. $\forall z \in \mathbb{C}$ *such that* $|z| > r$ *the series diverges.*

Proof. *Let us define at first* $r = sup\{r \in [0, \infty) : \sum_{n=0}^{\infty} |c_n| r^n < \infty\}$.
(1) *For any* $z : |z| < r$ *we have that the series converges absolutely, indeed:*

$$\sum_{n=0}^{\infty} |c_n||z|^n < \sum_{n=0}^{\infty} |c_n||r|^n < \infty \tag{4.2}$$

(2) *We now assume by absurd that there is a $z_1 > r$ and the series converges in z_1 ($\sum_{n=0}^{\infty} c_n z_1^n < \infty$). Since the series in z_1 is convergent, its elements has to be bounded, hence there is a $M \in \mathbb{R} : |c_n z_1^n| < M \ \forall n$. If we now take a z_2 s.t. $r < |z_2| < |z_1|$, for any z: $|z| < |z_2|$ we have:*

$$\sum_{n=0}^{\infty} |c_n||z|^n < \sum_{n=0}^{\infty} |c_n||z_2|^n = \sum_{n=0}^{\infty} |c_n z_1^n| \left|\frac{z_2}{z_1}\right|^n < M \sum_{n=0}^{\infty} \left|\frac{z_2}{z_1}\right|^n < \infty. \tag{4.3}$$

The last inequality follows from the fact that $|z_2| < |z_1|$ and the geometrical series is convergent. At the end we should have convergence inside $\tilde{r} = |z_2| > r$ but from the hypothesis r is the supremum of the radii of absolute convergence, so it has to be $r \geq \tilde{r}$ and hence the absurd.

4.3 Theoretical determination of the radius

The two most important methods to estimate the radius of convergence of the series (4.1) are the *ratio test* and the *root test*.

4.3.1 Root test

Theorem 4.3.1. ***(General root test)*** *Given the series*

$$\sum_{n=1}^{\infty} a_n. \tag{4.4}$$

Then the number $C = \limsup_{n\to\infty} \sqrt[n]{|a_n|}$ is such that the series converges absolutely if $C < 1$ and diverges if $C > 1$.

Corollary. ***(Power series root test)*** *If we define $\rho = \limsup_{n\to\infty} \sqrt[n]{|c_n|}$ then the power series (4.1) has radius of convergence $r = 1/\rho$ (taking care that we really mean ∞ if the denominator is zero).*

Proof (Theorem) *Let us start with the case $C < 1$. Fixed a natural number N, $\forall n \geq N$ we have, for some positive real k:*

$$\sqrt[n]{|a_n|} \leq k < 1 \qquad \Rightarrow |a_n| \leq k^n < 1 \tag{4.5}$$

But because $k < 1$ we have $\sum_{n=N}^{\infty} |a_n| \leq \sum_{n=N}^{\infty} k^n < \infty$ and therefore the whole series $\sum_{n=1}^{\infty} |a_n|$ is convergent, and the series (4.4) is absolutely convergent.
If $C > 1$, there must be some N such that if $n \geq N$ we will have

$$\sqrt[n]{|a_n|} > 1 \qquad \Rightarrow |a_n| > 1 \tag{4.6}$$

then $\forall n > N$ we know that $|a_n| \neq 0$ and therefore $a_n \neq 0$. Hence the series $\sum_{n=1}^{\infty} a_n$ has to diverge.

Proof (Corollary) *For a power series $\sum_{n=1}^{\infty} a_n = \sum_{n=1}^{\infty} c_n z^n$, we showed that the series converges if there exists an N such that for all $n \geq N$ we have:*

$$\sqrt[n]{|a_n|} = \sqrt[n]{|c_n z^n|} < 1, \tag{4.7}$$

that implies for the series to converge we must have $|z| < 1/\sqrt[n]{|c_n|}$ for all sufficiently large n. This means that $|z| < \limsup_{n\to\infty} 1/\sqrt[n]{|c_n|} = 1/\rho$. For analogous reason we can say that the series is divergent if $|z| > 1/\rho$. From the above definition of the radius of convergence it follows that $r = 1/\rho$ (with the meaning of an infinite radius if $\rho = 0$).

4.3.2 Ratio Test

Theorem 4.3.2. ***(Ratio test)*** *Given the series $\sum_{n=1}^{\infty} a_n$ then the number $D = \limsup_{n\to\infty} |a_{n+1}/a_n|$ is such that the series converges absolutely if $D < 1$ and diverges if $D > 1$.*

Corollary. ***(Power series ratio test)*** *If we define $\rho = \limsup_{n\to\infty} |c_n/c_{n+1}|$ then the power series (4.1) has radius of convergence $r = 1/\rho$.*

Proof(Theorem) *If D>1 we can find a $k < 1$ and an integer N such that for all $n \geq N$ we have $|a_{n+1}/a_n| < k$. This implies that:*

$$\begin{aligned} &|a_{N+1}| < k|a_N| \\ &|a_{N+2}| < k|a_{N+1}| < k^2|a_N| \\ &\dots \\ &|a_{N+p}| < k^p|a_N| \end{aligned} \tag{4.8}$$

This implies:

$$|a_n| < |a_N|k^{-N}k^n \tag{4.9}$$

and we have the convergence for the comparison with the geometrical series with $k < 1$. If $D > 1$ it follows that $\forall n > n_0$ for a certain n_0, the condition $a_n \to 0$ does not hold, hence we have the divergence.

The proof of the power series corollary immediately follows from this proof, as in the root test.

4.4 Practical extrapolation of the radius

We now want to define a practical tool to extrapolate the radius of convergence of the series (6.24). The approach we are going to use is the one suggested by Guttmann [27].

4.4.1 Domb-Sykes method

This method was used for the first time by Domb and Sykes [14]. If we have a function $f(z)$ that behaves like

$$f(z) \sim A\left(1 - \frac{z}{z_c}\right)^{-\lambda} + B \tag{4.10}$$

as $z \to z_c^-$, in absence of competing singularities one can Taylor expand it like the power series (4.1) and the n^{th} coefficient is given by:

$$c_n = A(z_c)\binom{n+\lambda-1}{n} z_c^{-n}. \tag{4.11}$$

Known this, one can now compute the ratio:

$$\frac{1}{r_n} = \frac{c_n}{c_{n-1}} = \frac{1}{z_c}\left(1 + \frac{\lambda - 1}{n}\right). \tag{4.12}$$

If A and B are *entire* functions (i.e. with no singularities in the finite complex z plane), one can even derive A and obtain the more precise estimate:

$$\frac{1}{r_n} = \frac{c_n}{c_{n-1}} = \frac{1}{z_c}\left(1 + \frac{\lambda - 1}{n} + \frac{c}{n^2} + O\left(\frac{1}{n^3}\right)\right), \tag{4.13}$$

where c is a parameter which depends on A, A' and z_c.

4.4.2 The Neville-Aitken extrapolation

The Neville-Aitken method has the goal to obtain a better accuracy in the estimation of critical parameters trough sequence extrapolation techniques. Given for instance the Domb-Sykes estimation of the radii Eq.4.13, we can notice that all the correction terms are all of the form n^{-k} with $k \in \mathbb{N}$. Neville extrapolation consists of eliminating high order correction terms. Suppose to have an original sequence $\{T_n^{(k)}\}$, we can construct "improved" sequences $\{T_n^{(k)}\}$ of the form:

$$T_n^{(k)} = \frac{1}{k}\left[nT_n^{(k-1)} - (n-k)T_{n-1}^{(k-1)}\right] \tag{4.14}$$

Consider for instance the ratios $r_n = c_n/c_{n+1}$ and set $T_n^{(0)} = r_n^{(0)} \equiv r_n$. Then one has:

$$r_n^{(1)} \equiv T_n^{(1)} = \frac{1}{z_c}\left[1 - \frac{c_1}{n(n-1)} + O\left(\frac{1}{n^3}\right)\right] \tag{4.15}$$

$$r_n^{(2)} \equiv T_n^{(2)} = \frac{1}{z_c}\left[1 + O\left(\frac{1}{n^3}\right)\right], \tag{4.16}$$

that is the leading correction term to $r_n^{(k)} = T_n^{(k)}$ is $O(1/n^{k+1})$. This improves relevantly the accuracy of the extrapolation of z_c.

4.4.3 Zinn-Justin's method

Still Guttmann reports one variant of the ratio method that is the Zinn-Justin method [27]. Continuing to assume the functional form (4.10) near the criticality, one can define the sequence:

$$s_n = -\left(\log \frac{c_n c_{n-2}}{c_{n-1}^2} \right)^{-1} \sim \frac{n^2}{\gamma - 1}. \tag{4.17}$$

One finds that following this definition, estimates of z_c can be obtained from:

$$z_{c,n}^{-1} = \left(\frac{c_n}{c_{n-2}} \right)^{1/2} \exp \left[- \frac{s_n + s_{n-1}}{(s_n - s_{n-1}) s_n} \right] \tag{4.18}$$

4.5 The Padé approximants

One of the major drawbacks of the ratio method is that if we have the functional form:

$$f(z) = \sum_{n=0}^{\infty} c_n z^n \sim A(z) \left(1 - \frac{z}{z_c} \right)^{-\lambda} + B(z) \tag{4.19}$$

and $A(z)$ has singularities at $|z| \leq z_c$ one has that the ratio method is not able to study such functions. A useful tool to solve this problem is the *Padé approximants* theory. Given the function $f(z)$, one can define the $[N/M]$ Padé approximant of $f(z)$ as:

$$[N/M] \equiv \frac{P_N(z)}{Q_M(z)} \equiv \frac{a_0 + a_1 z + \cdots + a_N z^N}{b_0 + b_1 z + \ldots b_M z^M}. \tag{4.20}$$

This ratio can be constructed known the first $M + N + 1$ Taylor coefficients of $f(z)$ and for simplicity we can set $b_0 = 1$. This ratio represents an approximation of $f(z)$ apart corrections $O(z^{N+1})$. To determine the coefficients of the two polynomials one has to solve two systems of equation. Starting from the equation:

$$f(z) = \frac{P_N(z)}{Q_M(z)} + O(z^{N+1}) \quad \Rightarrow \quad Q_M(z) f(z) - P_N(z) = O(z^{N+M+1}) \tag{4.21}$$

Then one can write the following system:

$$\begin{pmatrix} c_{N-M+1} & c_{N-M+2} \cdots & c_N \\ c_{N-M+2} & c_{N-M+3} \cdots & c_{N+1} \\ \vdots & \vdots & \vdots \\ c_N & c_{N+1} \cdots & c_{N+M+1} \end{pmatrix} \begin{pmatrix} b_M \\ b_{M-1} \\ \vdots \\ b_1 \end{pmatrix} = - \begin{pmatrix} c_{N+1} \\ c_{N+2} \\ \vdots \\ c_{N+M} \end{pmatrix}, \tag{4.22}$$

whereas the coefficients a_i:

$$\begin{aligned} a_0 &= c_0, \\ a1 &= c_1 + b_1 c_0, \\ &\vdots \\ a_N &= c_N + \sum_{i=1}^{min(N,M)} b_i c_{N-i} \end{aligned} \tag{4.23}$$

The importance of Padé approximant relies on the fact that it can be used as an analytic continuation of the series $f(z)$ beyond its radius of convergence.

Chapter 5

Chiral Random Matrix Theory

5.1 Gaussian Random Matrix Ensembles

Talking about *universality studies* in χRMT one usually refers to those studies whose aim is to show that the microscopic spectral density and the eigenvalue correlations near zero are stable against deformations of the matrix ensemble away from the gaussian probability distribution. Several studies have been made about these deformations, some of them can be found in Ref.[59]. The conclusion that emerges is that the microscopic spectral density and the eigenvalue correlations near zero exhibit a strong universality. However one has not to forget that outside the microscopic regime spectral properties of RMT diverges from those of real QCD.
Before defining a RM model which can reproduce the properties of the chiral phase transition of QCD let us introduce the *Gaussian Random Matrix Ensembles* (GRME) [34],[59] from which our random matrices will be extracted. The GRME can be obtained from two assumptions:

- the probability distribution of the matrices is invariant under unitary transformations;
- the matrix elements are statistically independent.

A large number of physical cases have been found to fall into a universality class of a random matrix ensemble with this two properties.
However there are a lot of cases where one has to relax one (or both) conditions. For instance in the following sections we will consider the substitution $W \to W + A$, with W a random matrix with a polynomial probability distribution $v(W)$ and A an arbitrary fixed matrix. Anyway, it was proved by Zinn-Justin [65] that even in this case the spectral correlations of the eigenvalues are given by GRME.

5.2 Introduction of the model

The first RM model for describing the spectrum of the euclidean Dirac operator was introduced by Shuryak and Verbaarschot [47]. The considerations that lead to definition of the model were the following. Consider the QCD partition function in Eq.(2.21) expressed as a sum over the sectors with defined topological charge

ν. Considering for instance the configurations with zero topological charge, it is important to notice that they could be even composed of spatially-well separated components with opposite topological charge. Such configurations give rise to the so called *almost zero* modes and play an important role in the chiral properties of the QCD partition function.
The central hypothesis of Ref.[47] is that the chiral properties of the QCD partition function are only determined by zero modes and almost zero modes of the Dirac operator. It is useful to think that such field configurations can be considered as a superposition of N_+ instantons and N_- anti-intantons (for a useful review about instantons see [45]). Let us define $N = N_+ + N_-$. Each isolated instanton has exactly one fermionic zero mode with a defined chirality. The total number of *exact* zero modes is the topological charge $\nu = N_+ - N_-$. With finite distances between the instantons, the remaining $N - \nu$ modes are no longer exact zero modes of the Dirac operator and therefore they give rise to mixing non-diagonal terms, that can be represented through a matrix W. In a instanton language, this matrix can be viewed as a sort of overlap matrix between instantons and anti-intantons. It can be proved that a that the Chiral Random Matrix model that we are going to introduce, reproduces the "zero mode" part of the QCD partition function with $N = N_+ - N_-$ zero (and almost zero) modes. Let us consider for instance the partition function at defined topological charge $\nu = N_+ - N_-$ and N_f flavors:

$$Z^{\beta}_{N_f,\nu}(m_1, \ldots, m_{N_f}) = \int DW \prod_{f=1}^{N_f} det(D + m_f) e^{-\frac{N\beta}{4} Trv(W^\dagger W)} \tag{5.1}$$

where:

$$D = \begin{pmatrix} 0 & iW \\ iW^\dagger & 0 \end{pmatrix}, \tag{5.2}$$

and W is an $N_+ \times N_-$ matrix extracted from a Gaussian Ensemble whose properties will be specified below. D is the matrix that replaces the euclidean Dirac operator of the previous sections[1]. The potential $v(\phi)$ is defined as:

$$v(\phi) = \sum_{k \geq 1} a_k \phi^k \tag{5.3}$$

It is possible [59] to check that the highest powers do not affect the microscopic spectral density of Eq.(2.24), therefore we can stop at the Gaussian term: $v(\phi) = a_1\phi \equiv \Sigma\phi$. The parameter β is called the *Dyson index* of the ensemble and it represents the number of independent real parameters that specify the matrix elements of W (see Appendix). For instance we can have:

1. real ($\beta = 1$)
2. complex ($\beta = 2$)
3. quaternion real [2] ($\beta = 4$)

[1] "Replaces" means that in the microscopic limit this matrix has the same eigenvalue density of the true euclidean Dirac operator of QCD.

[2] The *quaternions* can be defined as elements of a vector space $\mathbb{H} \in \mathbb{R}^4$. Given $\{1, i, j, k\}$ a basis of $\mathbb{H}$, each quaternion can be expressed as a linear combination $a\,1 + b\,i + c\,j + d\,k$, where $a, b, c, d \in \mathbb{R}$ and i, j, k respect the multiplication property $i^2 = j^2 = k^2 = ijk = -1$.

matrix elements. The partition function of Eq.(5.1) is invariant under the transformation:

$$W \to U^\dagger W V \tag{5.4}$$

where U is an $N_+ \times N_+$ matrix and V an $N_- \times N_-$ matrix which are orthogonal, unitary or symplectic matrices respectively for real, complex and quaternion real elements of W. For this reason the ensemble from which we take W can be called chiral Gaussian Orthogonal Ensemble (chGOE) for $\beta = 1$, chiral Gaussian Unitary ensemble (chGUE) for $\beta = 2$, chiral Gaussian Symplectic ensemble (chGSE) for $\beta = 4$.[3] It is important to say that if we want to reproduce QCD in fundamental representation with $N_c \geq 3$ the matrix elements of W have to be chosen complex and Dyson index is constrained to $\beta = 2$ [57]. An interesting analysis for all values of β is reported in Ref.[59].

This model reproduces the following properties of QCD:

- The $U_A(1)$ symmetry. As we have seen before, one of the consequences of the presence of this symmetry is that the Dirac operator eigenvalues are complex conjugated $\pm i\lambda_n$ or are zero. To see this it is sufficient to remember that the determinant of a block matrix made with matrices $A_{N_-\times N_-}$, $B_{N_+\times N_-}$, $C_{N_-\times N_+}$, $D_{N_+\times N_+}$, with A invertible, can be written as:

$$det\begin{pmatrix} A & B \\ C & D \end{pmatrix} = det(A)det(D - CA^{-1}B) \tag{5.5}$$

  Hence to find the eigenvalues:

$$\begin{aligned} det\begin{pmatrix} -\lambda\mathbb{I}_{N_-} & iW \\ iW^\dagger & -\lambda\mathbb{I}_{N_+} \end{pmatrix} &= det(-\lambda\mathbb{I}_{N_-})det(-\lambda\mathbb{I}_{N_+} - W\lambda^{-1}W^\dagger) \\ &= det(-\lambda\mathbb{I}_{N_-})det(-\lambda^{-1}\mathbb{I}_{N_+})det(\lambda^2\mathbb{I}_{N_+} + WW^\dagger) \\ &= (-)^{N_+ + N_-}\lambda^{|N_+ - N_-|}det(\lambda^2\mathbb{I}_{N_+} + WW^\dagger) = 0 \end{aligned} \tag{5.6}$$

  Since $WW^\dagger$ is hermitian it has real eigenvalues. If we call them ξ_n, from the previous equation it follows that $\lambda_n = 0$ or $\lambda_n = \pm i\sqrt{|\xi_n|}$, where $\xi_n \in \mathbb{R}$.

- The Dirac matrix has exactly $|\nu| = |N_+ - N_-|$ zero eigenvalues. This reproduces the structure of the topological sector ν of the QCD partition function. The proof follows directly from the previous point.

- The QCD *chiral symmetry* for zero quark masses of Eq.(2.15). Let us look for instance at the $\beta = 2$ case where the matrix elements of W are complex. The proof can be obtained writing the determinant as a Grassmann integral and putting $m_f = 0$ we have the terms $\bar{\Psi}^R iW^\dagger \Psi^R + \bar{\Psi}^L iW\Psi^L$ that are invariant under the transformation $\Psi^{R(L)} \to U_{R(L)}\Psi^{R(L)}$ and $\bar{\Psi}^{R(L)} \to \bar{\Psi}^{R(L)}U^{-1}_{R(L)}$, where $U_{R(L)} \in SU_{R(L)}(N_F)$. This is because W is the identity in flavor and W and U commute.
  For general β we have that the symmetry is implemented by the groups [57] $SU(2N_f)$ for $\beta = 1$, $SU(N_f) \times SU(N_f)$ for $\beta = 2$, $SU(N_f)$ for $\beta = 4$.

[3] The adjective "Gaussian" is used because we are choosing a gaussian potential for the probability distribution, otherwise in general it is omitted.

- The chiral symmetry is spontaneously broken at zero mass with breaking pattern [57] $SU(2N_f) \to Sp(2N_f)$ (the *symplectic* group[4] for $\beta = 1$, $SU(N_f) \times SU(N_f) \to SU(N_f)$ for $\beta = 2$, $SU(N_f) \to O(N_f)$ for $\beta = 4$ (the same as in QCD [54]), with a chiral condensate:

$$\Sigma = \lim_{N\to\infty} \frac{\pi\rho(0)}{N} \tag{5.7}$$

  where ρ is the eigenvalue density of D.

5.3 Chiral Random Matrix Models for the Chiral Phase transition at nonzero temperature

Here we present a RM model that tries to give a description of the chiral symmetry breaking phenomenon at nonzero temperature. This model was introduced in Ref.[31]. The original idea is to split the Dirac operator into two parts:

$$D = \gamma_0\partial_0 + R \tag{5.8}$$

If we use a chiral basis, we have a time dependence given by $exp[\pm i(2n+1)\pi T\tau)]$ (where τ is the euclidean time) and the first term gives us a sum of Matsubara frequencies $\omega_n = (2n+1)\pi T$. The simplest model for D is obtained by using the lowest Matsubara frequencies $\pm\pi T$ instead of the diagonal elements with positive (negative) Matsubara frequencies. However the first model of Ref.[31] used only one positive frequency πT, and we are going to study it. Restricting the analysis to the unitary case ($\beta = 2$) and choosing the sector with topological charge $\nu = 0$ ($N_+ = N_- = N/2$), we have a partition function:

$$Z_{\nu=0,N_f}(M) = \int DW \prod_{f=1}^{N_f} det(D + m_f) e^{-\frac{N\Sigma}{2} TrW^\dagger W} \tag{5.9}$$

where:

$$D = \begin{pmatrix} 0 & iW + iC \\ iW^\dagger + iC & 0 \end{pmatrix}, \tag{5.10}$$

and $C = \pi T \mathbb{I}_{N/2}$. More generally Wettig et al.[60] developed a detailed study of the possible C structure as a function of the temperature (see Appendix). This is inspired to a proportional-temperature-coupling between instantons and anti-intantons in the instanton liquid model. However, at this level we prefer to analyze the simplified T-dependence on the effective Matsubara frequency mentioned above.

Taking all the masses equal to m, this model predicts a second order phase transition related to the spontaneous symmetry breaking of the chiral symmetry with chiral condensate given by:

$$\left\langle \bar{\psi}\psi \right\rangle = \lim_{n\to\infty} \frac{1}{NN_f} \partial_m log Z \tag{5.11}$$

[4] A matrix S belongs to the symmetric group $Sp(2n) \Leftrightarrow S^T \Omega S$, where $\Omega = \begin{pmatrix} 0 & 1_n \\ -1_n & 0 \end{pmatrix}$.

If we take the chiral limit $m \to 0$ it can be shown that the behavior as a function of the temperature is:

$$\left\langle \bar{\psi}\psi \right\rangle = \Sigma\sqrt{1-(\Sigma\pi T)^2} \tag{5.12}$$

Therefore the critical temperature given by $T_c = 1/\pi\Sigma$. We have to stress that this model leads to a second order transition governed by *mean field exponents*, different from QCD with nontrivial critical exponents. For instance Ref.[31] computes near the transition two critical exponents $\beta \simeq 1/2$ and $\delta \simeq 3$, correspondent to the mean field values.

It is interesting to remark that the modification of the random matrix of Eq.(5.10) can be considered as a modification of the random matrix ensemble that does not preserve the unitary invariance, that is the replacement $W \to W + A$ written in the first section. It can be shown [61] that with the choice $A = \pi T$, the temperature parameter drastically modifies the spectrum of the new Dirac operator, but leaving untouched the microscopic spectral density which leads the phase transition.

5.4 Chiral Random Matrix Model at Nonzero Chemical Potential

To introduce a RM model for QCD at nonzero chemical potential, we remember that the QCD partition fuction at nonzero temperature T and quark chemical potential μ is:

$$Z(M,\mu,T) = Tr\, e^{\frac{H_{QCD}-\mu N}{T}} = \sum_{\alpha} e^{\frac{E_\alpha - \mu N_\alpha}{T}} \tag{5.13}$$

where H_{QCD} is the hamiltonian of QCD with eigenvalues E_α and N_α is the quark number operator. This partition function, for a mass matrix M, can be written as:

$$Z(m,\mu) = \langle \det(\gamma D + M + i\mu\gamma_0)\rangle_{S_{QCD}} \tag{5.14}$$

One can notice that the quark chemical potential μ appears in the Lagrangian in the form $\bar{\psi}(\mu\gamma_0)\psi$ and therefore the Dirac operator is modified in the form:

$$\partial_0 \to \partial_0 + \mu \tag{5.15}$$

This substitution deletes the anti-hermiticity of the Dirac operator. As reported in Ref.[61], many standard random matrix methods rely on convergence properties based on the (anti)hermiticity of the random matrix, hence direct application of most methods is not possible. However, there are many solutions to this problem, such as the *hermitization method* [18] of the Dirac operator, or the *replica trick method* [51].

A RM model of QCD at zero temperature and nonzero chemical potential can be obtained replacing the Dirac operator with:

$$D \to \mu\gamma_0 + R \tag{5.16}$$

where R is a matrix extracted from a chiral random ensemble. The partition function is the same as (5.9), but this time we have:

$$D = \begin{pmatrix} 0 & iW+\mu \\ iW^\dagger + \mu & 0 \end{pmatrix}. \tag{5.17}$$

A detailed study of this model is reported in Ref.[51],[29]. If we use such units where $\Sigma = 1$, a particularly simple form of the partition function is obtained for $N_f = 1$, which gives us:

$$Z(\mu) = \int d\sigma d\sigma^* [(\sigma + m)(\sigma^* + m) - \mu^2]^N e^{-N|\sigma|^2} \tag{5.18}$$

The integral can be evaluated in the limit $N \to \infty$ through the saddle point approximation, that gives us an order parameter of the transition near $m = 0$ equal to:

$$\sigma_0 = \begin{cases} 0 & for \quad \mu > \mu_c \\ \sqrt{1+\mu^2} & for \quad \mu < \mu_c \end{cases} \tag{5.19}$$

where $\mu_c \approx 0.53$[5]. It is interesting to study the analyticity properties of the partition function in the complex μ and m planes. This analysis will be done more in detail in the next chapter for Stephanov's model at nonzero T and μ. However it gives a confirmation that this model exhibits a first order transition at $\mu = \mu_c$ at $m = 0$ with the order parameter σ_0 of Eq.(5.19).

[5]In truth the critical μ can be obtained as a solution of the equation $Re[\mu^2 + log(\mu^2)] = -1$, therefore there is another solution that is $\mu_c = i$. This corresponds to the choice $\mu = i\pi T$ of the nonzero temperature model which gives us the known critical temperature at $\pi T = 1$ ($\Sigma = 1$)

Chapter 6

Stephanov's Random Matrix Model of QCD

6.1 Introduction to the model

We now introduce one of the first RM models able to reproduce some important features of the QCD phase structure in the (T, μ) plane. Such a model was theorized by Halasz, Jackson, Schrock, Stephanov and Verbaarschot in Ref.[30]. It represents an attempt to join the two different models of the previous sections, the first with $T \neq 0$, $\mu = 0$ [29],[51] and the second with $T = 0$, $\mu \neq 0$ [31],[60]. Since this model was consecutively studied in detail by Stephanov [49], from now on we will refer to this model as to *Stephanov's model*.
In the following sections we will introduce the main features of the model as in the original article. Then we will retrace and redemonstrate some of the intuitions of Stephanov. In particular we will reproduce the behavior of the partition function zeros in the μ plane (especially looking at the thermodynamic limit) and we will derive the nearest singularities of the free energy in such plane through a branching point analysis. As a next step we will extend the work of Stephanov analyzing the temperature and "volume" dependence of the Taylor coefficients of the free energy near $\mu = 0$ and we will extrapolate the radius of convergence through different methods. At the end we will extend the original model including all the Matsubara modes and we will analyze the properties at imaginary chemical potential, trying to modify the model in order to reproduce the Roberge-Weiss transition.

We start considering the SU(3) QCD partition function of Eq.(2.7) in presence of a baryon chemical potential μ_B without electroweak interactions and *two quarks*. As we will see later the number of flavors in the RM model is an irrelevant parameter, since for any N_f the model exhibits the same properties. However, we set $N_f = 2$ because the phase structure reproduced by this model is similar only to the one supposed for QCD with two flavors. For simplicity we can consider the sector with topological charge $\nu = 0$ (we will give the motivation for this assumption later) and from now on use the notation $Z_{\nu=0}(M, T, \mu_B) \equiv Z(M, T, \mu_B)$, where M is the mass matrix. Hence we have:

$$Z(M, T, \mu_B) = \int DA\bar{\psi}D\psi e^{-S_E} \tag{6.1}$$

where S_E is the Euclidean action:

$$S_E = \int_0^{1/T} dx_0 \int d^3x \left[\frac{1}{2g^2} TrF_{\mu\nu}F^{\mu\nu} - \sum_{f=1}^{N_f} \bar{\psi}_f \left(\not{\partial} + \not{A} + m_f + \frac{\mu_B}{N_c}\gamma_0 \right) \psi_f \right], \quad (6.2)$$

here $N_f = 2$ is the number of flavors, $N_c = 3$ is the number of colors. We consider the case with all equal quark masses $m_f = m$. As we know integrating out the fermionic degrees of freedom we obtain:

$$Z = \int DA \exp\left[-\frac{1}{2g^2} TrF_{\mu\nu}F^{\mu\nu} \right] det^{N_f} \left[\not{D} + m + \frac{\mu_B}{N_c}\gamma_0 \right] \quad (6.3)$$

where $\not{D} = \not{\partial} + \not{A}$ is the covariant derivative. From now on we will use the simplified notation $\mu_B \equiv \mu$.

6.1.1 Random Matrix partition function

As told before we introduce in this section the RM model of QCD of Ref.s[30], [49]. To reproduce the nonzero temperature and chemical potential QCD partition function of Eq.(6.3), looking at the RM models of the previous sections it is rather intuitive to require a partition function of the form:

$$Z_{RM} = \int dX exp\left(-\frac{N}{\sigma^2} TrXX^\dagger \right) det^{N_f}(D + m). \quad (6.4)$$

Here D is a $2N \times 2N$ matrix which approximates the Dirac operator $\not{D} + (\mu/N_c)\gamma_0$

$$D = \begin{pmatrix} 0 & iX + iC \\ iX^\dagger + iC & 0 \end{pmatrix}, \quad (6.5)$$

Because the operator D can assume only complex values, X is a complex $N \times N$ random matrix extracted from the Gaussian Unitary Ensemble ($\beta = 2$). Here we are replacing the dimension N_+ and N_- of the random matrix W of the previous sections with $m = n = N$. The motivation is that we know from QCD [59] that $\nu = |N_+ - N_-| \sim \sqrt{N_+ + N_-}$ therefore if $N_+ + N_-$ is big enough we can approximate $\nu \sim 0$. This is the reason why we consider only the sector with zero topological charge. X has a probability distribution:

$$P(X)dX = Kexp\left(-\frac{N}{\sigma^2} TrXX^\dagger \right) det^{N_f}(D + m)dX \quad (6.6)$$

where K is the normalization constant, σ^2 is the variance (we recall $\Sigma = 1/\sigma^2$, from Eq.(5.10)). C is a deterministic matrix which includes the temperature and chemical potential dependence of the model. The form of C takes into account the deterministic matrices of Sec.5.3 and 5.4 with linear dependence in the temperature and chemical potential. The only difference here is the use of *two* effective Matsubara $\pm\pi T$ frequencies instead of only the positive coupling πT If we call the proportionality coefficients a and b, we can define C as:

$$\begin{aligned} C_k &= a\pi T - ib\mu/N_c \qquad \text{if k=1 ... N/2,} \\ &= -a\pi T - ib\mu/N_c \qquad \text{if k=N/2+1 ... N.} \end{aligned} \quad (6.7)$$

We chose to use a coupling $\sim +\pi T$ for the lowest half of the X eigenvalues and $\sim -\pi T$ for the highest half. This linear ansatz is really naive but leads to interesting results, as we are going to show. The parameters a, b, σ of the model are determined as written in Ref.[30]. The chiral condensate of the model is calculated as:

$$\left\langle \bar{\psi}\psi \right\rangle = \frac{1}{N_f V_4} \frac{\partial \, log Z_{RM}}{\partial m} \tag{6.8}$$

From current algebra we know that $\left\langle \bar{\psi}\psi \right\rangle |_{T=\mu=m=0} \approx 2fm^{-3}$. Using Eq.(6.4) we have that:

$$\left\langle \bar{\psi}\psi \right\rangle_{T=\mu=m=0} = \frac{N}{2V_4\sigma} \approx \frac{n_{inst}}{2\sigma}, \tag{6.9}$$

where $n_{inst} = N/V_4 \approx 0.5fm^{-3}$ is the average density of instantons (or anti-instantons) in our instanton model. Thus we have that σ is fixed to $\sigma \approx 0.5fm^{-1} \approx 100MeV$. It can be seen that the parameters a and b depend on the values of T_c, the critical temperature of the second order line at $m = \mu = 0$ and μ_c, the critical chemical potential of the first order line at $m = T = 0$. In particular, from $T_c \approx 160MeV$ it follows that $a \approx 0.2$. The parameter b, which connects the model with the density scale, is fixed by $\mu_c \approx 1200MeV$ to $b \approx 0.13$.
It is useful to use σ as a unit of mass of the model and absorb the terms πa and b/N_c in the definitions of T and μ. This is equivalent to measuring T in units of $T_c = \sigma/\pi a \approx 160MeV$, μ in units of $\sigma/bN_c \approx 2.27GeV$ and m in units of $\sigma \approx 100MeV$.

6.1.2 Thermodynamic limit and finite size case

In χRMT, N is interpreted as the volume of space-time. In a certain sense this corresponds to use units where $N/V = 1$ so that σ^2 can be written as $\sigma^2 N/V$ and the exponential of Eq.(6.4) becomes correctly dimensionless. It is now interesting to compare the model at finite matrix size N with the one obtained in the so-called *thermodynamic limit*, i.e. $N \to \infty$. One of the advantages of this RM model is that both the thermodynamic limit and the finite size case are well manageable and it is quite easy (for instance using programs like *Wolfram Mathematica*) to study the finite size dependence and the convergence of the results for high values of N.

The *thermodynamic limit* $N \to \infty$ of the partition function can be obtained through the following mathematical steps:

- write the determinant in Eq.(6.4) as a Grassmann integral;
- perform the gaussian integration over X;
- use the Hubbard-Stratonovich transformation to eliminate the fermionic terms through the insertion of auxiliary $N_f \times N_f$ matrices Φ.

The whole procedure is clearly explained in the Appendix. The final form of the

thermodynamic partition function results to be:

$$\begin{aligned} Z_{RM} &= \int D\Phi \exp\left[-NTr(\Phi\Phi^\dagger)\right] det^{N/2} \begin{pmatrix} \Phi+m & \mu+iT \\ \mu+iT & \Phi^\dagger+m \end{pmatrix} det^{N/2} \begin{pmatrix} \Phi+m & \mu-iT \\ \mu-iT & \Phi^\dagger+m \end{pmatrix} \\ &= \int D\Phi \exp\left[-N\Omega(\Phi)\right] \end{aligned} \tag{6.10}$$

where

$$\begin{aligned} \Omega(\Phi) =& Tr\Bigg[\Phi\Phi^\dagger - \frac{1}{2}\ln\{[(\Phi+m)(\Phi^\dagger+m) \\ & - (\mu+iT)^2][(\Phi+m)(\Phi^\dagger+m) - (\mu-iT)^2]\}\Bigg] \end{aligned} \tag{6.11}$$

and Φ are $N_f \times N_f$ complex matrices, so that the integration is performed over $2N_f^2$ real variables. The $N \to \infty$ limit is reached through the *saddle point* approximation, that means:

$$\lim_{N\to\infty} \frac{1}{N} \log Z_{RM} = -min_{\{\Phi\}}\Omega(\Phi) \tag{6.12}$$

The function $\Omega(\Phi)$ can be considered as an effective potential that controls the phase transition of the model. Apart from a multiplicative T factor, it can be considered as the density of free energy. For real m it is expected for the saddle point to be reached taking $\Phi \equiv \phi \mathbb{I}_{N_f \times N_f}$, where $\phi \in \mathbb{R}$, so that Eq.(6.11) can be written as:

$$\Omega(\phi) = N_f\left[\phi^2 - \frac{1}{2}\ln[(\phi+m)^2 - (\mu+iT)^2][(\phi+m)^2 - (\mu-iT)^2]\right] \tag{6.13}$$

Eqn.(6.13) has to be minimized as a function of the real parameter ϕ to obtain the correct expression of the partition function in the thermodynamic limit.

To write the expression of the partition function for the *finite size* case, it is sufficient to integrate Eq.(6.10) in the "flavor" variables and then manipulate the result using some combinatorial identities. Apart from a constant factor, we obtain[49]:

$$\begin{aligned} Z_{RM}^{(N)} = & \sum_{k_1,k_2=0}^{N/2} \binom{N/2}{k_1}\binom{N/2}{k_2}(N-k_1-k_2)!\,{}_1F_1(k_1+k_2-N;1;-m^2N) \\ & \times [-(\mu+iT)^2N]^{k_1}[-(\mu-iT)^2N]^{k_2}. \end{aligned} \tag{6.14}$$

Here ${}_1F_1(a;b;c)$ is the Kummer confluent hypergeometric function.[1] Consequently, the effective potential of the finite size case can be defined as:

$$\Omega^{(N)} = -\frac{1}{N}\log Z_{RM}^{(N)}, \tag{6.15}$$

and in the thermodynamic limit it becomes equal to Eq.(6.12). The partition function of Eq.(6.14) represents a finite polynomial in the variables μ and m, so that it is very simple to find numerically the zeros in the complex μ and m planes. This will be better explained in the next section.

[1] In general ${}_1F_1(a,b,c) = \sum_{n=0}^{\infty} \frac{a^{(n)}}{b^{(n)}}\frac{c^n}{n!}$, where $a^{(n)} = a(a+1)\dots(a+n-1)$ is the rising factorial. For $b=1$, as happens in our case, the function reduces to the Laguerre polynomial and the sum turns out to be finite ${}_1F_1(a;1;c) = L_a(c) = e^c L_{|a|-1}(-c) = e^c \sum_{k=0}^{|a|-1}\binom{|a-1|}{k}\frac{1}{k!}c^k$, for $a<0$

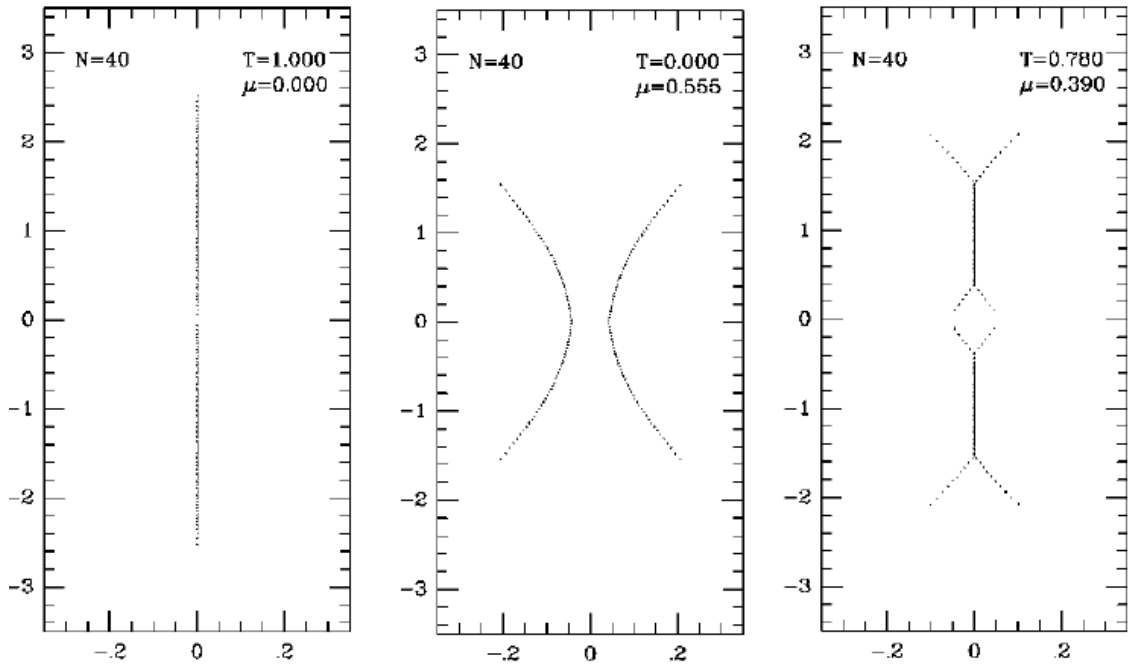

Figure 6.1: Complex mass plane zeros of the finite N partition function for different values of T and μ. Figure taken from Ref.[30].

6.1.3 Complex zeros of the partition function

We now want to study the phase transition properties of this RM model of QCD looking at the complex singularities of the effective potential defined for the finite size case in Eq.(6.11) and in the thermodynamic limit in Eq.(6.15).
As reported in Sec.3.1 and Sec.3.2.12, Yang and Lee [63],[64] showed that non-analyticities appear in the thermodynamic limit when the zeros of the partition function pinch the real axis of the relevant parameters (see Fig.3.1). This can cause a discontinuity of the order parameter of the phase transition.
In the previous section we told that the finite N partition function is a polynomial in the mass and chemical potential. Therefore we can think at first to perform the analysis in the complex *mass* plane. The plot of Fig.6.1 taken from Ref.[30] shows the zeros of the finite N partition function Eq.(6.14) in the complex m plane as with T and μ as external parameters. When the "zeros line" pinches the real axis near $m = 0$ in the thermodynamic limit this corresponds to a non-analytic behavior of the free energy and to a discontinuity of the order parameter $\left\langle \bar{\psi}\psi \right\rangle$.

More interesting for our purposes is to concentrate on the complex *chemical potential* singularities.
In Sec.3.2.12, we said that the singularities are given by the μ-zeros of the finite-size partition function (6.14). In the thermodynamic limit the zeros coalesce into a $1D$ line (the *Stokes boundary*) whose endpoints are called the *branching points*. To obtain the branching points of the system we have to impose for the effective potential $\Omega(\phi, \mu)$ (at fixed T and μ) to have the first and the second derivative in ϕ equal to

zero. Therefore it is necessary to solve the following system:

$$\frac{\partial\Omega(\phi,\mu)}{\partial\phi}=0, \qquad \frac{\partial^2\Omega(\phi,\mu)}{(\partial\phi)^2}=0 \tag{6.16}$$

for unknown ϕ and μ. The second equation gives us the particular μ at which two saddle point solutions ϕ_1 and ϕ_2 merge into one. We will see soon how two of the real branching point solutions correspond with the spinodal lines of the first order chiral transition. The Stokes boundaries are calculated imposing that the real part of thermodynamic effective potential Ω (i.e. the *electrostatic potential* in the analogy of Sec.3.2.12) is continuous for such ϕ_1 and ϕ_2.

$$\left.\frac{\partial\Omega(\phi,\mu)}{\partial\phi}\right|_{\phi=\phi_1=\phi_2}=0, \qquad Re\Omega(\phi_1)=Re\Omega(\phi_2) \tag{6.17}$$

In Fig.6.2 we computed the zeros of the N=120 partition function (6.14) in the complex μ^2 plane as a function of the temperature for the $m=0$ and the $m=0.07$ (7 MeV) cases. We know that in the massless case the Stokes boundaries (not shown here) for all the temperatures lower than T_c reach the real μ^2 axis. Instead for nonzero mass the branching points are complex for temperatures higher than the critical one (look for instance at $T=T_c$ for $m=0.07$). The first real branching point appears at $T=T_E$: this signal represents (as we will see below) a useful way to detect the critical point in the (T,μ) phase diagram.
Another interesting picture is obtained plotting the distance from the origin of the branching points at various temperatures (Fig.6.3). As we will see in the following section, these points represent the *nearest singularities* that limit the Taylor expansion in μ of the effective potential. They are purely real (and therefore physical singularities) only for $T\leq T_E$, where the line depicts one of the two spinodal lines of the first order transition. The minimum distance from the origin is reached at a temperature $T_{min}\sim 1.05\,T_c$, where the singularity is complex.

6.1.4 Chiral condensate and phase diagram

In this section we are going to reproduce the phase diagram of this RM model of QCD.
To depict the phase diagram one has at first to minimize the effective potential (6.11). Before doing this, let us analyze for a moment how to obtain the *chiral condensate* of the model, that in the massless case is an order parameter for the phase transition. We previously defined the chiral condensate as:

$$\left\langle\bar{\psi}\psi\right\rangle=\frac{1}{VN_f}\frac{\partial\, log Z_{RM}}{\partial m} \tag{6.18}$$

Given the form of Eq.(6.10), after minimizing the potential one finds that:

$$\left\langle\bar{\psi}\psi\right\rangle=\frac{N}{VN_f}2Re\,Tr\left\langle\Phi_0\right\rangle, \tag{6.19}$$

where Φ_0 is the minimizing matrix. If the saddle point equation admits solution $\Phi_0=\phi_0\mathbb{I}_{N_f}$, hence we have that $\left\langle\bar{\psi}\psi\right\rangle\propto\phi_0$. So, ϕ_0 can be thought as the order

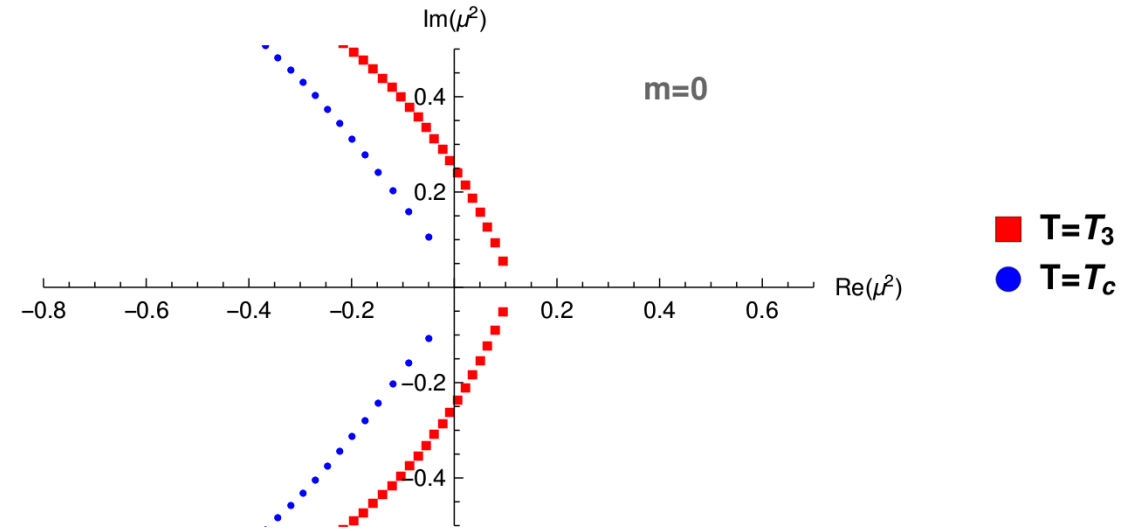

(a) *m=0*

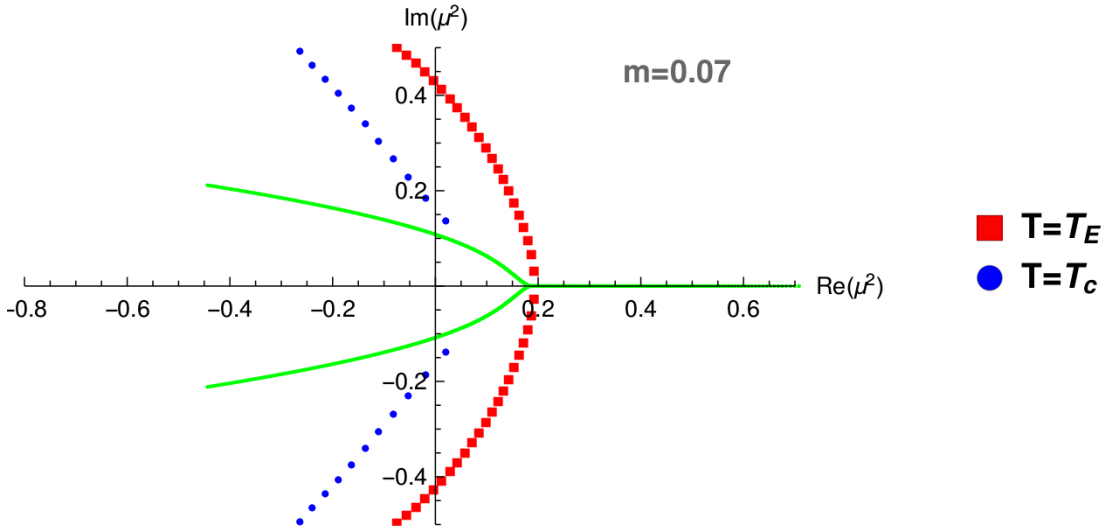

(b) *m=0.07*

Figure 6.2: Computed zeros of the N=120 partition function in the complex μ^2 plane at $m = 0$ for $T = T_c$ and $T = T_3$ (temperature of the tricritical point at m=0) (Fig.(a)) and at $m = 0.07$ for $T = T_c$ and $T = T_E$ (Fig. (b)). The plot of the Stokes boundaries is omitted. For $m = 0$, it can be shown that for all $T < T_c$ the Stokes boundaries end touching the real axis, hence the "branching point line" coincides with the $Re(\mu^2)$ axis. For $m = 0.07$, the branching point line is represented in green as a function of the temperature. Below T_E the singularities are real and define one of the two spinodal lines.

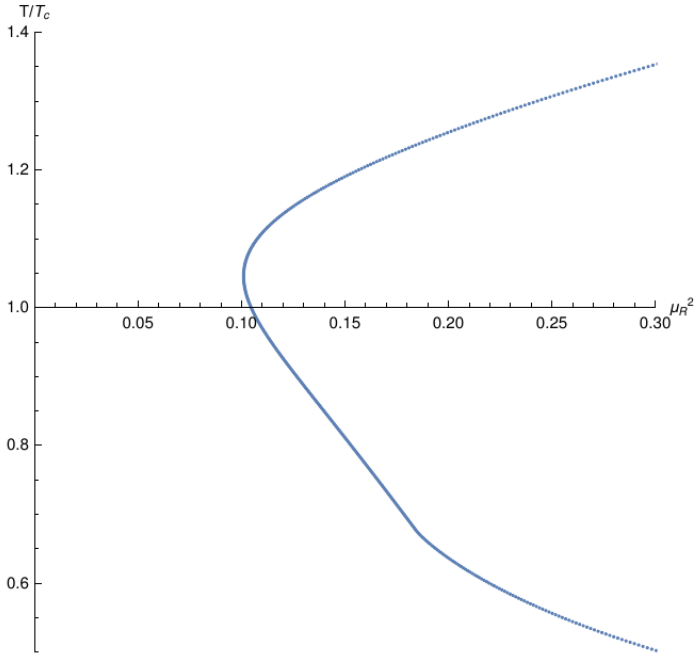

Figure 6.3: Plot of the nearest singularity as function of the temperature, for $m = 0.07$. The minimum distance is reached for a temperature T^* just above T_c. At $T = T_E \approx 0.67$ the line have a non-analyticity (to know more see Ref. [49]) and below T_E the line is one of the two *spinodal lines*.

parameter of the chiral transition in the massless case. Hence a first way to reproduce the phase diagram is to plot the behavior of ϕ_0 as a function of T and μ. We have computed and plotted this behavior in Fig.6.4. One can clearly visualize the first order line along the sharp discontinuity, whereas the second order line is where ϕ_0 smoothly approaches zero.

Let us now derive the phase diagram analyzing the effective potential Ω. It shares similar features with the Landau-Ginzburg one of Sec.3.2.11 in the following sense: it has not a power law but its minimization gives us a fifth degree equation in the ϕ variable, exactly what happens in the $\sim \phi^6$ potential. Therefore some important properties of the phase diagram can still be obtained through an analogous analysis of the coefficients.

Case $m = 0$. The $m = 0$ case is simplified, because the minimization gives us a fourth degree equation, exactly solvable in an analytical way:

$$\phi^4 - 2\left(\mu^2 - T^2 - \frac{1}{2}\right)\phi^2 + (\mu^2 + T^2)^2 + \mu^2 - T^2 = 0 \tag{6.20}$$

Following the analogy with the Landau-Ginzburg potential of Sec.3.2.11 to extract the second order line it is sufficient to impose that two of the four roots of (6.20) become zero (we set $a = 0$ in Eq.(3.28) and we have a quartic potential near the origin $\Omega \sim b(\mu, T)\phi^4$):

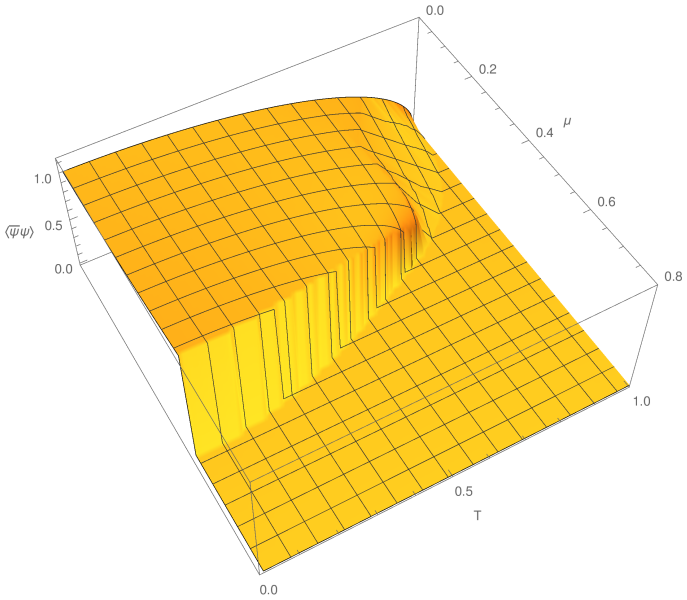

Figure 6.4: Chiral condensate of the RM model as a function of T and μ at $m = 0$. It is clear the sharp discontinuity along the first order line and the smooth approach to zero along the second order line.

$$(\mu^2 + T^2)^2 + \mu^2 - T^2 = 0 \tag{6.21}$$

Furthermore the ending point of this line is easily obtained by putting the other two roots equal to zero ($a = b = 0$, $\Omega \sim c(T, \mu)\phi^6$).

$$\mu^2 - T^2 - \frac{1}{2} = 0, \tag{6.22}$$

which gives us a triple point near $T_3 = 1/2\sqrt{\sqrt{2}+1} \approx 0.776$ and $\mu_3 = 1/2\sqrt{\sqrt{2}-1} \approx 0.332$. The first order (*triple*) line of the model is simply deduced requiring that the depth of the two minima far from the origin is equal to the one at $\phi = 0$. The obtained equation for the triple line is:

$$\begin{aligned} \mu^2 - T^2 + \frac{1}{2} + \frac{1}{2}\sqrt{1 - 16\mu^2 T^2} - \frac{1}{2}\log\Big(\frac{1 + \sqrt{1 - 16\mu^2 T^2}}{2}\Big) \\ + \log(\mu^2 + T^2) = 0, \end{aligned} \tag{6.23}$$

and the phase diagram of the massless case is shown in Fig.6.5.

Case $m \neq 0$. For nonzero mass the minimization of (6.11) is now given by a fifth order polynomial, whose zeros in general are not analytically findable. As told before in this case the chiral symmetry is explicitly broken, we no more have an order parameter and the second order line is replaced by an *analytic crossover*.
To obtain the first order line a useful strategy can be to fix the temperature (starting from $T = 0$) and choose the suitable μ so that the potential has the two lowest

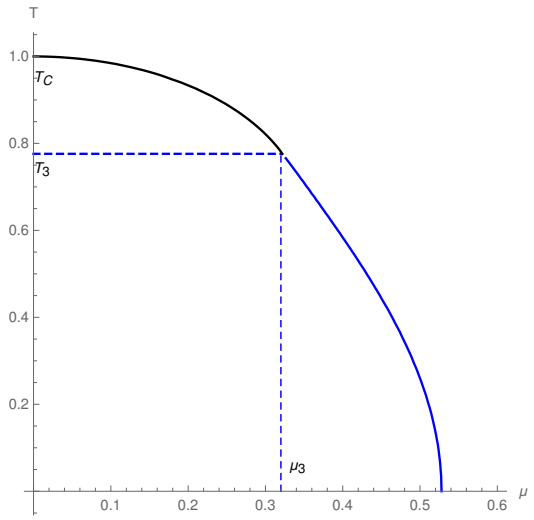

Figure 6.5: Phase diagram of the RM model of QCD at $m = 0$. In blue the first order line and in black the second order one. The tricritical point (T_3, μ_3) is where such two lines join.

minima of the same depth. Of course this approach stops working when we reach the critical endpoint: we no more have a coexistence of two different phases and only one absolute minimum of the effective potential dominates. Using this method and varying the mass inside a proper range $m \in [0, 1.2]$ (that is $[0, 120]$ MeV) the result is the one of Fig.6.6. Varying the mass with constant steps, the first order lines seem to be almost equi-spaced in the (T, μ) plane and the critical temperature $T_E^{(m)}$ slightly increases with the mass.

Spinodal lines

The spinodal lines delimit a region around the first order line where the minimum at $\phi = 0$ (that is the chirally restored phase) can exist as a metastable state. Inside this region the effective potential has three (local) minima and the crossing of the spinodal line towards the first order line is characterized by the appearance of a new local minimum. This can be seen for instance in the plots of the effective potential near the two spinodal points at $T = 0.4$ in Fig.6.7.

The spinodal lines have their origin in the phase diagram at the (tri)critical point. It has been demonstrated (Ref.[44]) that along the isothermal[2] spinodal lines of the first order chiral phase transition the baryon number susceptibility diverges, while it is finite along the crossover and the first order phase boundaries (only in the hypothesis that such transition happens in equilibrium). Consequently, singular fluctuations of baryon number varying the collision energy in heavy ion collisions have been proposed as possible signals for the QCD critical endpoint [44]. Knowing this, it is plausible to expects for the free energy to have a singular behavior near the spinodal lines (as we will see Taylor expanding the effective potential Ω in the baryon

[2]In general the *isothermal* and the *isoentropic* spinodal lines are determined by the conditions $(\partial P/\partial V)|_T = 0$, $(\partial P/\partial V)|_S = 0$, where P is the thermodynamic pressure, V is the volume and S is the entropy of the system.

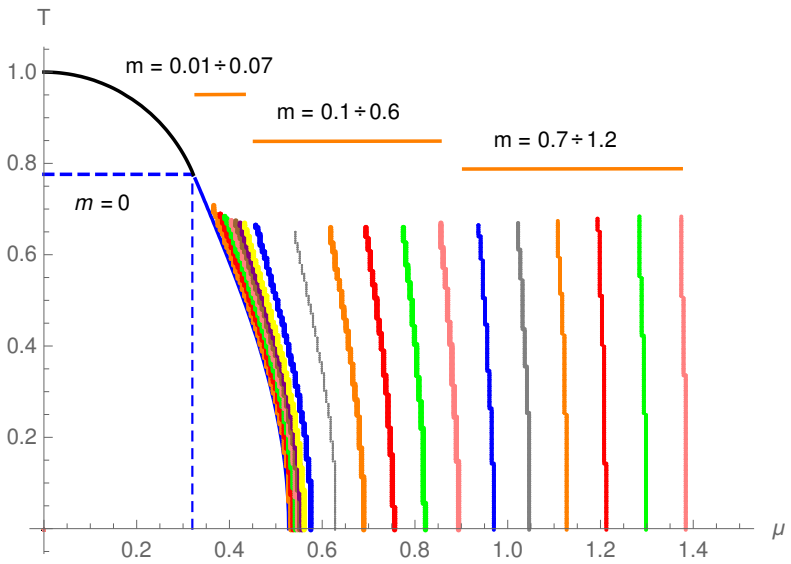

Figure 6.6: Phase diagram of the RM model of QCD for increasing masses.

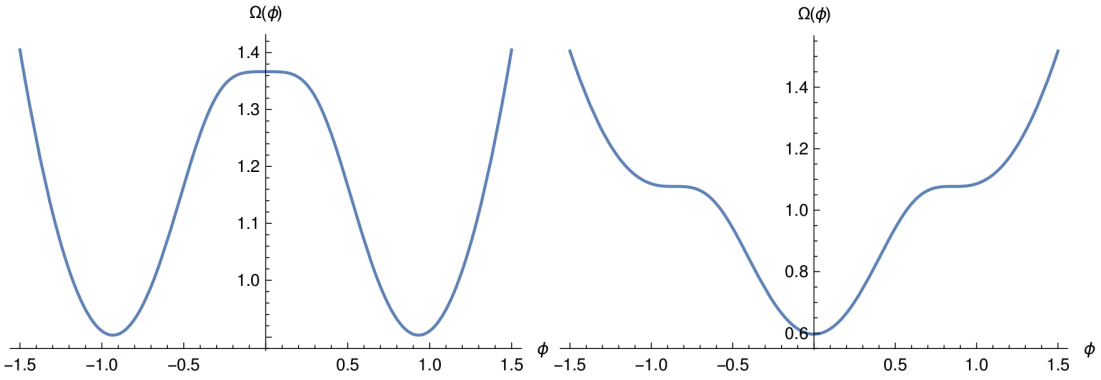

Figure 6.7: Effective potential $\Omega(\phi)$ in the massless case at $T = 0.4$ for two points lying on the spinodal lines. The left figure refers to the "left" spinodal line (or *supercooling* line), where a new minimum at $\phi = 0$ appears. The right figure refers to the "right" spinodal line (or *superheating* line), where two new symmetric minima at $\phi \neq 0$ appear.

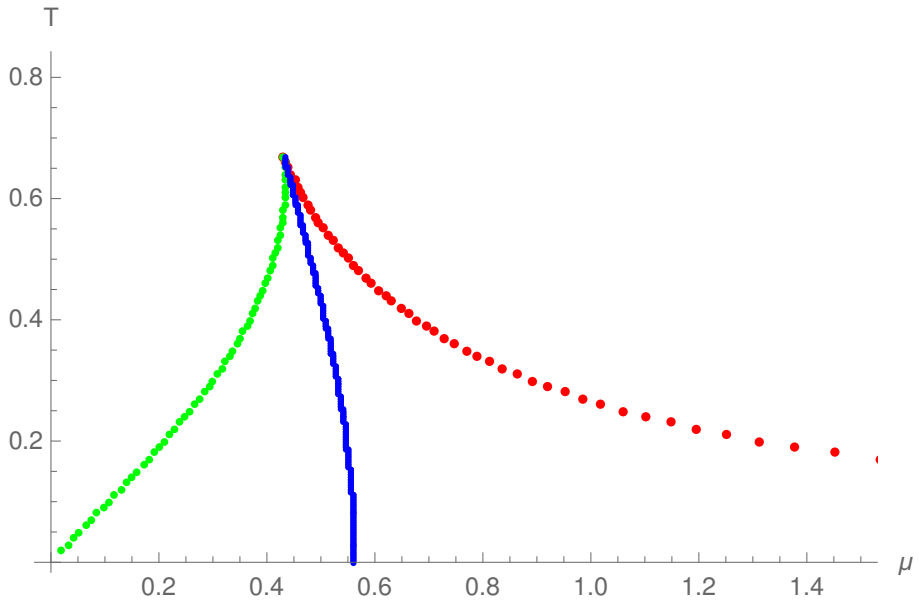

Figure 6.8: Spinodal lines (the red and the green lines) for the first order line (blue line) at $m = 0.07$.

chemical potential μ). In the $m = 0$ case, the two spinodal lines can be seen as the continuation of the second order line that branches at the tricritical point. The line that continues inside the broken symmetry region can be labelled as the *supercooling* spinodal line, whereas the one that continues outside as the *superheating* one [30][3]. To draw them a possibility is to choose for each temperature the correct real μ singularities from the branching point system of Eq.(6.16). The $m = 0.07$ spinodal lines, together with the first order line, are shown in Fig.6.8. We can notice that the superheating spinodal line is obtained from the plot of the nearest singularities of the Taylor expansion of Ω in μ (Fig.6.3), taking only the points with $T < T_E$.

One could ask why the nearest singularity that limits the Taylor expansion is represented by the superheating line and not by the supercooling one. As can be seen in Fig.6.7 for $m = 0$, Taylor expanding from $\mu = 0$ at fixed temperature ($T < T_E$) we are moving in the (T, μ) diagram inside the broken symmetry region, and crossing the supercooling line a new "restored" local minimum appears at $\phi = 0$. However this does not affect the expansion because we are still inside the broken region. When we arrive at the *superheating* spinodal line, we are definitively crossing the point where the last "broken" local minima disappears, and this has effects on the Taylor expansion of the free energy.

[3]Usually one refers to *supercooling* in analogy with the first order phase transition of a liquid, when one lowers the temperature of the liquid below the freezing point without it becoming a solid. Similarly, one intends *superheating* when one increases the temperature of the liquid higher than its boiling point without it boiling.

6.1.5 Taylor series of the free energy

In this section we study more deeply some techniques to detect the singularities of the free energy in the (T, μ) plane. We are in particular interested in those methods that we can used even in LQCD, like the Taylor expansion analysis. For instance, to have information about the position of the critical endpoint of the first order line in the (T, μ) plane of Fig. 6.6 we can consider a Taylor expansion of the effective potential (that is the free energy apart a T factor) in the baryon chemical potential near $\mu = 0$. This expansion should have temperature-dependent finite radius of convergence below the critical temperature T_E, whose amplitude should be bounded - for each temperature - by the distance to the superheating spinodal line. For temperatures higher that T_E the nearest μ singularity assumes complex values, hence it is not physical. Therefore given the effective potential (6.11), holding the temperature T at and the mass m at fixed values, we proceed in defining the Taylor series in the baryon chemical potential near $\mu = 0$, that is:

$$\Omega(m, T, \mu) = \sum_{n=0}^{\infty} \frac{1}{n!} \frac{\partial^n \Omega(m, T, \mu)}{\partial \mu^n}\bigg|_{\mu=0} \mu^n \equiv \sum_{n=0}^{\infty} c_n(m, T)\mu^n \tag{6.24}$$

Since Ω is *even* in the chemical potential (look at Eq. (6.11)), it follows that only the even coefficients c_{2k} ($k \in \mathbb{N}$) are nonzero. An important thing to appreciate about our RM model is that this expansion can be performed very easily both in the finite size and in the thermodynamic case. This will be really useful to analyze finite size effects and the convergence of the coefficients and the estimated radii as $N \to \infty$.

6.2 Results

All the computational analysis of this section is realized with the program Wolfram Mathematica 10.3. There is a practical difference in the derivation of the coefficients between the thermodynamic and the finite size case. In the first we have proceeded by solving numerically the minimization of the potential (6.11) (finding numerically a solution of a fifth-degree equation) and then expanding the minimized $\Omega_{min}(m, T, \mu)$ in the μ variable. The estimation of the highest "thermodynamic" coefficients has to deal with rounding errors that lead to very noisy estimates. This causes the presence of a limited number of available coefficients to determine the radius of convergence. Instead the expansion of the finite size potential (6.15) concerns a finite order polynomial and the program allows to reach higher order coefficients with a great precision.

6.2.1 Taylor coefficients

Fixing the value of the mass on $m = 0.07$ (7Mev) [4] we show in Fig.6.9 the computed coefficients for the finite N=120 case as functions of the temperature. As we told above, the even-dependence on μ of the potential makes nonzero only the even coefficients.

[4] We want to follow the Ref.[49] that uses this value of the mass to compare its results with ours.

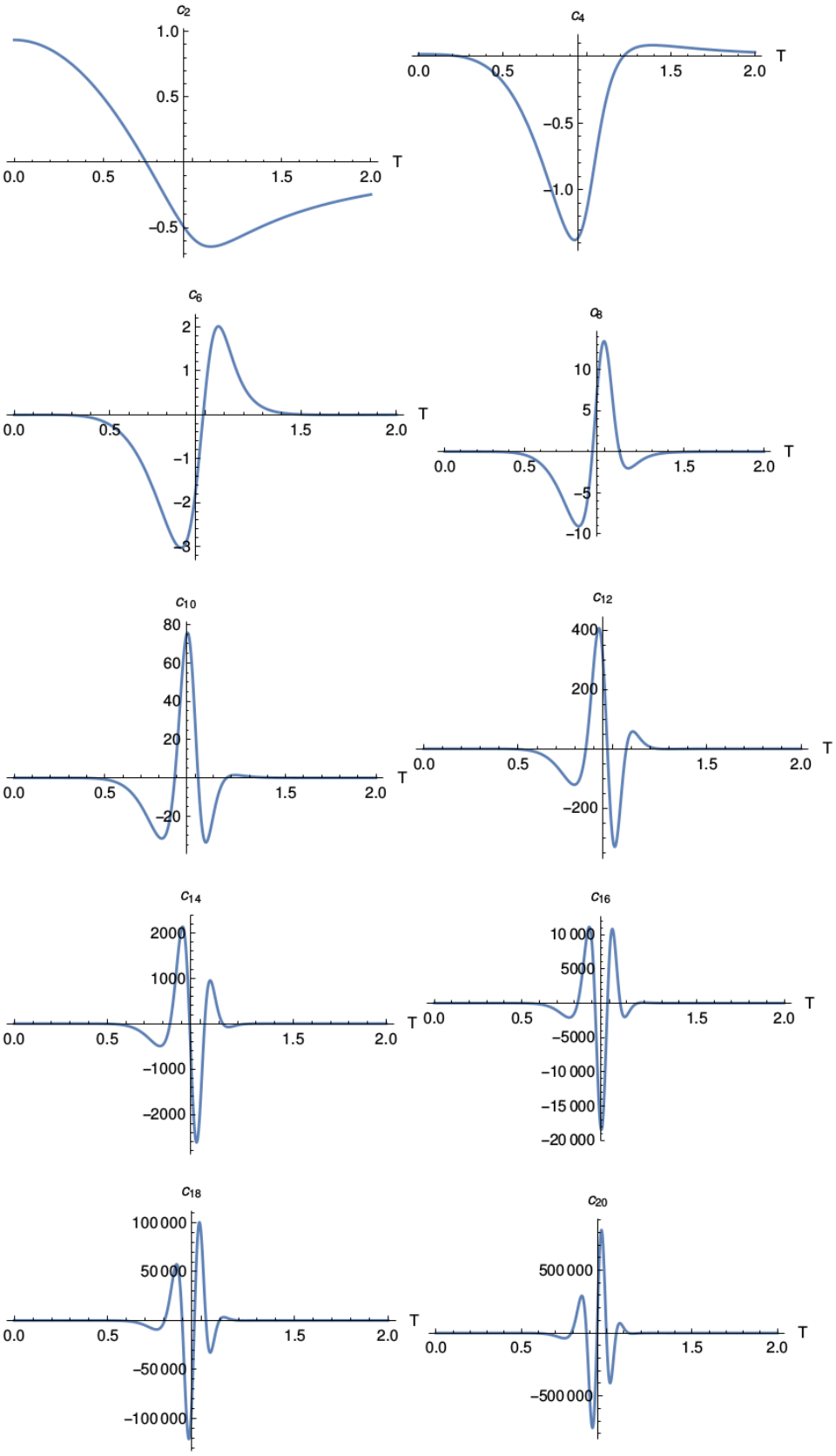

Figure 6.9: Taylor coefficients for $m = 0.07$ and $N = 120$ as function of the temperature. The figures are centered around $T^* = 0.95$.

We can notice that the oscillations in temperature of the coefficients are stronger in the range $T \sim [0.5 \div 1.5]$. The figure is centered around a temperature that we label with T^*. The temperature oscillation, especially for the higher coefficients, seems to be symmetric around this point. In the $N = 120$ case we have $T^* \backsimeq 0.95$ but moving toward the thermodynamic limit ($N \to \infty$) such temperature increases up to become slightly higher than $T_c = 1$. It is plausible for T^* to coincide in the thermodynamic limit with the pseudocritical temperature at which the crossover line of the chiral transition reaches the $\mu = 0$ axis for a given quark mass.

6.2.2 Comparison of finite size and thermodynamic coefficient

The same computation of the coefficients can be made in the thermodynamic case. It is interesting to see how the finite size coefficients approach the $N \to \infty$ ones. For example in Fig.6.10 it is possible to compare the temperature dependence of the $N = 50$ coefficients with the thermodynamic ones. Here it is easier to see that the temperature T^* increases with N.

An interesting topic to study is the convergence of the finite size coefficients with increasing N (that is the "volume" of the model) near the critical temperature T_E. We anticipate that a consistent estimate of the critical temperature for this RM model at $m = 0.07$ is $T \backsimeq 0.670$, so we choose to fix this temperature and to increase N. The first intuitive ansatz for trying the fit of the increasing-N coefficients is the simple exponential one. But a better fit that turns out to be successful is the sum-of-exponentials one, that is:

$$c_n(N) = c_n^{\infty} + A\, e^{-N/N_{high}} + B\, e^{-N/N_{low}} \tag{6.25}$$

where c_n^{∞} is the thermodynamic value of the n^{th} coefficient at the chosen temperature and N_{high} and N_{low} two typical matrix sizes. Fig. 6.11 shows some fitted coefficients.

It is possible to plot the values of N_{high} and N_{low} as functions of the expanding order n (Fig.6.12). The one that leads the convergence at high N is the lowest, N_{low}. It results that both N_{high} and N_{low} decrease almost linearly increasing the expanding order n.

6.2.3 Computation of the radii and radius of convergence estimation

Since we are able to compute the Taylor coefficients of the effective potential, the following step is to estimate the radius of convergence at various temperatures. The goal is to detect the position of the critical point and to reproduce the location of the super-heating spinodal line. We are now going to use the mathematical tools introduced in the Chap.4.

A possible attempt could be to study the convergence of the "root" radii $\{|c_n|^{-1/n}\}$ but such sequence results to be slowly convergent [27]. We can instead consider the sequence of "ratio" radii $\{|c_n/c_{n+1}|\}$ that is more rapidly convergent than the previous one. Furthermore this ratio sequence choice allows an easier extrapolation

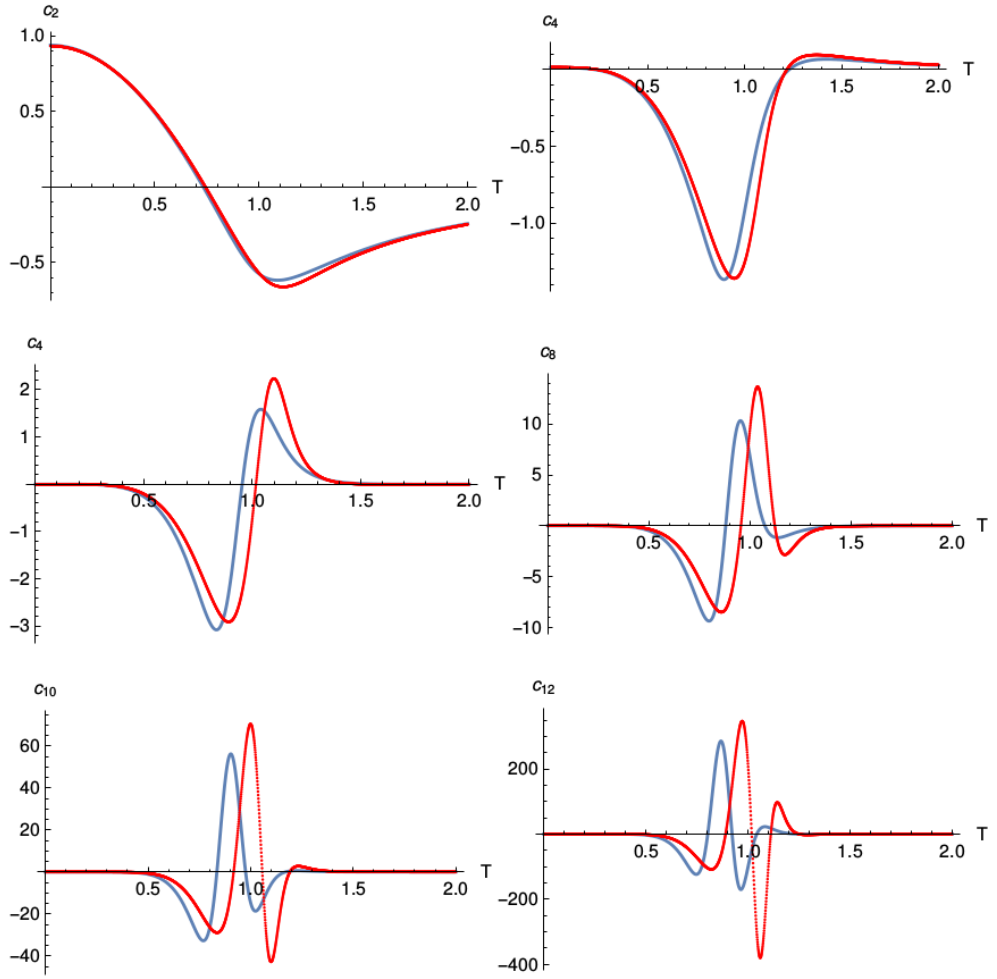

Figure 6.10: Some Taylor expansion coefficients for $m = 0.07$ at $N = 50$ (blue line) and $N = \infty$ (red line) as functions of the temperature

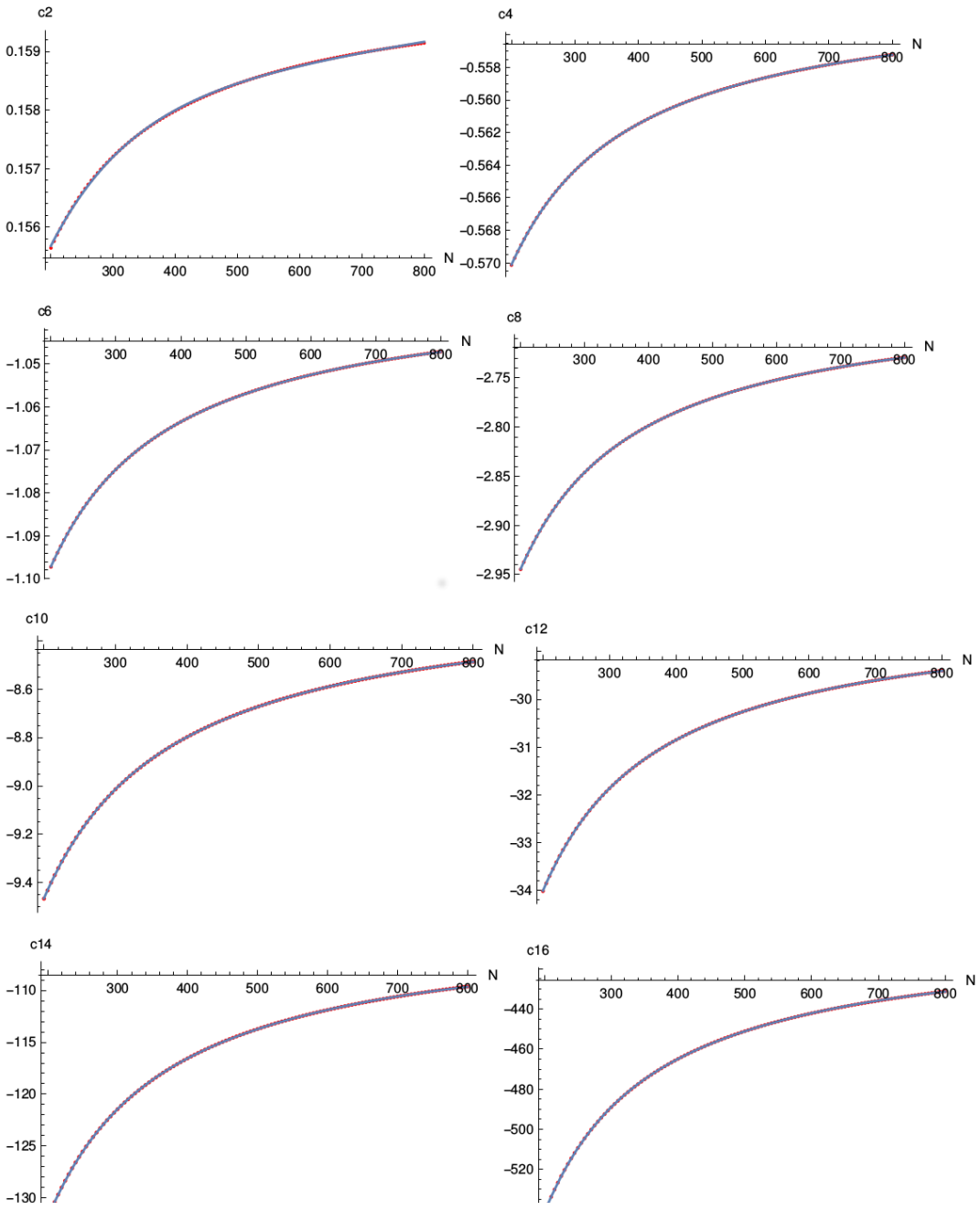

Figure 6.11: Some of the increasing-N coefficients (red points) fitted with the sum-of-exponential ansatz (blue line).

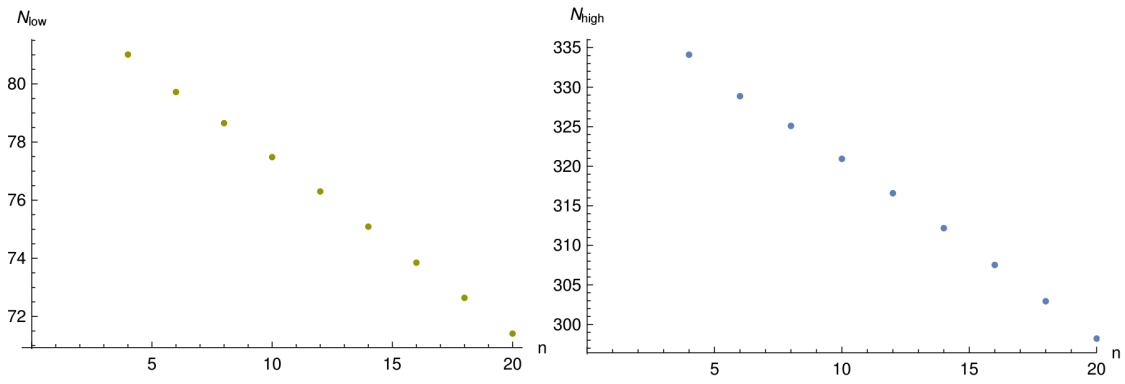

Figure 6.12: Behavior of the two typical matrix sizes N_{high} and N_{low} as function of the expanding order n.

of the critical parameters with respect to the root one. So, in this section we will focus mainly on the ratio methods to estimate the wanted radius of convergence.

Ratio test

As remarked by Balduzzi [6], it is interesting to analyze the nature of the nearest singularity that the ratio test is able to detect. Because the series of interest has only even terms, changing the variable to $t = \mu^2$ the series becomes $f = \sum_{n=0}^{\infty} c_{2n}\mu^{2n} = \sum_{n=0}^{\infty} c_{2n}t^n$. This causes for the sequence to extrapolate the radius to be $\{\sqrt{|c_n/c_{n+2}|}\}$. Let us now explicitly look at the *sign* of c_n/c_{n+2}. Near the criticality [5] the leading term of the free energy is supposed to be of the form: $f(\mu) \sim 1/(\mu - \mu_c)^{\lambda}$, so that the behavior of the $2n^{th}$ coefficient is $c_{2n} \sim [(\lambda + 2n)!/\lambda!]\ \mu_c^{-2n}$. Hence we have that near the criticality:

$$r_n^2 = \frac{c_n}{c_{n+2}} \sim \mu_c^2 \qquad \Rightarrow \qquad \mu_c \text{ is } \begin{cases} \text{Imaginary} & \text{if} \quad r_n^2 < 0; \\ \text{Real} & \text{if} \quad r_n^2 > 0; \end{cases} \tag{6.26}$$

In Fig.6.13 we show the first ratio radii for $N = 120$ and the ratio sign (in red), index of the opportunity to have a real singularity. The peaks and the zeros of each radius are reached at those temperatures for which respectively the denominator and the numerator of r_n vanishes and the ratio changes sign.

[5] We intend for *criticality* the critical endpoint or the spinodal line.

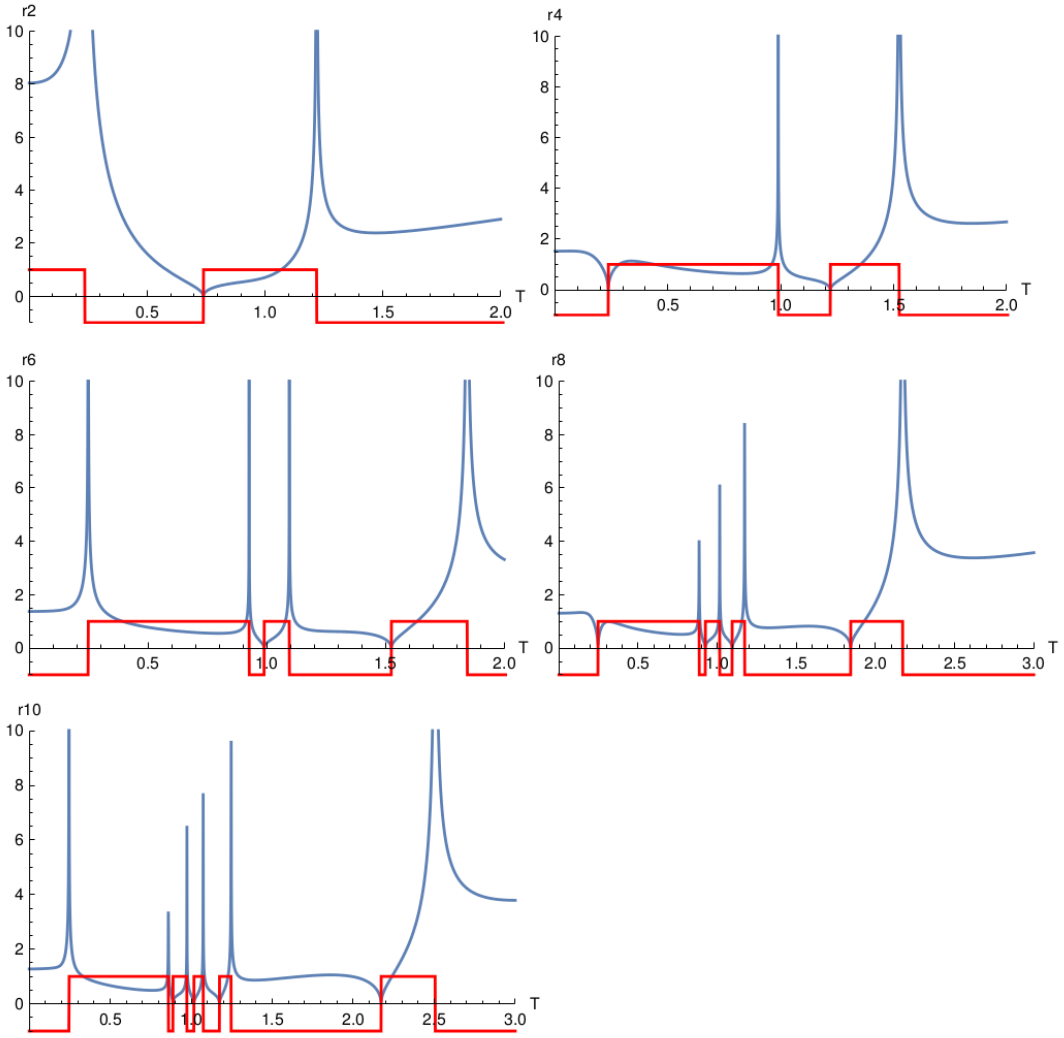

Figure 6.13: First ratio radii in the $N = 120$ case with the sign of the ratio $sign[c_n/c_{n+2}]$ (red).

.

It is interesting to notice that for each radius the high temperature region is *sign oscillating* (that means in general a complex μ singularity) whereas the low temperature region is *almost* totally characterized by a positivity of the sign (i.e the singularity in μ is real). Decreasing the temperature from $T > 1$, the point at which the sign stops oscillating can be used as an estimation for the critical temperature (this will be better shown below). At very low temperatures the positivity unexpectedly ceases near $T = 0.28$ where an imaginary singularity in μ becomes the nearest one. To understand what happens it is useful to look again at the branching points of the effective potential in the μ plane (Fig.6.14). For high temperatures the nearest singularity is purely real, therefore the sign is positive. Near $T \sim 0.28$ and below the nearest singularity becomes the one on the imaginary axis, therefore the sign of the ratio flips. This behavior is considered as an artifact of the RM model, not expected

to be present in QCD.

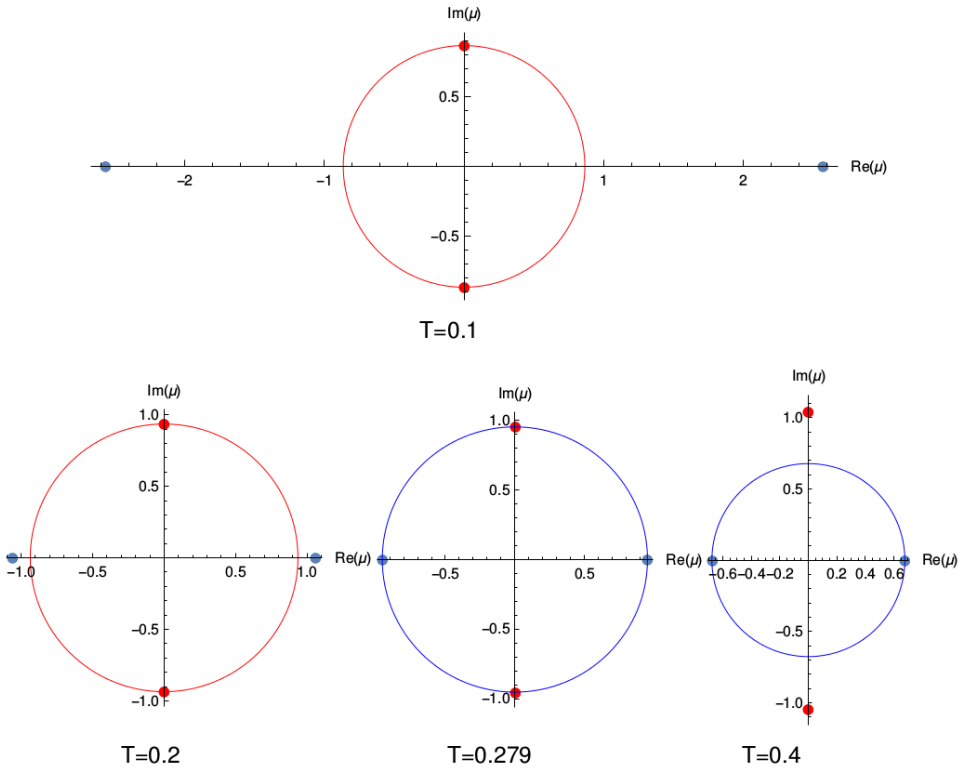

Figure 6.14: Nearest singularity at low temperature. In red the imaginary singularities, in blue the real ones. At $T = 0.1$ the nearest singularity is purely imaginary, at $T = 0.279$ the imaginary one equals in modulus the real one, at higher temperatures the nearest one is the real one and the ratio sign is positive.

.

Domb-Sykes method

Known the estimated radii sequence we can use the methods described in Sec.4.4 to extrapolate the convergence radius for each temperature and try to reproduce Fig.6.3, the plot of the nearest μ^2 singularity deduced from a branching point analysis. In particular we can start using the Domb-Sykes method, and with this purpose we proceed:

- computing for different temperatures and for different matrix sizes N the radii r_n;
- fitting the sequence $\{1/r_n\}$ with the ansatz Eq.(4.13) estimating μ_c and the critical exponent λ for each temperature.

In Fig.6.15 we show the fits (implemented with the program *Gnuplot*) for some temperatures of the inverse radii $1/r_n$ as functions of *1/n*. Since the convergence works for high n we exclude the lowest coefficients, and the behavior is very linear-like in a certain range of temperature.

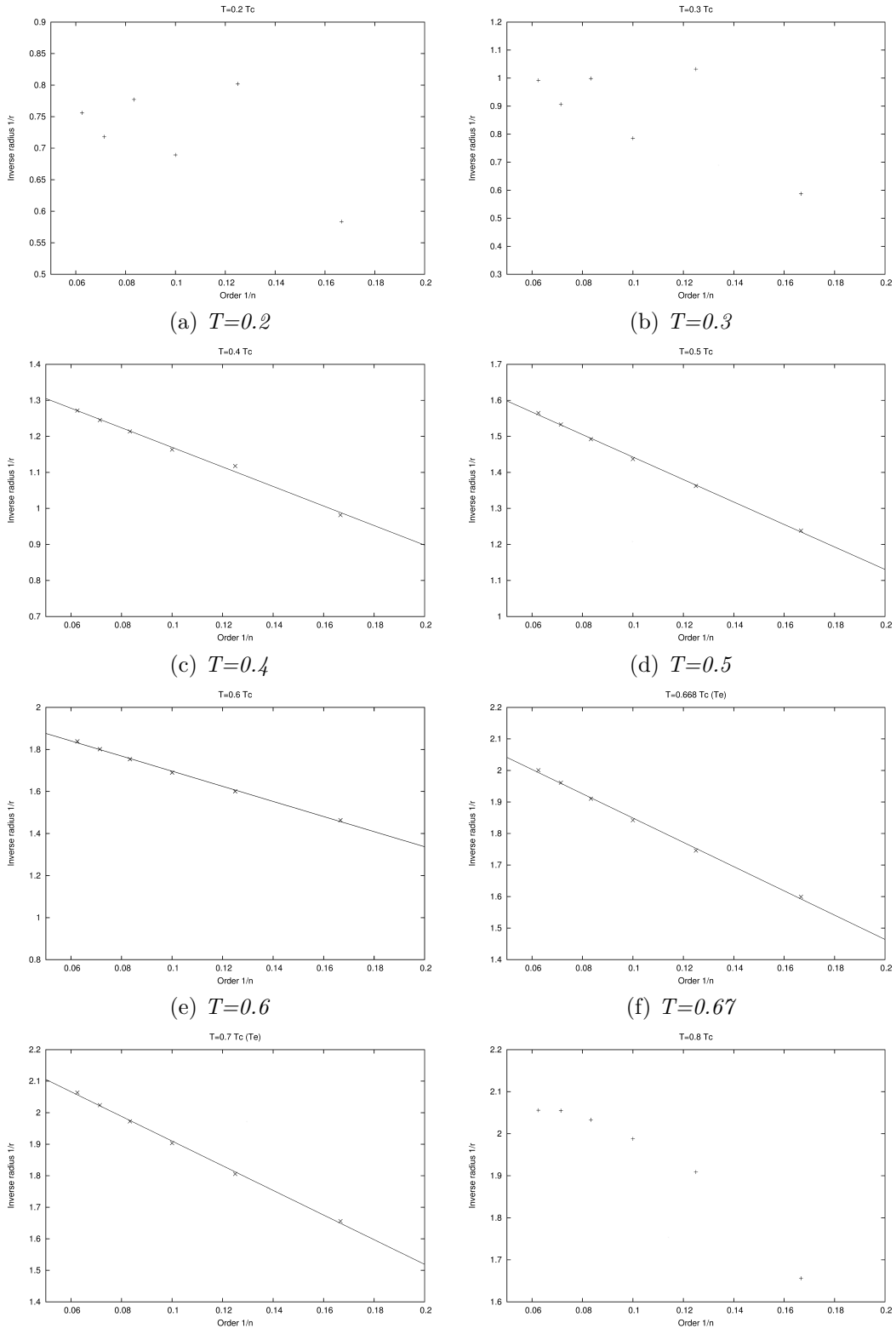

(a) *T=0.2* (b) *T=0.3*

(c) *T=0.4* (d) *T=0.5*

(e) *T=0.6* (f) *T=0.67*

(g) *T=0.7* (h) *T=0.8*

Figure 6.15: Inverse radii as a function of the inverse expansion order. The straight fit ceases to work at low temperatures (due to the imaginary singularity) and for high temperatures, where the spinodal line ends and the singularity becomes complex

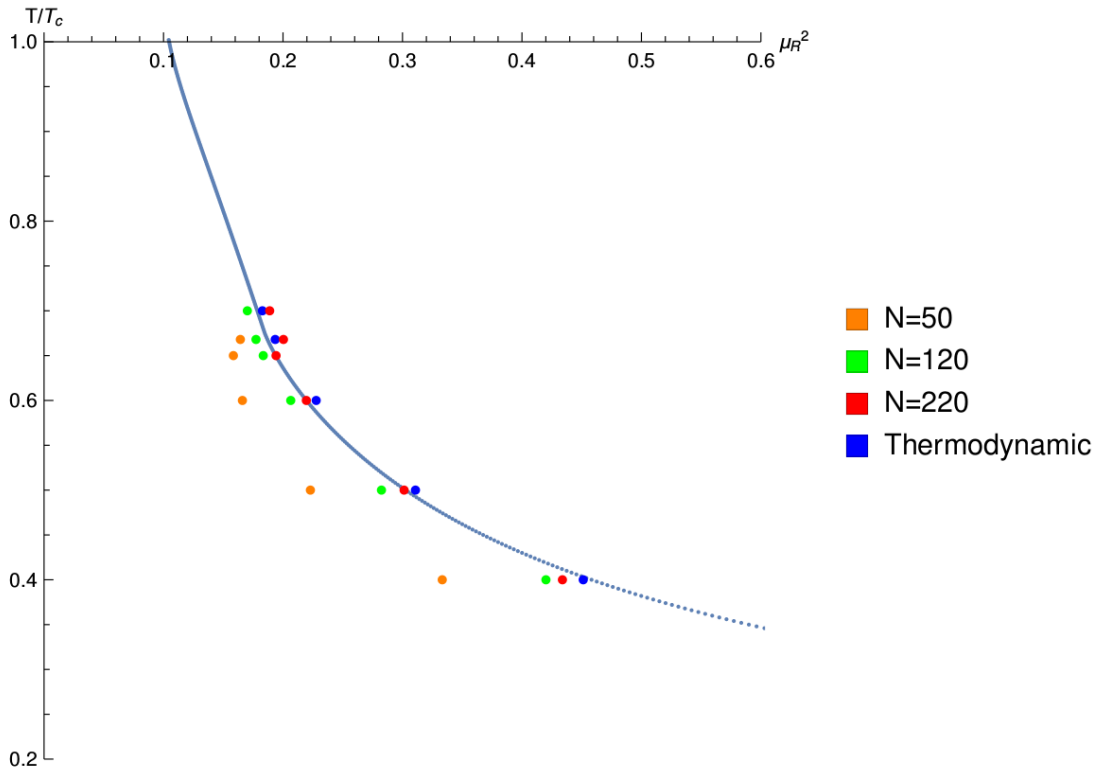

Figure 6.16: Plot of the extrapolated singularities from the ratio test with the Domb-Sykes method at $N = 50$, $N = 120$, $N = 220$ and $N = \infty$. The errorbars of the fitted values are not included for a better visualization.

From these fits it is possible to extrapolate the nearest real singularity for each particular temperature. Below the critical temperature $T_E \simeq 0.67$ the line of singularities for the effective potential is represented by the super-heating line in Fig.6.8. At this point we can try to reproduce the nearest-singularity plot of Fig.6.3. Varying the temperature and the matrix size N, and extrapolating the criticalities from the radii fits, the obtained figure is Fig.6.16. The correspondence between the branching-point estimated line and the fitted radii is quite good. From this figure it is possible to analyze the finite size effects, indeed is clearly visible how the finite size singularities approach to the thermodynamic ones in the $N \to \infty$ limit.
The Domb-Sykes ansatz stops working at high temperatures $T \gtrsim 0.7$ (above the critical point the singularity is in general complex) and at low temperatures, when the unphysical imaginary singularity started to dominate.[6]

[6] An imaginary singularity in μ corresponds to a real singularity in μ^2 on the negative axis, that should be related to an alternate sign pattern of the coefficients c_{2n}, c_{2n+2}. This is verified, indeed the ratio sign is always negative at low temperatures. In principle the Domb-Sykes method should be able to detect even such singularities, but some fitting attempts with parabolic corrections to the Domb-Sykes method lead to overestimation of the position of the imaginary singularity.

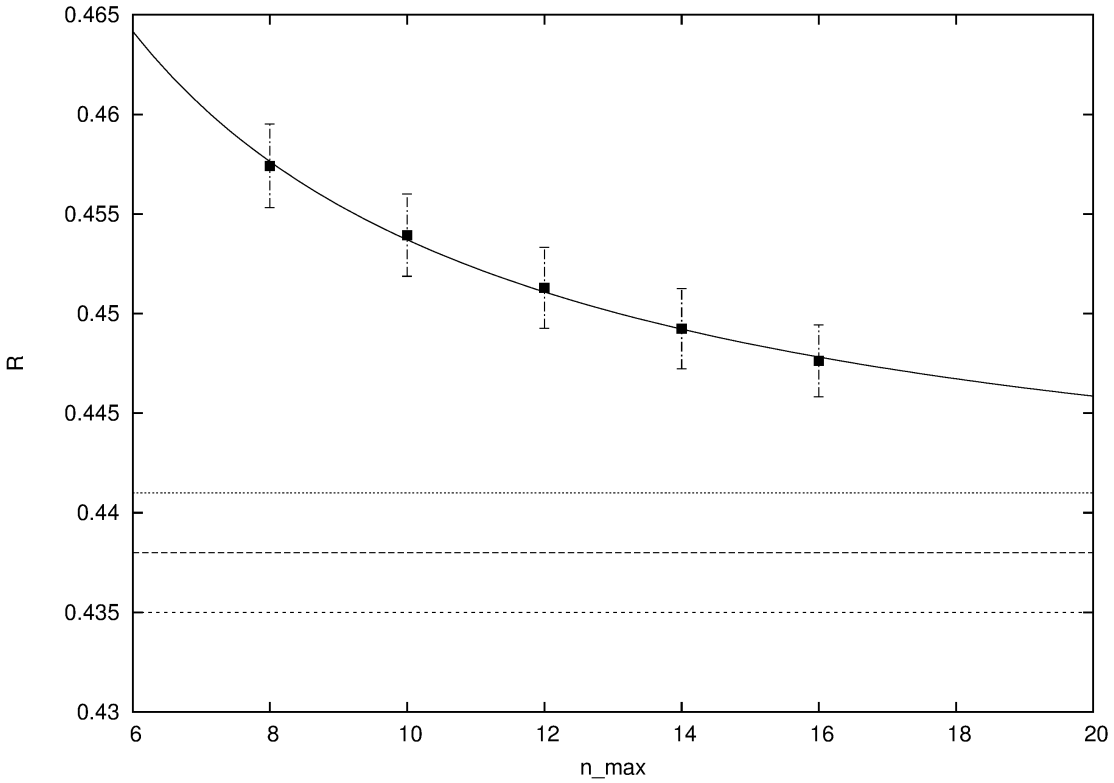

Figure 6.17: Behavior of the estimated radius of convergence at the critical temperature T_E increasing the maximum expansion order n_{max}. The fit is performed with an ansatz $R(n_{max}) = R_\infty + b/n_{max}^{3/2}$ that gives us $R_\infty = 0.438(3)$.

Another interesting check to perform is to analyze how the position of the extrapolated singularity changes varying the maximum order of the expansion, n_{max}. This can be useful especially if one has only few available coefficients, to understand how their number affects the estimation of the singularity. The result at the temperature T_E is reported in Fig.6.17, that shows a decreasing radius increasing the maximum order. It is well fitted by a function $R(n_{max}) = R_\infty + b/n_{max}^{3/2}$, that gives as result $R_\infty = 0.438(3)$.

The next interesting parameter of the fit is the exponent λ of Eq.(4.10). To predict its value it is useful to look at what Stephanov suggests [49]. In QCD the critical point for nonzero mass defined by (T_E, μ_E) is of the class of the 3D Ising model, whereas the RMT is governed by the *mean field theory* universality. One can see that the leading perturbation near the critical point is *magnetic field like*. This derives from the fact that one has for the mean field theory the scaling dimensions $y_t = 1/\nu = 2$ and $y_h = \beta\delta/\nu = 3$. Since both t and h couple linearly with $\mu - \mu_E$, the magnetic field dominates the response to $\mu - \mu_E$ near the critical point [49]. From universality arguments we know that the behavior of the singular part of the free energy near the critical point is:

$$\Omega \sim h^{1+1/\delta} g(th^{-1/\beta\delta}) \tag{6.27}$$

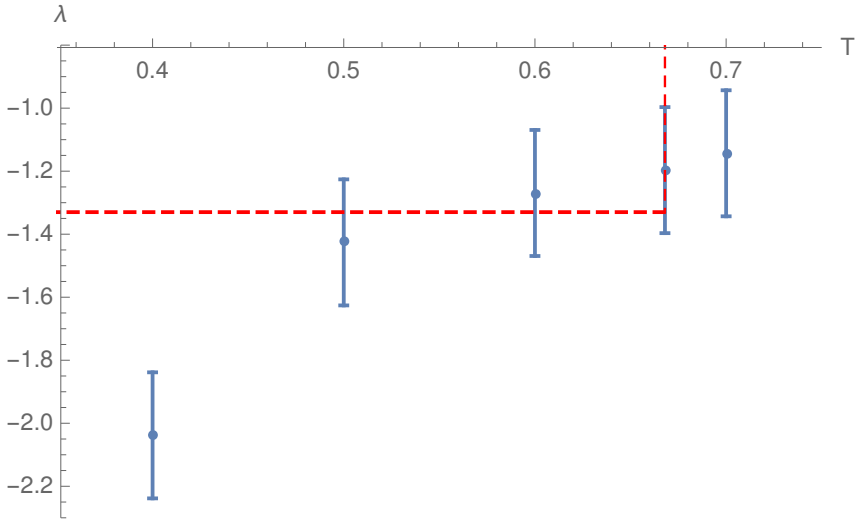

Figure 6.18: Exponent λ from the ansatz Eqn.4.10. Near the critical point ($T_E \backsimeq 0.67$) the fitted value is consistent with the theoretical one $\lambda = -4/3$.

where $g(x)$ is an analytic function near $x = 0$. Since near μ_E we have that $\mu - \mu_E \sim h$, and as written in Eqn.(4.10) $\Omega(\mu) \sim A(1 - \mu/\mu_E)^{-\lambda} + B$, using the mean field value $\delta = 3$ we obtain:

$$-\lambda = 1 + \frac{1}{\delta} \quad \lambda = -\frac{4}{3} \approx -1.33 \tag{6.28}$$

near the critical point. In the Fig.6.18 we show the values of λ in the case of mass $m = 0.07$ as function of the temperature. We can notice that near $T = T_E$ the prediction for λ is, within the errors, in accordance with the fitted value $\lambda = -1.2(2)$.

The parameter λ can even be related with the critical exponent of the baryon susceptibility at the critical point

$$\chi_{\mu\mu} = \frac{\partial n_B}{\partial \mu} = -\frac{\partial^2 \Omega}{\partial \mu^2} \tag{6.29}$$

Near the critical point the susceptibility behaves as:

$$\chi_{\mu\mu} \sim (\mu - \mu_E)^{-\gamma_\mu} \tag{6.30}$$

It should be clear that $\lambda + 2 = \gamma_\mu$, hence near the critical point a value of $\lambda = -4/3$ is in accordance with the mean field prediction $\gamma_\mu = 2/3$ [44]. As we can notice the value of $|\lambda|$ decreases along the spinodal line approaching the critical point. This cause for γ_μ to increase: the divergence of the baryon susceptibility becomes stronger near the endpoint, as reported even in Ref.[44].

Zinn-Justin method

Known the thermodynamic Taylor coefficients, the Zinn-Justin method of Sec.4.4.3 allows to construct the sequence $\{s_n\}$ of Eqn.(4.17) with three of them $s_n = f(c_n, c_{n-1}, c_{n-2})$ and successively the sequence μ_n^c of Eqn.(4.18) that should approach to the correct singularity for sufficient high n. For this purpose, we choose for

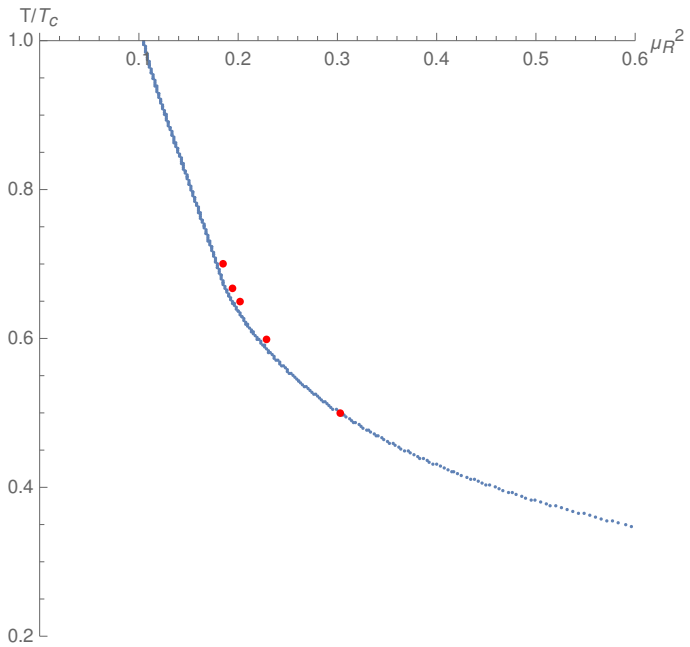

Figure 6.19: Plot of the extrapolated singularities from the Zinn-Justin ansatz of Eqn.4.18 at $N = \infty$.

each temperature the *highest* n estimation for the criticality and we put this values onto the nearest singularity plot obtaining the result is in Fig.6.19. The agreement with the spinodal line seems to be good, even in this case.

Neville-Aitken method

The Neville-Aitken method, given the original sequence of the estimated radii, allows to redefine new sequences $\{r_n^{(k)}\}$ whose convergence to the asymptotic value is more rapid. For instance we can try to determine in such way the asymptotic radius of convergence at the critical temperature T_E redefining the sequences $\{r_n^{(1)}\}$ and $\{r_n^{(2)}\}$ whose correction from the asymptotic value is $O(1/n^2)$ and $O(1/n^3)$ respectively, as reported in Sec.4.4.2. Here we show in Fig.6.20 the fits for the square of these sequences. As we can see the convergence is more rapid just in the second step, where the asymptotic value is given by $R_\infty = 0.437(4)$. However in our case this method does not represent a great improvement with respect to the Domb-Sykes one. One of the problems is that in every step one loses one degree of freedom, even though we see that just in the second step the correction with respect to the asymptotic value is sufficiently small.

Padé approximants

Given a finite number of $N+M+1$ coefficients, one can try to reconstruct the form of Ω_{min} through a Padé approximant $[N/M] = P_N(z)/Q_M(z)$. We know that near the criticalities Ω behaves like $\Omega_{min}(\mu) \sim (1-\mu/\mu_c)^{-\lambda}$. Since $\lambda \approx -1.33$ near the critical endpoint (and in general is negative), in correspondence of $\mu = \mu_c(T)$ the function should have zeroes. Knowing this, we tried, starting from the thermodynamic

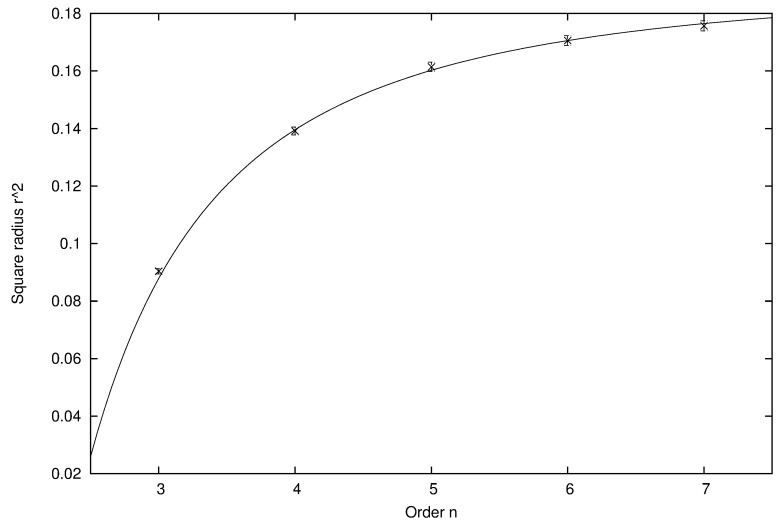

(a) $(r_n^{(1)})^2$

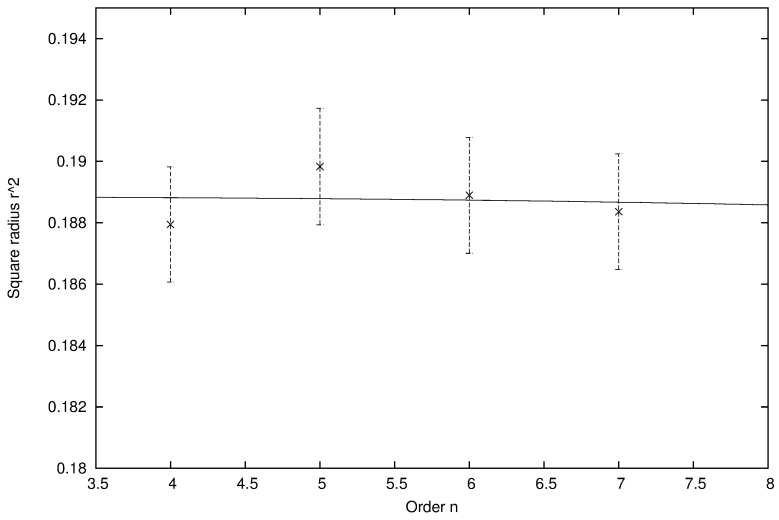

(b) $(r_n^{(2)})^2$

Figure 6.20: Neville-Aitken extrapolations for the corrected sequences $(r_n^{(1)})^2$ and $(r_n^{(2)})^2$. The correction with respect to the asymptotic value $R_\infty = 0.437(4)$ is $O(1/n^2)$ and $O(1/n^3)$ respectively.

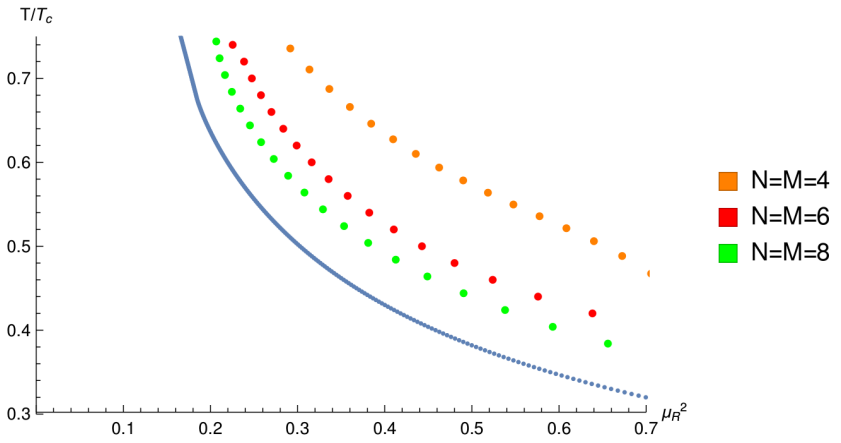

Figure 6.21: Plot of the criticalities of Ω deduced through Padé approximants $[N, M]$

.

coefficients, to reconstruct different Padé approximants varying N and M and looking at the behavior of the zeros. We varied the temperature and computed the zeros and the poles of the Padé approximants $[N/M]$ paying attention for the poles to not cancel the zeros. Varying the temperature it is possible to recognize those zeros that are near the expected criticalities and whose temperature behavior is similar to the one seen in the previous sections. If we plot in particular such zeros as a function of the temperature in the nearest singularity plot we obtain the behavior of Fig.(6.21). We show for simplicity the zeros obtained from the Padé approximants with $N = M = 4\,, 6\,, 8$. It is possible to see that increasing the order, the line of zeros approaches to the spinodal line.
However this method, applied to the RM model does not provide any advantage. The convergence to the line of criticalities seems to be slow. Furthermore is not clear what a valid estimation of the critical point can be. Indeed the behavior of a complex criticality that becomes real below a certain temperature seem to be verified only starting from $N = 8$ and even in such case it leads to a not still correct estimation.

6.2.4 Location of the critical point

We are now going to compare the different methods, some of which described in the previous section, to estimate the location of the critical point of the RM model for a finite mass $m = 0.07$, i.e the ending point of the first order transition line of the diagram in Fig.6.6.

Branching point analysis in complex μ plane. As we described in the Sec.6.1.3, one estimation of the critical point consists in determining the temperature T_E at which for the first time we have a real branching point of the effective potential Ω in the complex μ plane. Such an estimation, as reported in Fig.6.2, leads to $T_E = 0.674(2)$, $\mu_E = 0.430(3)$.

End of the minima degeneracy

Known the expression of the effective potential as a function of the parameter ϕ we know that on the first order line there is a degeneracy of the two absolute minima, index of two coexisting phases. For obtaining the phase diagram in Fig.6.6 it is sufficient to iteratively vary the temperature T from below and then choose every time the μ that gives such equally-deep absolute minima. Using this procedure we can find the temperature at which this degeneracy ends and the corresponding chemical potential. The obtained values are: $T_E = 0.668(4)$, $\mu_E = 0.432(4)$.

End of ratio sign oscillation

Looking at the plot of ratio radii in Fig.6.13, we told that an oscillation at high temperatures of $sign[c_{n+2}/c_n]$ has to be related with a complex μ singularity of the Taylor expansion. Decreasing the temperature it is possible to detect the point at which the ratio sign stops its oscillation, hence the singularity starts to be real.[7] To perform the analysis with a bigger sample of radii, we choose to study the finite size case with $N = 120$. Looking at the Fig.6.22 it is possible to notice that the "oscillation-endpoint" moves toward lower temperatures increasing the expanding order. If one wants to extrapolate the critical T and μ, one choice is the point $(T_E^{(n)}, \mu_E^{(n)})$ after the last peak when the ratio reaches a minimum (Fig. 6.22). Plotting these points as functions of the expanding order and then trying an exponential fit (i.e $\mu_E(n) = \mu_E(\infty) + b\, e^{-n/\tilde{n}}$) one obtains the result of Fig. 6.23 and the fitted values of $\mu_E \equiv \mu_E(\infty) = 0.433(1)$ and $T_E \equiv T_E(\infty) = 0.602(6)$. The result for the μ criticality seems to be coherent with the previous estimates more than the T one[8]. This can be caused from the arbitrariness to choose the end-of-oscillation point, more widely variable in T than in μ.

[7] This is not true at very low temperatures where there is an unphysical imaginary singularity that, however, does not affect this estimation.

[8] In truth a little correction should be necessary due to the fact that we are considering the finite N=120 case, whereas the transition happens in the thermodynamic limit. But this computation is just as example.

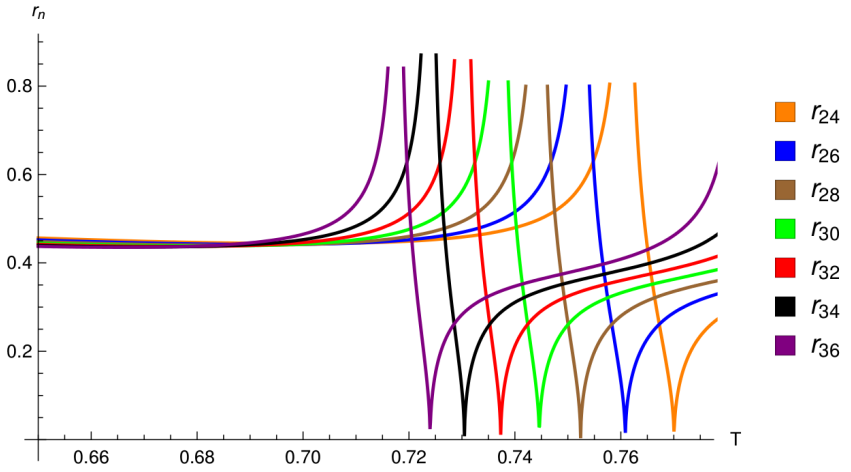

Figure 6.22: Behavior of the $N = 120$ ratio radii near the last oscillation of the ratio sign.

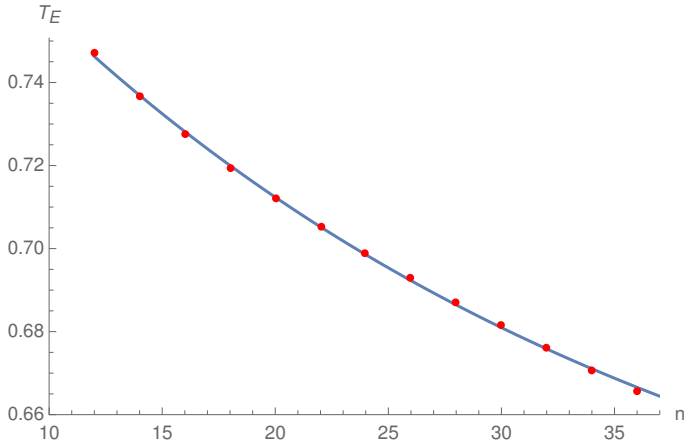

(a) $T_E^{(n)}$

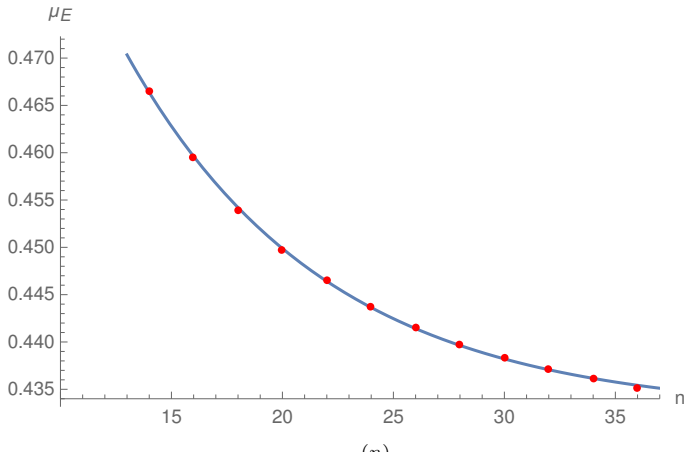

(b) $\mu_E^{(n)}$

Figure 6.23: Estimated μ_E and T_E from the minimum of the $N = 120$ ratio radii after the end-of-sign-oscillation point.

Fit extrapolations

An estimation of the critical point can be tested from the ratio radii extrapolation suggested by Domb-Sykes and from the Zinn-Justin method. It is plausible to think that both the first ansatz of Eq. (4.13) and the second of Eq. (4.18) should cease to work once overpassed the critical point, because of the appearance of a complex singularity for $T > T_E$. In truth the fits with both methods continue working quite well even for temperatures slightly higher than the T_E estimated through other ways (look for instance at the T=0.7 case in Fig.6.15). This is maybe due to the fact that the imaginary part of the singularity is still much smaller than the real one, so the ansatz continues to be acceptable at first.

One of the things one can do is to insert the critical temperature obtained with other methods as an external input and then to estimate the related μ_E. Using for instance the estimate $T_E = 0.668(4)$, we obtain $\mu_E = 0.441(2)$ with the Zinn-Justin method and $\mu_E = 0.448(4)$ with the Domb-Sykes method.

6.3 Stephanov's model with all the Matsubara frequencies

6.3.1 Introduction of the model

The model we have studied in the previous sections has the advantage to describe a mean field chiral phase transition with the only temperature dependence on the lowest Matsubara frequency $\omega_0 = \pi T$. As reported in Ref.[48] (and as we are going to show), for sufficiently high temperatures and zero chemical potential the zero mode is the only one that leads the transition and the chiral condensate is exclusively described by only such degree of freedom. However the model fails at low temperatures. We would like to know what can change adding *all* the Matsubara frequencies $\omega_n = (2n+1)\pi T$ to the model, or at least an higher number of them. For this purpose we consider a partition function of the form:

$$Z = \int DX exp(-NTrXX^\dagger) \prod_n det^{N_f} \begin{pmatrix} m & iX + i\Omega_n + \mu \\ iX^\dagger + i\Omega_n + \mu & m \end{pmatrix} \tag{6.31}$$

We are using for μ, T and m the units defined in at the beginning of this chapter. As in the model with only one Matsubara frequency, we consider for the "instanton" basis a coupling in temperature of opposite sign in the following sense:

$$\Omega_n = \begin{pmatrix} \omega_n \mathbb{I}_{N/2} & 0 \\ 0 & -\omega_n \mathbb{I}_{N/2} \end{pmatrix} \tag{6.32}$$

After several passages reported in Appendix, we obtain as final form of the partition function:

$$Z = exp[-\Omega(\{\bar{y}\}, m, T, \mu)] \tag{6.33}$$

where $\Omega(\{y_i\}, m, T, \mu)$ is an effective potential, $\{y_i\}$ is an infinite set of parameters whose index $i = 1, 2 \ldots$ refers to the Matsubara modes and $\{\bar{y}_i\}$ are those parameters

that minimize the potential. The explicit expression of Ω is:

$$\begin{aligned}\Omega(y,m,T,\mu) &= \sum_{n=0}^{\infty}\left[y_n^2 - \frac{1}{2}log\Big[[(y_n+m)^2-(\mu+i\omega_n)^2][[(y_n+m)^2-(\mu-i\omega_n)^2]\Big]\right] \\ &\equiv \sum_{n=0}^{\infty}\Omega_n(y_n),\end{aligned} \tag{6.34}$$

where

$$\Omega_n(x,m,T,\mu) = x^2 - \frac{1}{2}log\Big[[(x+m)^2-(\mu+i\omega_n)^2][[(x+m)^2-(\mu-i\omega_n)^2]\Big] \tag{6.35}$$

Hence the obtained effective potential can be expressed as a sum of *independent* potentials, each one related to a specific Matsubara mode. The chiral condensate in the massless case can be computed as (see Appendix):

$$\left\langle\bar{\psi}\psi\right\rangle = \sum_{n=0}^{\infty}\frac{2N}{V}\bar{y}_n\frac{(\bar{y}_n^2+\omega_n^2-\mu^2)}{(\bar{y}_n^2+\omega_n^2-\mu^2)^2+4\mu^2\omega_n^2} = \sum_{n=0}^{\infty}\frac{2N}{V}\bar{y}_n, \tag{6.36}$$

where the last equality follows from the chiral limit ($m\to 0$) of the saddle point equation:

$$y_n = \frac{(m+y_n)\left((m+y_n)^2+\omega_n^2-\mu^2\right)}{\left((m+y_n)^2+\omega_n^2-\mu^2\right)^2+4\mu^2\omega_n^2} \tag{6.37}$$

One of the non-trivial solutions of this equation is:

$$y_n^2 = \frac{1}{2}\left[(1-2(\omega_n^2-\mu^2)+\sqrt{1-16\mu^2\omega_n^2}\right]. \tag{6.38}$$

Hence y_n assumes real values only in a certain range of (T,μ). This can be better understood in the $\mu=0$ case, already analyzed by Stephanov [48] for $N_f=1$. The nonzero solution in such case is:

$$y_n = \sqrt{1-\omega_n^2} = \sqrt{1-(2n+1)^2(T/T_c)^2} \tag{6.39}$$

that exists only for those n such that $1-\omega_n^2\geq 0$. When T is close to T_c, only the $\omega_0=\pi T$ frequency contributes to the chiral condensate, not the others. This is no more true at temperatures very lower than T_c. For instance if we write $T=\alpha T_c$, it is possible to see that at $\alpha=1/3$ even ω_1 starts to contribute to the chiral condensate. In general when $\alpha=1/(2n+1)$ we have to take into account the first ω_n frequencies. Therefore the model at $\mu=0$ considered in Sec.5.3 is valid only for $T\gtrsim 0.33\,T_c$.

Taking $n=0$ the expression Eq.(6.36) is exactly the same of the case with only the zero mode [48] [30] . It would be reasonable to expect that the presence of more Matsubara frequencies can affect in some way the phase boundary of the chiral phase transition, due to a different vanishing of the order parameter with respect to the $n=0$ case. In the following section we will see that this is not the case: the phase boundary it is not modified including an arbitrary large number of Matsubara modes.

6.3.2 Phase diagram of the model

The phase diagram of the model in the *massless* case can be derived imposing for the chiral condensate (6.36) to be an order parameter for the transition, that is to vanish crossing the phase boundary.
For this purpose, we can at first consider to modify the initial model adding a finite number $\bar{n}$ of Matsubara frequencies. This puts an upper limit in the sums of the chiral condensate and the effective potential. For instance let us consider a model with the first $\bar{n} = 5$ Matsubara modes and analyze the behavior at high and low temperatures. Being a sum of independent terms, the global minimum of the effective potential Ω is a simple superposition of the global minima of the potentials $\Omega_n(y_n)$ related to the specific Matsubara modes.
In Fig.(**??**.a) we can analyze the behavior of such potentials starting from a point on the first order line $(T_H^{first}, \mu_H^{first})$ at high temperatures. As we have seen before, at high temperatures (the first figure) the highest modes do not contribute to the chiral breaking, indeed only the mode ω_0 shows a nonzero order parameter in the proximity of the phase boundary. Holding fixed the chemical potential μ_H^{first} and decreasing the temperature inside the broken region (far from the phase boundary), the highest modes start to contribute modifying the value of the nonzero order parameter.

Secondly in Fig.(6.24.b) we approach a point on the phase diagram $(T_L^{first}, \mu_L^{first})$ at a fixed low temperature T_L increasing the chemical potential inside the broken region. We can see that the despite the the high modes contribute, this does not affect the breaking because the "order parameters" y_i start to vanish approaching the first order line from the highest to the lowest. Hence the parameter y_0 is the one that determine the position of the point where the chiral symmetry breaking takes place. To better visualize this, we can for instance look at the different temperature behavior of the $\{y_i\}$ at $\mu = 0$ and the related chiral condensate (the sum of them) in Fig.6.25. The "critical temperature" for each mode is at $T_c^{(n)} = 1/(2n+1)$, hence $T_c^{(0)}$ is the highest and this causes $T_c = T_c^0$.

A similar behavior happens even at $\mu \neq 0$: this means that the phase diagram is not modified varying the number of Matsubara modes of the theory.

This is clear in Fig.6.26 where the phase diagram is computed using a model with a number of Matsubara modes of $\bar{n} = 1, 3, 5$. The profile is the same, due to the motivations given above.

6.3.3 Imaginary chemical potential and the *quasiperiodicity*

Given the potential of Eq.(6.34), one can notice that in the chirally restored phase, i.e. when the order parameters y_i are all zero, the effective potential is *almost* invariant under the transformation:

$$\omega_n = (2n+1)\pi T \rightarrow \omega_n + 2k\pi = \omega_{n+k} \tag{6.40}$$

If one defines the infinite Matsubara summation in the range $i = 0 \ldots \infty$ a shift $\omega_n \rightarrow \omega_{n+k}$ would cause for the first k frequencies to be "not replaced" after the

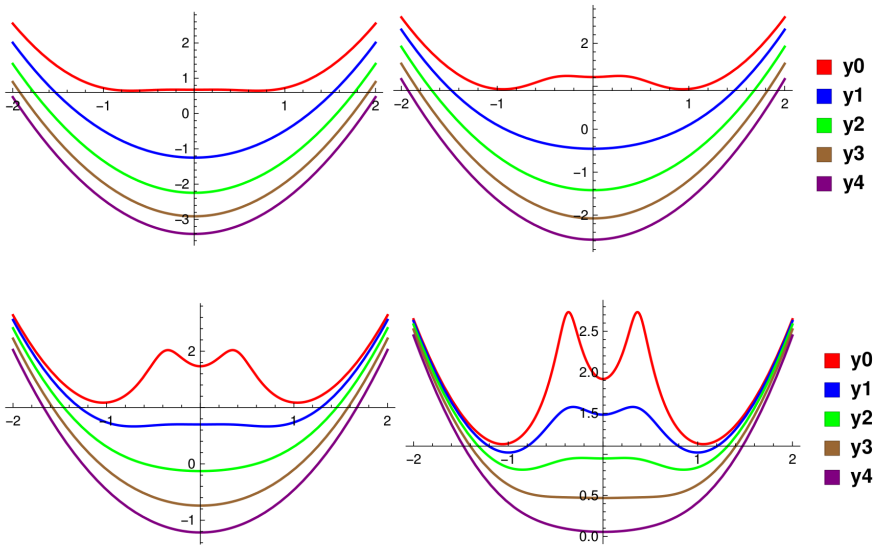

(a) $\mu_H^{first} = 0.37$. $T_H^{first} = 0.60$, $T = 0.40$, $T = 0.20$, $T = 0.10$ *(from left to right, up to down)*

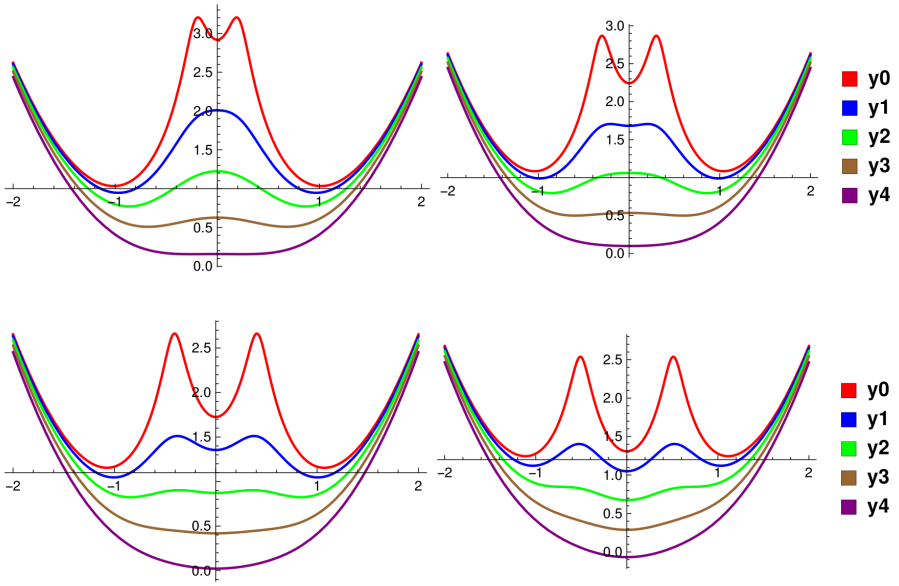

(b) $T_L^{first} = 0.10$. $\mu = 0.21$, $\mu = 0.31$, $\mu = 0.41$, $\mu_L^{first} = 0.51$ *(from left to right, up to down)*

Figure 6.24: **(a)** Plot of the effective potentials $\Omega_n(y_n)$ decreasing the temperature at $\mu_H^{first} = 0.37$. The first point is on the first order line at "high" temperature, with only the zero mode involved. Decreasing the temperature we are inside the broken region and even the higher modes start to contribute to the chiral condensate. **(b)** Plot of the effective potentials $\Omega_n(y_n)$ increasing the chemical potential at $T_L^{first} = 0.10$. We start from a point inside the broken region at low temperature, where even the high modes contribute. Increasing the μ we reach the phase boundary: the last "order parameter" y_i that vanishes is the lowest one (y_0).

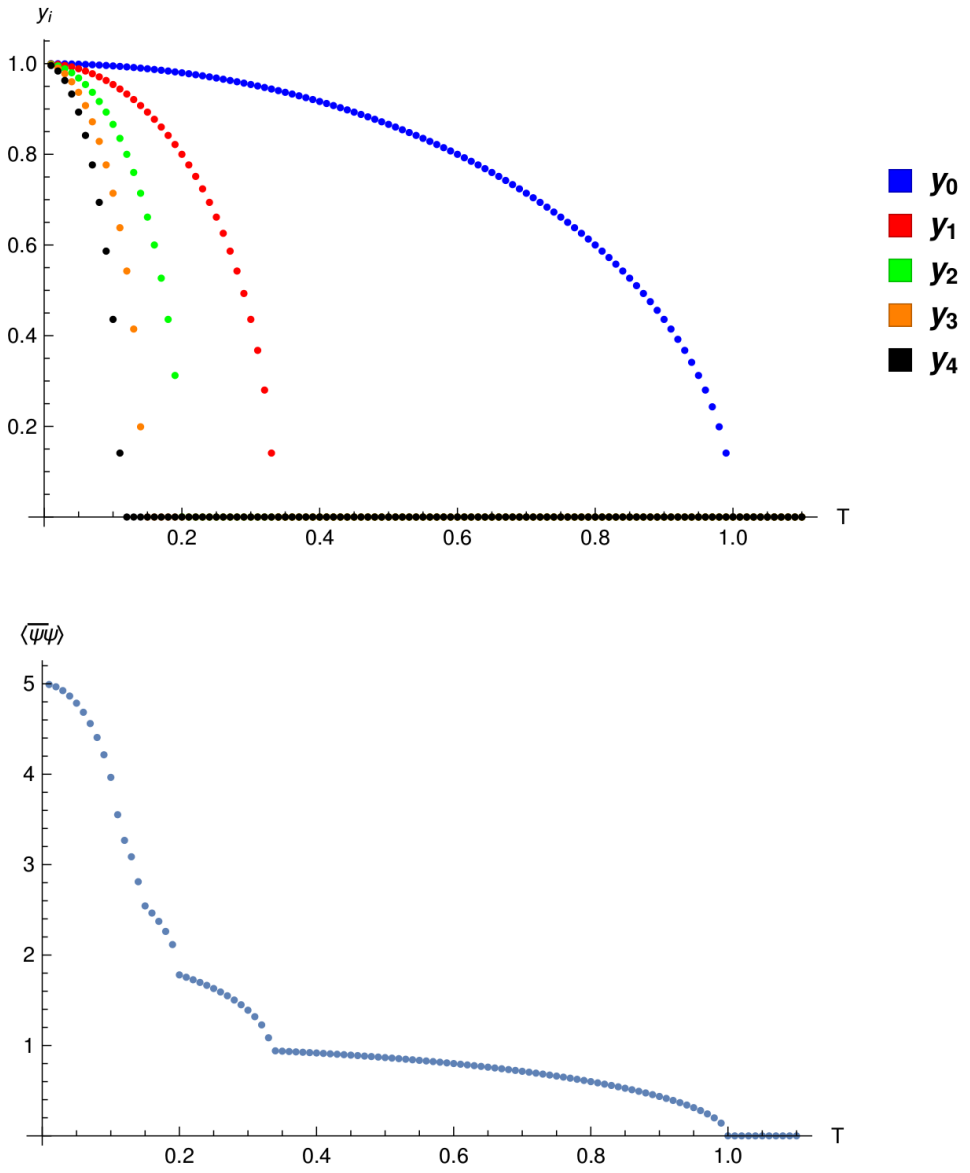

Figure 6.25: Temperature behavior of the $\{y_i\}$ as functions of the temperature (*up*) and the related chiral condensate (*down*). The "critical temperature" for each mode is at $T_c^{(n)} = 1/(2n+1)$, hence $T_c^{(0)}$ is the highest and this causes $T_c = T_c^0$.

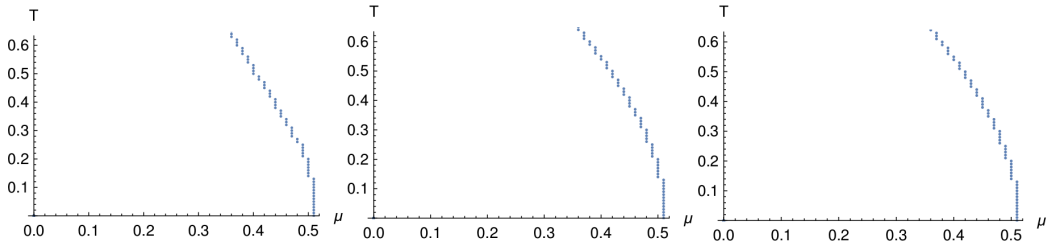

Figure 6.26: Plot of the first order line in the massless case of models with a number of Matsubara modes of $\bar{n} = 1, 3, 5$. The results are exactly the same, both for high and low temperatures.

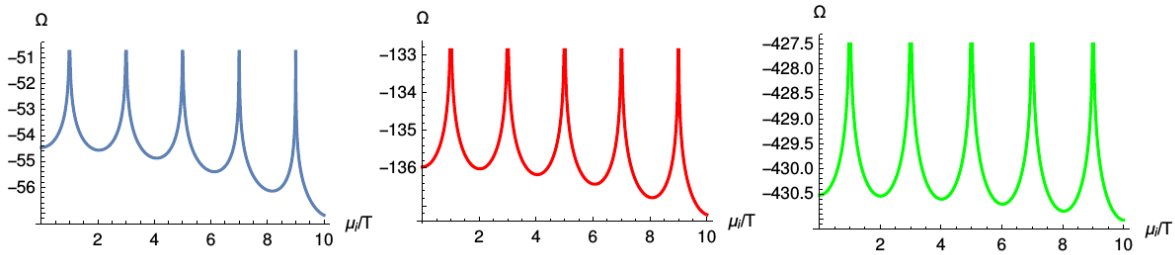

Figure 6.27: 2π-quasiperiodicity in the restored phase of the effective potential Ω as function of μ_i/T (in units of π), for $\bar{n} = 10$ (blue), 20 (red), 50 (green). As expected the periodicity improves increasing the number of Matsubara frequencies.

shift.[9]. This can be avoided redefining the summation from $i = -\infty, \ldots, \infty$. In truth in the model we are analyzing we are able to deal with only a finite number $\bar{n}$ of frequencies, hence the finiteness of the summation cause for the periodicity to be verified not exactly and only for small k. Furtermore the symmetry Eq.(6.40) is not verified in the broken phase, when the y_i assumes nonzero (and in general different) values. However the only thing that matters is the difference $y_i - y_{i\pm1}$ and if both modes are "broken" (i.e nonzero) such difference seems to be not so high.
If we now turn on an imaginary chemical potential μ_i, in such conditions this *quasiperiodicity* in principle allows us to shift periodically the variable μ_i/T without affecting relevantly Ω. Indeed the transformation:

$$\mu_i/T \to \mu_i/T + 2k\pi \tag{6.41}$$

modifies the effective potential in a way equivalent to Eq.(6.40). Therefore we expect see a quasiperiodicity of Ω in the variable μ_i/T. The following Fig.6.27 shows the improvement of the quasiperiodicity of 2π of the effective potential increasing the number of Matsubara modes ($\bar{n} = 10$, 20, 50). This behavior however is respected only at low μ_i/T.

[9]This happens because we would have $\omega_0 \to \omega_k$, $\omega_1 \to \omega_{k+1}$,... hence the first k frequencies would not be replaced after the shift.

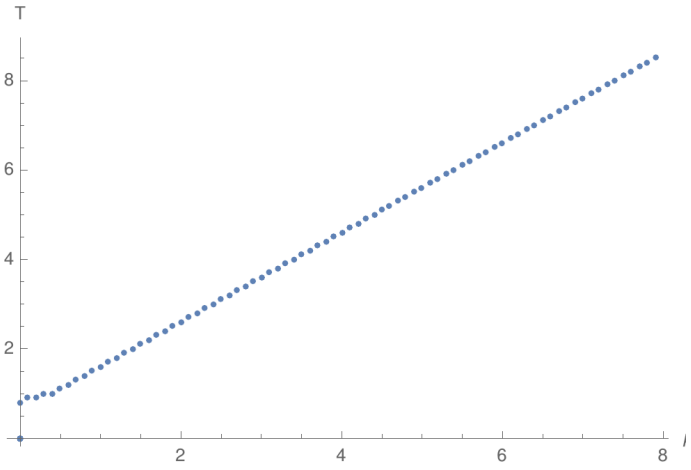

Figure 6.28: Second order line at imaginary chemical potential for a model with $\bar{n} = 10$. As in the real μ case, the zero mode is the only to lead the transition.

It has been verified that with both the "truncation schemes" of the Matsubara frequency sum, that is summing over the positive $(i = 0, \ldots, \infty)$ or even over the negative $(i = -\infty, \ldots, \infty)$ frequencies the oscillation pattern is similar and it does not vary substantially decreasing the temperature and going inside the chiral symmetry broken region.

Let us now try to plot the phase diagram of the model in the *massless* case at imaginary chemical potential, including at first $\bar{n} = 10$ Matsubara frequencies. We could ask if some signal of periodicity appears in the phase boundary increasing μ_i/T. We can see in (Fig.6.28), that as what happens in the real μ case, again the zero mode dominates the transition. The higher modes play a role at low temperature, but near the second order line the order parameters y_i with $i \neq 0$ are zero and the last parameter to vanish is y_0, that leads the position of the phase boundary. The result is that the behavior of the second order line is almost linear in the diagram (T, μ). No periodicity appears in the phase boundary because the highest modes do not play any relevant role there.

6.3.4 High temperature behavior

We are now going to analyze the high T behavior of the free energy density f in the RM model with a finite number of Matsubara frequencies $\bar{n}$. For this purpose we choose some values of $\bar{n}$ and we fit for $m = \mu = 0$ the potential $\Omega^{\bar{n}}_{min}(T)$ in the high temperature region. As example we report in Fig.6.29 the fit for $\bar{n} = 10$. It results that:

$$\Omega^{\bar{n}}_{min}(T) \sim -log(T^{2\bar{n}}) \quad \Rightarrow f^{\bar{n}} \sim -T\, log(T^{2\bar{n}}) \tag{6.42}$$

As expected from the logarithmic dependence on the temperature form of the potential (6.34), we have that the free energy diverges as $\sim -T\, log(T)$ instead of the wanted $\sim T^4$ trend.

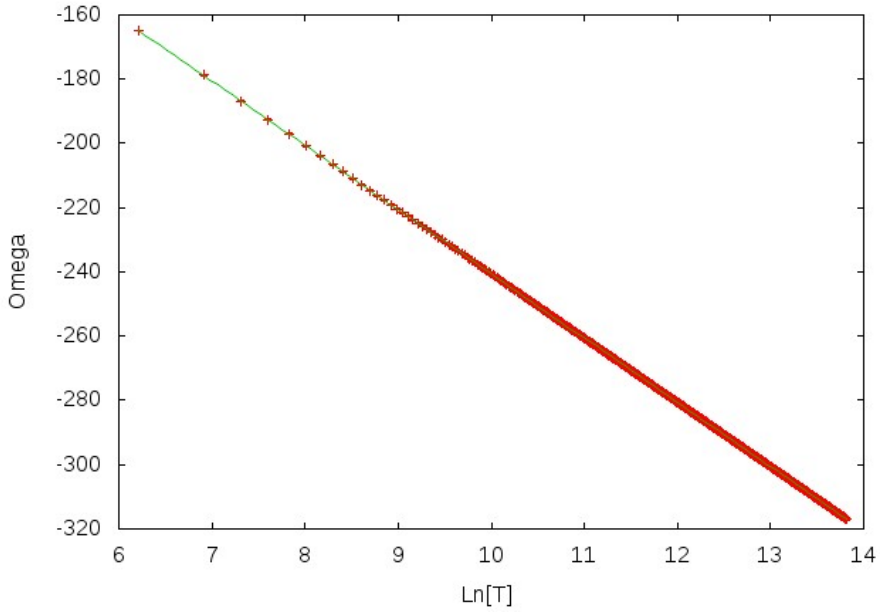

Figure 6.29: Ω_{min} for $m = \mu = 0$ at high temperature as a function of $Log(T)$ for $\bar{n} = 10$. The divergence is $\sim -log(T^{20})$.

6.4 Attempts to modify the Random Matrix model at imaginary chemical potential

A still open issue regards the capability of the RM to reproduce the phase structure of QCD even at *imaginary* chemical potential. For instance is this model able to exhibit something similar to the Roberge-Weiss transition at $\mu_{q,I}/T = (2k+1)\pi/3$ described in Sec.3.2.8? Does this model have anything similar to a $Z(3)$ center symmetry? Is it possible to replay a kind of Polyakov loop?
Before trying to answer these questions, we have to notice that the model of the previous sections, apart the good effort undertaken with the insertion of all the Matsubara modes, is not able to reproduce the *periodicity* of $2k\pi$ of the partition function in the imaginary baryon chemical potential, a property strictly related to the quantization of the baryon charge.

6.4.1 The Morita-Nakamura model

An attempt in this direction was implemented by Morita and Nakamura [36]. Without absorbing the constant terms inside the definitions of T and μ, they modified the effective potential of Eq.(6.11) through the substitution:

$$\frac{b}{N_c}\mu + i\pi aT = \pi aT\left(i + \frac{b}{a\pi N_c}\frac{\mu}{T}\right) \longrightarrow \pi aT\left(i + \frac{b}{a\pi N_c}2sinh\frac{\mu}{2T}\right) \tag{6.43}$$

This modified potential becomes:

$$\begin{aligned}\Omega^{MN}(\Phi)/N_f = \phi^2 - \frac{1}{2}\ln\Big\{\Big[(\phi+m)^2 - \tilde{T}^2\Big(Asinh(\mu/2T)+i\Big)^2\Big] \\ \times\Big[(\phi+m)^2 - \tilde{T}^2\Big(Asinh(\mu/2T)-i\Big)^2\Big]\Big\}\end{aligned} \tag{6.44}$$

where $\tilde{T} = a\pi T$ and $A = 2b/a\pi N_c$. It is easy to see that Ω has the correct periodicity of 2π in μ_i/T. We remember that μ here is the *baryon* chemical potential. If we are interested in reproducing a periodicity of $2k\pi T/3$ in the imaginary *quark* chemical potential, we can proceed simply substituting by hand $\mu = 3\mu_q$. More elegantly we can try to split the determinant of the original partition function in three new determinants in which μ/T is shifted by $2i\pi/3$ and $4i\pi/3$ (that is $det[f(\mu/T)] \to det[f(\mu/T)]\, det[f(\mu/T + i2\pi/3)]\, det[f(\mu/T + i4\pi/3)]$) and consider now μ as the *quark* chemical potential.

The "split" potential hence is:

$$\begin{aligned}\Omega^{MN}_{split}(\Phi)/N_f = \phi^2 - \frac{1}{6}\ln\{&[(\phi+m)^2 - \tilde{T}^2(Asinh(\mu/2T)+i)^2] \\ &\times[(\phi+m)^2 - \tilde{T}^2(Asinh(\mu/2T)-i)^2] \\ &\times[(\phi+m)^2 - \tilde{T}^2(Asinh(\mu/2T+2i\pi/3)+i)^2] \\ &\times[(\phi+m)^2 - \tilde{T}^2(Asinh(\mu/2T+2i\pi/3)-i)^2] \\ &\times[(\phi+m)^2 - \tilde{T}^2(Asinh(\mu/2T+4i\pi/3)+i)^2] \\ &\times[(\phi+m)^2 - \tilde{T}^2(Asinh(\mu/2T+4i\pi/3)-i)^2]\}\end{aligned} \tag{6.45}$$

We can now try to deduce the phase diagram of this model. At real μ the Morita-Nakamura modification exhibit a similar structure to the original model only at $\mu/T \ll 1$ (indeed $sinh(x) \approx x$ for $x \to 0$) with the usual pattern of second order (crossover)-first order line for zero (nonzero) mass. The "split" potential only modifies the magnitudes in the phase diagram. This is clearly shown for $m = 0.05$ in Fig.6.30.

At imaginary μ in the massless case both models show a second order line (continuation of the real μ one) which starts from $(T/T_c = 1, \mu_i/T = 0)$ for the first and $(T/T_c = 1.757, \mu_i/T = 0)$ for the second that oscillates with a really small amplitude in μ_I/T with a period of $2k\pi$ (for Ω^{MN}) and $2k\pi/3$ (for Ω^{MN}_{split}). This is shown in Fig.6.31.

As expected both models are not able to reproduce the QCD-expected Roberge Weiss transition lines, as already supposed by Morita and Nakamura in their article.

6.4.2 The insertion of a *Polyakov phase*

We still stay for this moment on the Morita-Nakamura model. The last effort in inducing a kind of RW transition is to take into account the Polyakov loop in the RM theory following the hint of Stephanov [48]. The basic idea is to introduce the phase of the averaged Polyakov loop $\psi_p \equiv arg\ \langle\ell\rangle$ as a shift in the imaginary chemical potential. We can suppose that for temperature higher than a certain T^* we have $\psi_p = 0$, whereas below T^* the effective potential Ω has to be minimized even with respect to ψ_p (in addition to ϕ), which can assume only three discrete values. To summarize:

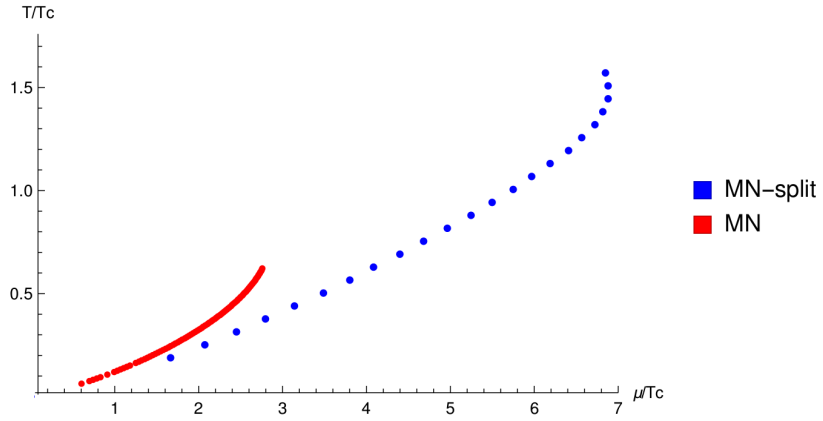

Figure 6.30: First order line of the Morita-Nakamura model (red) and of the "split" model (blue) and at $m = 0.005$ at real chemical potential. The normalizations of T and μ are different with respect to the original Stephanov's model.

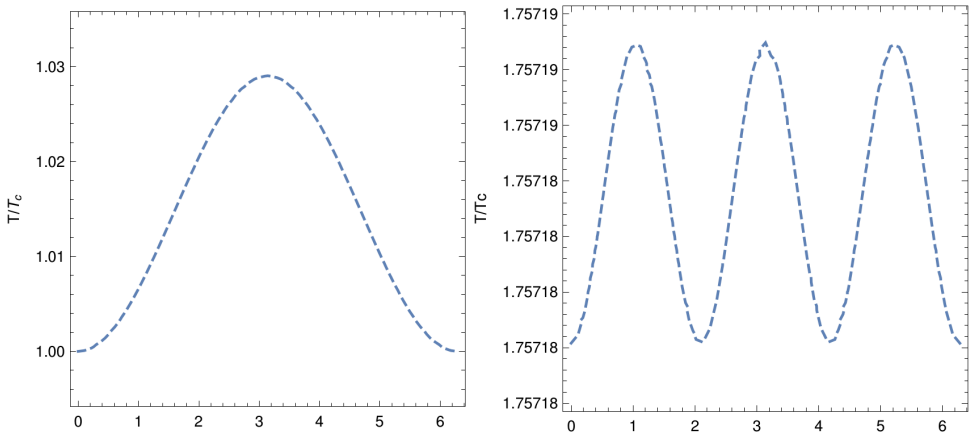

Figure 6.31: Second order lines at imaginary chemical potential in the standard Morita-Nakamura model (2π periodic, *left*) and in the "split" modification ($2\pi/3$ periodic, *right*). In the second plot the line starts at $T_c^{split} \approx 1.757\, T_c$.

$$\begin{aligned} &\text{If } T > T^* \qquad \psi_p = 0. \\ &\text{If } T < T^* \qquad \psi_p = \begin{cases} 0 \\ \frac{2\pi}{3} \\ \frac{4\pi}{3} \end{cases} \end{aligned} \tag{6.46}$$

We will talk more about T^* at the end. The article of Stephanov does not consider any chemical potential, but introduce the Polyakov phase as a shift in the Matsubara frequencies $\omega_n = (2n+1)\pi T + \psi_p$. Since we want to hold the periodicity in μ_I/T, we choose to modify the Morita-Nakamura model shifting the *quark* chemical potential $\mu_i^Q/T \to \mu_i^Q/T + \psi_p$. We choose to insert the factor $1/N_c = 1/3$ inside the argument of *sinh* and to have the quark chemical potential $\mu_Q = \mu_B/N_c$. After this we introduce the shift with ψ_p:

$$\begin{aligned} \Omega(\phi)/N_f = \phi^2 - \frac{1}{2}\ln\{&[(\phi+m)^2 - (\pi a T)^2\left(\frac{2b}{\pi a} sinh\left(\frac{\mu_Q + i\psi_p}{2T}\right) + i\right)^2] \\ &\times[(\phi+m)^2 - (\pi a T)^2\left(\frac{2b}{\pi a} sinh\left(\frac{\mu_Q + i\psi_p}{2T}\right) - i\right)^2]\} \end{aligned} \tag{6.47}$$

It is now possible to analyze the minima of the effective potential as a function of ψ_p. For instance, taking the simplified case of $m = 0$ and going to high temperatures, this ensures us to have only a minimum at $\phi = 0$. We can see that for $\mu_i^Q/T = \pi/3$, π, $5\pi/3$ (that is $(2k+1)\pi/N_c$) we have that Ω "changes" the value of ψ_p to be minimized:

$$\begin{cases} \mu_i^Q/T = \pi/3, & \psi_p = 0 \longrightarrow 4\pi/3 \\ \mu_i^Q/T = \pi, & \psi_p = 4\pi/3 \longrightarrow 2\pi/3 \\ \mu_i^Q/T = 5\pi/3, & \psi_p = 2\pi/3 \longrightarrow 0 \end{cases} \tag{6.48}$$

This behavior is shown in Fig.6.32.
We can now compute the average quark density of this modified model and plot it as a function of μ_i^Q/T. Admitting only $\psi_p = 0$ (i.e for $T < T^*$) we have a continuous behavior, whereas, minimizing the potential even with respect to the three possible value of Polyakov phase ($T > T^*$), we obtain for the quark density to be discontinue every $(2k+1)\pi/3$, as happens in the RW transition.
The problem is the temperature T^*. We would like that such a critical temperature (that in principle should be equal to the T_{RW} obtained through lattice simulations) could arise naturally from the model. But we have inserted it by hand as an external parameter and this really sounds like an artificial trick.

To conclude we can say that the chiral Random Matrix model seems to be constitutively not able to reproduce in a natural way the Roberge-Weiss transition and in general the phase structure at imaginary quark chemical potential. The absence of the gauge degrees of freedom leads to an artificial introduction of the effects of a Polyakov loop through a shift in the fermionic boundary conditions. Furthermore the Morita-Nakamura modification alters the interpretation of the

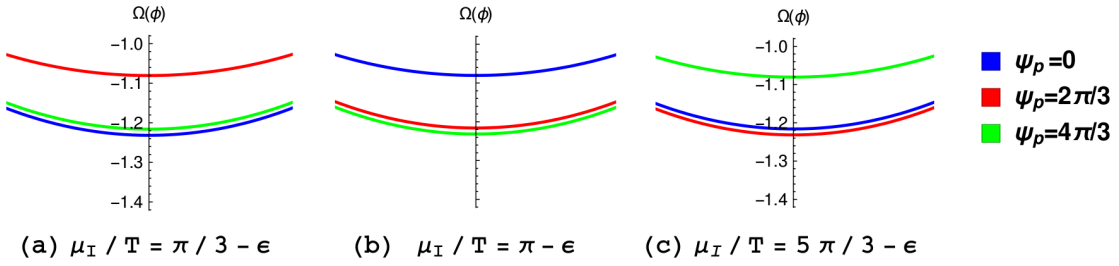

Figure 6.32: Minimum in $\phi = 0$ of the effective potential at $m = 0$ and $T = 3$ for the different values of the Polyakov phase. The "correct" minimum in every figure is the lowest one. In the three figures we show the "jump" in the values of ψ_p when $\mu_I/T = (2k+1)\pi$.

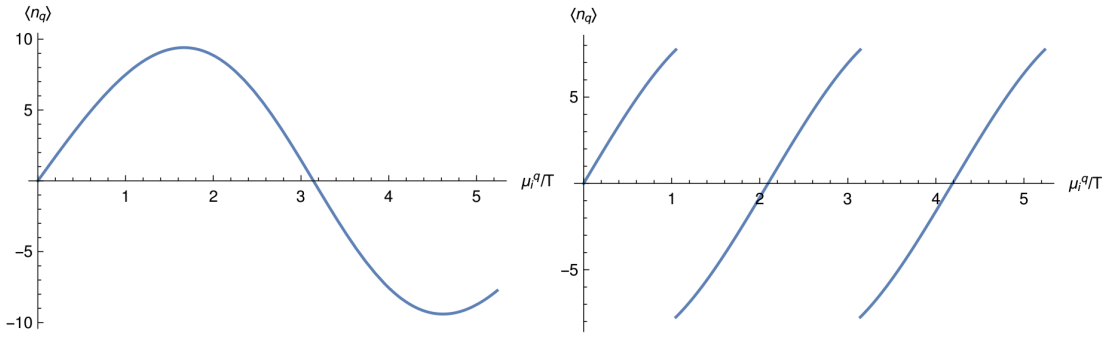

Figure 6.33: Imaginary part of the average quark density as a function of μ_i^Q/T. On the *left* we have the behavior at $T < T^*$ and on the *right* for $T > T^*$. Including the three different values for ψ_p discontinuities arise at $\mu_i^Q/T = (2n+1)\pi/N_c$.

boundary conditions of the fermions in the RM model as usually intended. Indeed to save the periodicity we implement the shift as $\omega_n + Tsin(\mu_i^Q/T + \psi_p)$ instead of the natural way $\omega_n + \mu_i^Q + \psi_p T$. However an interesting article that try to reproduce the center symmetry through a Random Matrix model for the eigenvalues of the Polyakov loop was proposed by Bruckmann in Ref.[10], although it is really different from the usual approach of the χRMT. Maybe it could be taken as an inspiration for future works.

Chapter 7

An attempt with LQCD data

The RM model has the advantage to be expressed as a function of an effective potential and hence to be analytically solvable. In principle Taylor expanding in μ such effective potential one could obtain coefficients of arbitrary high order and estimate the radius of convergence of the series with an high precision, detecting the nearest singularity at different temperatures. In this sense the RM model can be seen as a really interesting *toy model* to compare the efficiency and the limits of different methods of radii extrapolation.
We have now to increase the level of the challenge trying to analyze Lattice QCD (LQCD) data and check if the previous methods are still useful or not. In LQCD we have not the fortune to know an analytic form of the partition function, but we have to approximate the path integral through Monte Carlo simulations on the lattice. Using the technique of the *imaginary chemical potential* described in Sec.3.2.7 we are able to perform simulations at nonzero μ_I and extrapolate informations about the real-μ region avoiding the sign problem.

As a first exercise we can check if we succeed or not in the estimation of the radius of convergence from a Taylor expansion in μ_I of an observable which has a known singularity on the $\mu_I > 0$ axis. We remember that the connection with the lattice units is: $\hat{m} = am$, $\hat{\mu} = a\mu$, $T = 1/aN_t$, where a is the lattice size, $\hat{m}$, $\hat{\mu}$ are the adimensional mass and chemical potential. Taken $N_f = 2$, we know that the baryon number n_B can be used as an order parameter for the Roberge-Weiss transition at $\mu_{q,I}/T = \pi/3$. We choose a value of the mass $\hat{m} = 0.2$ for which the endpoint of the RW line is of the second order (look at Sec.3.2.9 about the *Columbia plot*). The baryon number is purely imaginary for imaginary chemical potential, hence when we write n_B from now on we mean its imaginary part. The lattice we are using is $N_s \times N_t = 48 \times 4$. In Fig.7.1 we show the very precise lattice data.

Known that $\theta = \mu_{q,I}/T = \hat{\mu}_{q,I} N_t$, to fit this data we have used an ansatz for the free energy of the form (we call $\hat{\mu}_{q,I} \equiv \hat{\mu}$):

$$f(\hat{\mu}) = a_1 \, cos(3N_t\hat{\mu}) + a_2 \, (1 - cos(3N_t\hat{\mu} - \pi))^{a_3} \tag{7.1}$$

which respects the $2\pi/3N_t$ periodicity and the parity in $\hat{\mu}$. This form of the free energy gives us the wanted behavior near the RW criticality. Indeed if we expand the "singular" part of the free energy for little $\bar{\hat{\mu}} = \hat{\mu} - \pi/3N_t$ we have:

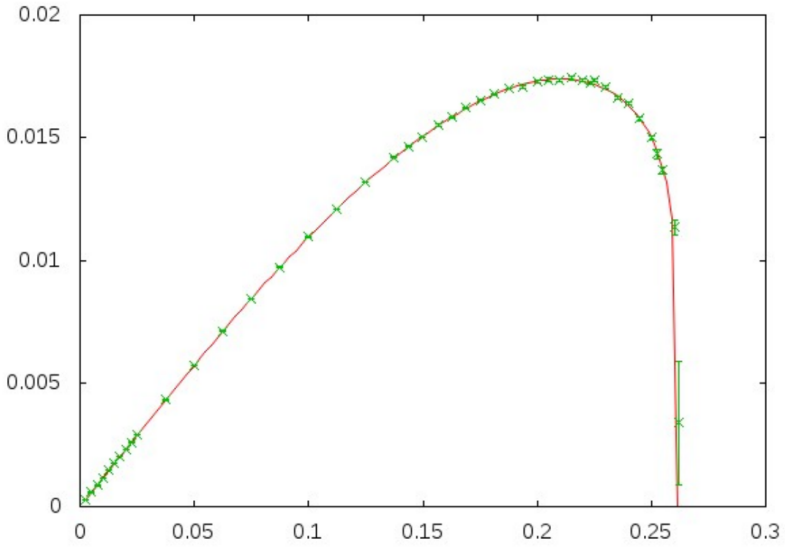

Figure 7.1: Imaginary part of the baryon number as function of $\hat{\mu}_{q,I}$ with a mass of $\hat{m} = 0.2$ for which the RW endpoint is of the second order.

$$f_{sing} \sim (\bar{\hat{\mu}}^2)^{a_3-1} \tag{7.2}$$

From Eqn:(7.1) it follows that the ansatz for the baryon number is:

$$n_B(\hat{\mu}) = \tilde{a}_1\, sin(3N_t\hat{\mu}) + \tilde{a}_2\, sin(3N_t\hat{\mu} - \pi)(1 - cos(3N_t\hat{\mu} - \pi))^{a_3-1} \tag{7.3}$$

Near the criticality:

$$n_B \sim \bar{\hat{\mu}}(\bar{\hat{\mu}}^2)^{a_3-1} = \bar{\hat{\mu}}^{2a_3-1} \tag{7.4}$$

To understand the physical meaning of the exponent a_3, let us remember that the universality class of this second order phase transition is the one of the 3d Ising model. The imaginary chemical potential can be interpreted as a magnetic field and the baryon number as the magnetization. Hence the critical exponent should be $m \sim h^{1/\delta}$, with $\delta \simeq 4.79$. From this we expect a value of a_3:

$$2a_3 - 1 = +1/\delta \qquad \Rightarrow \qquad a_3 \simeq +0.60 \tag{7.5}$$

Using the ansatz Eq.(7.3) and fitting around the criticality we find $a_3 = +0.58(1)$.

We now want to try to extrapolate such criticality through a radius of convergence estimation of the baryon number Taylor expansion in $\hat{\mu}_{q,I}$ near the origin. To do this we need to estimate as many coefficients as we can from the data. We fit the data with a truncated polynomial in $\hat{\mu}_{q,I}$, assuming for the fitted coefficients to be approximated to the ones of the Taylor series around the origin. We have to hope in this way to obtain a sufficiently high number of coefficients in order to perform one of the techniques of the previous sections to extract the radius of convergence.
To fit the data we proceed varying either the degree of the polynomial and the fitting range, to verify the numerical stability of the coefficients and if exists a

maximum degree over which the fit fails. Extending the range of the fit we have to be careful because approaching the criticality, by definition, the Taylor expansion of the function (7.3) *is not equal* to the function itself. The other problem is that if one wants only to use data far from the criticality, the best polynomial fit results to have only few powers, hence only few radii would be available for the radius of convergence estimate. On the other hand, increasing the fit range, the polynomial fit seems to require more and more powers, but there is not a real stability of the coefficients (apart the first two-three).

It results that the sign of the fitted cofficients is alternate.[1] In principle no one ensures us that this alternate pattern is extended for *all the coefficients* and not only for the available ones, but let us suppose this is true. If the sign is not *definitively* constant, then the singularity can be in general complex (lying at a distance R but with an arbitrary phase). The nearest singularity in general could not lie on the direction of the expected one. This seems to be the case: for a series with alternate signs, the position of the nearest singularity is on the *"negative real"* axis. We are considering a series $\sum_{n=1}^{\infty} c_{2n+1}\hat{\mu}^{2n+1} = \sqrt{t}\sum_{n=1}^{\infty} c_{2n+1}t^n$ (with $t = \hat{\mu}^2$) hence the singularity should be in the $Re(t) < 0$ direction, or purely imaginary in $\hat{\mu}$. The only thing that the radius of convergence can tell us is the maximum distance below which the singularity that we want to find *is not* present.

However we can try to check if the methods used to extrapolate a radius of convergence in the RM model result to be useful even in this case to determine the location of a singularity, wherever it is. Since the series of the baryon number is odd in $\hat{\mu}$ let us suppose for the baryon number to have a behavior in proximity of the *nearest* singularity of the form: $n_B(t) \approx A(t)(1 + t/t_c)^{-\lambda} + B(t)$, where $t = \hat{\mu}^2$. We have assumed this behavior because, as assumed above, the singularity should be onto the negative real axis $t_c < 0$. Even in such a case we should be able to use the Domb-Sykes method to extrapolate the singularity. Expanding the previous ansatz for the baryon number around $t = 0$ and computing the ratio of two consecutive coefficients:

$$\frac{1}{R_n^2} = \frac{c_n}{c_{n-1}} = -\frac{1}{t_c}\left(1 + \frac{\lambda - 1}{n} + O\left(\frac{1}{n^2}\right)\right) \tag{7.6}$$

Notice that if $t_c < 0$ in the $n \to \infty$ limit we have the correct sign for the radius.
Before working with the simulated data, it can be interesting to see if the ansatz (7.3) for the baryon number is able or not to localize the RW singularity through a radius of convergence extrapolation. Taylor expanding it around $\hat{\mu} = 0$ (with the theoretical value of $a_3 = +0.60$), we can deduce a sequence of estimated radii and try to extrapolate the radius of convergence á la Domb-Sykes (7.6) but now for a *positive* singularity. Performing a linear fit (see Fig.7.2) we correctly obtain $\hat{\mu}_c = 0.27(2)$ that is compatible with the theoretical prediction $\pi/12 \approx 0.26$.

Let us look at the data. We analyzed the variation of the degree of the fitting

[1] This does not happen if we consider the ansatz (7.3), for which definitely there is a constant sign of the coefficients and this corresponds to a singularity on the positive real axis, as what happens at $\hat{\mu} = \pi/3N_t$.

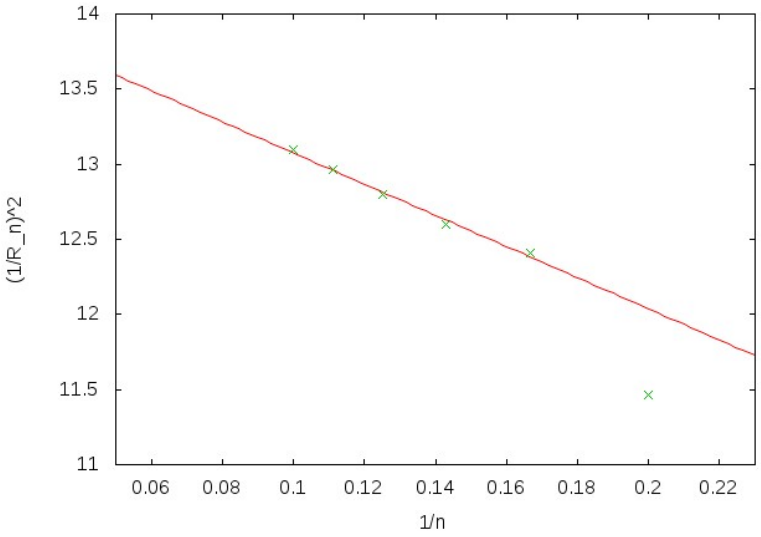

Figure 7.2: Domb-Sykes estimation for the radius of convergence of the Taylor series of the function $n_B(\hat{\mu}) = \tilde{a}_1\, sin(3N_t\hat{\mu}) + \tilde{a}_2\, sin(3N_t\hat{\mu} - \pi)(1 - cos(3N_t\hat{\mu} - \pi))^{a_3 - 1}$ near $\hat{\mu} = 0$. The extrapolated value $\hat{\mu}_c = 0.27(2)$ is compatible with the RW singularity at $\pi/12 \approx 0.26$.

polynomial and the range of fit to determine the coefficients. We succeed in estimating the coefficients up to the nineth different from zero (or c_{19} in the $\hat{\mu}$ expansion).
At this point we try to perform the linear fit (7.6). The first ratios can be excluded from the fit since the Domb-Sykes method works only asymptotically in n. Looking at Fig.(7.3.a), a curious thing that can be noticed is that, even taking into account the errors, the value of the estimated radii R_n^2 seems to systematically *increase* with n, instead of decreasing like in the previous example or like in RM model. This a priori does not exclude the possibility of a finite radius of convergence to exist. As shown in Fig.(7.3.a) a fit of $1/R_n^2$ provide us a *positive* estimation of t_c, (hence a *negative* estimation of the ratio) of $t_c = 0.03(2)$. Such behavior holds even with the parabolic corrections.
To obtain a positive estimation of the radius therefore we decide to try a parabolic fit in $(R_n)^2 = -t_c(1 + (1 - \lambda)/n + b/n^2)$ instead of $1/(R_n)^2$. Since we have only few measures, the estimated values vary significantly depending of the number of excluded low order radii. For instance excluding the first three radii from the fit we obtain $|\hat{\mu}| = 0.16(24)$ whereas excluding the first two $|\hat{\mu}| = 0.41(23)$. Both estimates could in principle be compatible with an imaginary singularity closer to the origin with respect the RW one (situation that could justify an alternating sign of the coefficients), but even with the RW singularity. However no precise estimates seem to be feasible in this way. The methods of radius estimation of the truncated Taylor series in this case do not seem to work well as in the Random Matrix model case. Maybe this is due to an imprecise estimation of the coefficients, or even to a different singular behavior of the function near the unwanted singularity with respect to the supposed one. Even the Zinn-Justin or the Padé approximants methods do not

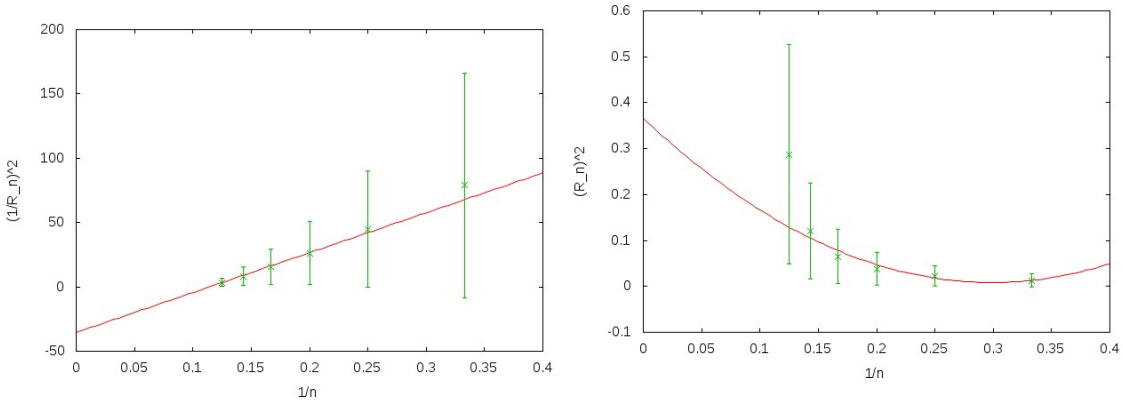

(a) $1/(R_n^2)$ with $1/n$ (b) R_n^2 with $1/n$

Figure 7.3: Linear and parabolic Domb-Sykes fits respectively for $1/(R_n^2)$ and R_n^2.

to provide clear informations. This does not mean that all this methods are not applicable in LQCD, but the particularity of the chosen data makes them not really useful.

Chapter 8

Conclusions

8.1 Achievements

Stephanov's model seems to be the simplest RM model that reproduces some of the main features of the phase structure of QCD with two flavors. In this work we studied deeply the advantages and the limits of such model, especially analyzing the behavior of the zeros of the partition function in the complex μ plane, the branching points of the effective potential Ω, the location of the phase boundaries, the critical endpoint and the spinodal lines.
We performed at fixed temperature a Taylor expansion of the minimized Ω_{min} (i.e the free energy apart a T factor) in the chemical potential near $\mu = 0$ and then studied the temperature behavior of the coefficients, together with their convergence to the thermodynamic values increasing the matrix size N. We analyzed the sequence of estimated radii of convergence $\{r_n = \sqrt{c_n/c_{n+2}}\}$ as a function of the temperature and the sign of the ratio c_n/c_{n+2} as a significant criterion to have or not a real singularity.
We tried to verify the efficiency of different mathematical methods to estimate the radius of convergence of a series whose only few coefficients are known. In particular the Domb-Sykes and the Zinn-Justin methods seem to provide extrapolations of the radii of convergence that are in good agreement with the location of the spinodal line estimated through a branching points analysis. Even the Neville-Aitken extrapolation seems to allow a good estimation of the radius already in the second step, eliminating the leading corrective terms in the $(1/n)$ expansion. The Padé approximation did not proved to be a useful method to estimate the critical point, differently for instance from what found in a 3D Potts model study of Ref.[6]. It seems to be able to asymptotically locate the of the spinodal line but the convergence to the exact values is rather slowly.
A study of the extrapolated radii as function of the maximum available order n_{max} in the Taylor expansion has been performed, showing a decreasing behavior of the estimation increasing the order ($\sim 1/n_{max}^{3/2}$). An estimation for the parameter λ of the ansatz $\Omega_{min}(\mu) \sim (1 - \mu/\mu_c)^{-\lambda}$ near the critical point, related with the critical exponent δ through $1/\delta = 1 - \lambda$ has lead to the result $\lambda = -1.2(2)$, in accordance with its predicted mean field value $\lambda_{MF} \simeq -1.33$.

We modified Stephanov's model including all the Matsubara modes, with the

intent to verify whether the phase structure could change. We verified that including an arbitrary number of Matsubara modes the phase boundary does not change, because the leading term near the transition is still the one related to the lowest Matsubara frequency. We computed the high T behavior of the free energy density at $T = \mu = 0$, verifying that $f(T) \sim T\, log(T^{2\bar{n}})$ (instead of the expected $\sim T^4$ for QCD) where $\bar{n}$ is the number of frequencies included in the model.

As a next step we tried to understand if the RM model is able or not to reproduce the features of the phase diagram at imaginary chemical potential. With this purpose we considered at first the standard Morita-Nakamura modification to ensure periodicity of $2k\pi$ in μ/T, and secondly we split the fermionic determinant to obtain periodicity of $2k\pi/3$. At zero masses, the phase structure is given by an oscillating continuation of the second order transition line from real μ. As a next step we tried to insert the influence of the Polyakov loop by imposing that the imaginary chemical potential was shifted by a discrete phase ψ_p over a certain temperature T^* and we have minimized Ω even with respect to ψ_p. This leads to encouraging jumps of the Polyakov phase and to discontinuities of the quark density at the Roberge-Weiss points. However the main problem is that such temperature T^* has been inserted externally and in a totally arbitrary way.

The last effort was to apply the previous mathematical tools to extrapolate a LQCD singularity, that is the Roberge-Weiss singularity of the baryon number at $\mu_I/T = \pi/3$. A precise estimation of the coefficients through a polynomial fit in such case was a really difficult challenge. Furthermore, the alternate sign pattern makes the nearest singularity not the RW one, and the Domb-Sykes and other methods seem to not be able to detect it efficiently.

8.2 Limits of the model and future challenges

After having shown all its advantages, it is important at the end of this work to focus honestly on the constitutive limits of the original Stephanov's RM model, without forgetting that it still remains a *model* of QCD. This can be the only way for trying to improve it in the future or to proceed toward other directions. Let us make a list of some of them:

- This model predicts for a zero mass a second-order phase transition for *any* number of flavors, but we know that this is a feature only of the two-flavors-QCD: this model is only valid at $N_f = 2$.
- Ref.[29] also shows that the schematic model of the QCD partition function (6.10) is not able to reproduce the zero-temperature Fermi-Dirac distribution.
- Such model is not able to reproduce the μ independence of the partition function in the low density phase.
- This model is not able to reproduce the known 2π periodicity in $\mu_{I,B}/T$ related

to the quantization of the baryon charge.[1]

- Such model is not able to provide real predictions for the phase diagram of QCD because the physical values are outside the *microscopic range* inside which all equivalences are allowed. Furthermore it predicts a *mean field* chiral transition.

In addition to these points, it would be important to introduce more clearly in the RM approach the gauge fields and the color degree of freedom, as well as the center symmetry and the Polyakov loop behavior.[2] However we think that an introduction in the model of something similar to the color symmetry could be a non trivial task. Indeed one of the advantages of Stephanov's RM model is the fact that the integral that reproduces some of the global symmetries of the QCD partition function can be treated analytically. Introducing further degrees of freedom we could have integrals that we are able to treat only numerically and no one ensures us that drawbacks similar to the *sign problem* do not arise.
The relative facility to describe the chiral phase transition and the QCD phase structure in the (T, μ) plane through such a simplified model as Stephanov's one, makes the application of the Random Matrix models to the QCD phase diagram an interesting topic of study and a better knowledge and improvement of similar methods a worth challenge for the future.

Considerations can be even made about the ability of the RM model to allow relatively precise estimation of the criticalities in the (T, μ) plane using only a finite number of Taylor coefficients of the free energy in the μ expansion near the origin. To perform the Domb-Sykes extrapolation in the thermodynamic limit, for instance, we used the knowledge of 8 coefficients (up to c_{16} in the μ expansion, since the odd terms were zero). An interesting figure is Fig.6.17, that shows the fit extrapolation as a function of the number of available coefficients. For instance it can be noticed that a fit with 4 available estimated radii $\{r_n\}$ provides an almost 2% higher radius of convergence than a fit with 8 coefficients.
What happens in LQCD? An instructive investigation of the critical endpoint of QCD at $N_f = 2$ through a Taylor expansion of the baryon number susceptibility χ_B can be found for instance in Ref.[25]. Here the coefficients χ_B are computed up to the 6th order (χ_B^0, χ_B^2, χ_B^4, χ_B^6) [3] and it is analyzed their temperature dependence and the finite volume effects near the critical region. An estimation of the radius of convergence through the root method and the ratio method is performed approaching the thermodynamic limit and it provides estimations for T_E and μ_E. Derivation of high order coefficients clashes with the difficulty of computing high order derivatives of the partition function Z. Indeed they can be written through expectation values of operators involving traces of inverses and derivatives of the Dirac operator whose computational cost is high.

[1] Attempts to solve the last two problems can be found in a never-published paper of Halasz Ref.[28]

[2] An attempt to introduce the color be found in the Vanderheyden-Jackson model [55] in the Appendix, whereas a model for the Polyakov loop is the Bruckmann one [10]

[3] Because of CP symmetry it comes out that only the even coefficients are nonzero.

Appendix A

The Dyson index

When we introduced the partition function of the RM model (Eq(5.1)) we have seen that the matrix elements of W can be defined to assume real, complex or quaternion real values. This corresponds to different values of β, the *Dyson index*, that is the number of real parameters needed to specify the matrix elements. Without going into details, it is interesting to see how the nature of such matrix elements can be related to particular symmetries of the euclidean Dirac operator. The first who studied such problem applied to RMT was Verbaarschot [56], inspired by a work of Dyson [16]. We have previously seen that because of the anticommutation rule $\{\gamma_5, D\} = 0$ the euclidean Dirac operator $D = \gamma_\mu \partial_\mu + i\gamma_\mu A_\mu$ can be reduced in the chiral basis to the form:

$$D = \begin{pmatrix} 0 & iW \\ iW^\dagger & 0 \end{pmatrix} \tag{A.1}$$

1. Taking $N_c \geqslant 3$, for fermions in the fundamental representation the matrix elements of the Dirac operator are complex, $W_{ij} \in \mathbb{C}$. This leads to $\beta = 2$.

2. Let us consider the case of $N_c = 2$. In such case the Dirac operator has a further symmetry. Indeed if we define with C the charge conjugation operator ($\gamma_\mu^* = -C\gamma_\mu C^{-1}$), K the complex conjugation operator, σ_i the Pauli matrices, it is possible to derive [56] that:

$$[C^{-1}\sigma_2 K, D] = 0 \tag{A.2}$$

Such a operator has the property:

$$(C^{-1}\sigma_2 K)^2 = 1 \tag{A.3}$$

that allows to find a basis in which the Dirac operator has *real* matrix elements, $W_{ij} \in \mathbb{R}$. Hence $\beta = 1$.

3. The third class is obtained considering the *adjoint representation*. In such case we have that the Dirac operator can be expressed in the form:

$$D_{ab} = \gamma_\mu \partial_\mu \delta_{ab} + f^{abc}\gamma_\mu A_\mu^c, \tag{A.4}$$

where f^{abc} are the structure constants of $SU(N_c)$. In such case the further symmetry is:

$$[D, C^{-1}K] = 0 \tag{A.5}$$

where the operator which commutes with D:

$$(C^{-1}K)^2 = -1 \tag{A.6}$$

In this case Dyson suggests that the Dirac operator can be diagonalized by a symplectic transformation[1] , that is equivalent to say that the elements are real quaternions (if we define $W^{\dagger}_{l,m} = a_1 1 + a_2\, i + a_3\, j + a_4\, k$ with $a_i \in \mathbb{R}$ and $\{1, i, j, k\}$ a basis of $\mathbb{R}^4$, we have that $W^{\dagger}_{l,m} = \bar{W}_{l,m}$, where $\bar{W}_{l,m} = a_1 - a_2\, i - a_3\, j - a_4\, k$ is the quaternion conjugate). This implies that $\beta = 4$.

More generally it is possible to see that a Dyson index β different than two, is related with the presence of so-called *antiunitary symmetries*, i.e. the existence of a unitary operator U which "anti-unitarily" commutes with the hamiltonian H:

$$[H, UK] = 0. \tag{A.7}$$

This relation implies $(UK)^2 = 1$ or $(UK)^2 = -1$, which corresponds to $\beta = 1$ and $\beta = 4$ respectively [57].[2] For $N_c \geq 3$ in the fundamental representation we have no anti-unitary symmetries (no such a U exists), the hamiltonian is hermitian and $\beta = 2$.

[1] A symplectic matrix M respects the property: $M^T \Omega M = \Omega$, where $\Omega = \begin{pmatrix} 0 & \mathbb{I} \\ -\mathbb{I} & 0 \end{pmatrix}$

[2] This happens because $(UK)^2 = UKUK = UU^*$ is unitary and for the Schur's lemma $UU^* = \lambda\mathbb{I}$ for the irreducible representations. Hence we have $UU^* = UU^*$, $\lambda^* = \lambda \Rightarrow \lambda \in \mathbb{R}$. Since UU^* is unitary, $|\lambda| = 1$ and $\lambda = \pm 1$.

Appendix B

The final form of the partition function

Let us derive the final form of the partition function in the case of an infinite number of Matsubara modes (6.34) and for the only zero mode case (6.10). For this purpose we start from the expression:

$$Z = \int DX exp(-NTrXX^{\dagger}) \prod_{n} det^{N_f} \begin{pmatrix} m & iX + i\Omega_n + \mu \\ iX^{\dagger} + i\Omega_n + \mu & m \end{pmatrix} \tag{B.1}$$

We are using for μ, T and m the units defined in Chap.6. As in Stephanov's model with only one Matsubara frequency, we consider for the "instanton" basis a coupling in temperature of opposite sign in the following sense:

$$\Omega_n = \begin{pmatrix} \omega_n \mathbb{I}_{N/2} & 0 \\ 0 & -\omega_n \mathbb{I}_{N/2} \end{pmatrix} \tag{B.2}$$

The determinant can be written as a Grassmann integral, and if we explicit all the indexes:

$$\begin{aligned} = \int DXD[\Psi\Psi^*] exp\Bigg[- N \sum_{a,b=1}^{N} X_{ab} X^{\dagger}_{ba} + \sum_{f=1}^{N_f} \sum_{a,b=1}^{N} \sum_{m,n=0}^{\infty} \Psi^{*a,f}_{m} \\ \times \begin{pmatrix} m & iX + i\Omega + \mu \\ iX^{\dagger} + i\Omega + \mu & m \end{pmatrix}^{ab,fg}_{mn} \Psi^{b,g}_{n} \Bigg], \end{aligned} \tag{B.3}$$

where we have that "a, b" are the indexes of the "instanton basis", "f, g" are the flavor indexes and "m, n" are related to the specific Matsubara modes. It is useful to remark that $\Omega \equiv \omega_n \delta_{mn} \delta^{fg} \gamma_5^{ab}$, $X \equiv \delta_{mn} \delta^{fg} X^{ab}$, and m and μ are proportional to the identity in all the indexes. The measure $D[\Psi\Psi^*] = \prod_{m,n;a,b}^{f,g} d\Psi^{f}_{m,a} d\Psi^{*g}_{n,b}$.
If we write explicitly the right-handed and the left-handed part of the fermions, $\Psi = (\Psi_R, \Psi_L)$:

$$\begin{aligned} = \int DXD[\Psi\Psi^*] exp\Bigg[- N \sum_{a,b=1}^{N} X_{ab} X^{\dagger}_{ba} + \sum_{f=1}^{N_f} \sum_{a,b=1}^{N} \sum_{m,n=0}^{\infty} \Big[\Psi^{*a,f}_{R,m} m \Psi^{a,f}_{R,m} + \Psi^{*a,f}_{L,m} m \Psi^{a,f}_{L,m} \\ + \Psi^{*a,f}_{R,m} (iX + i\Omega + \mu)^{ab}_{mn} \Psi^{b,f}_{L,n} + \Psi^{*a,f}_{L,m} (iX^{\dagger} + i\Omega + \mu)^{ab}_{mn} \Psi^{b,f}_{R,n} \Big] \Bigg] \end{aligned} \tag{B.4}$$

If we now perform the Gaussian integration in X we obtain:

$$\begin{aligned} &= \int DX\, exp\Bigg[\sum_{f=1}^{N_f}\sum_{a,b=1}^{N}\sum_{m,n=0}^{\infty}\Big[-NX_{ab}X^{\dagger}_{ba} + \Psi^{*a,f}_{R,m}iX_{ab}\Psi^{b,f}_{L,m} + \Psi^{*a,g}_{L,n}iX^{\dagger}_{ab}\Psi^{*b,g}_{R,n}\Big]\Bigg] \\ &= exp\Bigg[-\frac{1}{N}\Psi^{*a,f}_{R,m}\Psi^{b,f}_{L,m}\Psi^{*b,g}_{L,n}\Psi^{a,g}_{R,n}\Bigg] \end{aligned} \tag{B.5}$$

and replacing:

$$\begin{aligned} = \int D[\Psi\Psi^*]\, exp\Bigg[\sum_{f=1}^{N_f}\sum_{a,b=1}^{N}\sum_{m,n=0}^{\infty}\Big[&-\frac{1}{N}\Psi^{*a,f}_{R,m}\Psi^{b,f}_{L,m}\Psi^{*b,g}_{L,n}\Psi^{a,g}_{R,n} + \Psi^{*a,f}_{L,m}m\Psi^{*a,f}_{L,m} \\ &+ \Psi^{*a,f}_{L,m}(iX + i\Omega + \mu)^{ab}_{mn}\Psi^{*b,f}_{R,n} + \Psi^{*a,f}_{R,m}(iX^{\dagger} + i\Omega + \mu)^{ab}_{mn}\Psi^{*b,f}_{L,n}\Big]\Bigg] \end{aligned} \tag{B.6}$$

It can be noticed that we have only quadratic and quartic terms in the fermion variables. We can use the Hubbard-Stratonovich transformation to eliminate the quartic term. If we take $Q^{fg}_{mn} = \psi^{*f}_{L,m}\psi^{g}_{L,n}$, the Hubbard-Stratonovich transformation consists in:

$$exp\left[-NTrQQ^{\dagger}\right] = \int dY exp\left[-NTr[YY^{\dagger}] - iQY^{\dagger} + iYQ^{\dagger}\right], \tag{B.7}$$

where $Y \equiv Y^{fg}_{mn}$ is a non trivial matrix in the flavor and Matsubara indexes. Known that $\Psi_L = i\sigma_2\Psi_R$, we have that $Q^{\dagger fg}_{mn} = -\psi^{*f}_{R,m}\psi^{g}_{R,n}$ this identity we have:

$$\begin{aligned} = \int DYD[\Psi\Psi^*]\, exp\Bigg[\sum_{f=1}^{N_f}\sum_{a,b=1}^{N}\sum_{m,n=0}^{\infty}\Big[&-NY^{fg}_{mn}Y^{\dagger gf}_{nm} + \Psi^{*a,f}_{R,m}(Y^{fg}_{m,n} + m)\Psi^{*a,g}_{R,n} \\ &+ \Psi^{*a,f}_{L,m}(Y^{\dagger fg}_{m,n} + m)\Psi^{*a,g}_{L,n} + \Psi^{*a,f}_{L,m}(i\Omega + \mu)^{ab}_{mn}\Psi^{*b,f}_{R,n} \\ &+ \Psi^{*a,f}_{R,m}(i\Omega + \mu)^{ab}_{mn}\Psi^{*b,f}_{L,n}\Big]\Bigg] \end{aligned} \tag{B.8}$$

Remembering the opposite-sign dependence in temperature of Ω, and integrating in the fermionic variables:

$$= \int DY \exp\left[-NTr(YY^{\dagger})\right] det^{N/2}\begin{pmatrix} Y+m & \mu+iM \\ \mu+iM & Y^{\dagger}+m \end{pmatrix} det^{N/2}\begin{pmatrix} Y+m & \mu-iM \\ \mu-iM & Y^{\dagger}+m \end{pmatrix}, \tag{B.9}$$

where $M \equiv \omega_n\delta_{mn}\delta^{fg}\delta^{ab}$. This is the final form of the partition function, whose features take into account the model of Ref.[30] with only one Matsubara frequency at nonzero μ and T and the model of Stephanov [48] with all the Matsubara frequencies but with zero chemical potential.

At this point we have to do a little digression. We promised in Chap.(6) the explicit

proof of the final form of the partition function with only the lowest Matsubara mode and N_f flavor, Eq.(6.10). The proof is exactly the one we have just shown, simply removing the summation on the frequencies (keeping only $n = 0$) and substituting $Y \equiv Y^{fg}_{mn} \to \Phi \equiv \Phi^{fg}$, where Φ is a $N_f \times N_f$ matrix.

The partition function of Eq.(B.9) can be expressed as a function of an effective potential $\Omega(Y)$. Indeed:

$$= \int DY \exp\Bigg[- NTr\{YY^\dagger - \frac{1}{2} log\Big[[(Y+m)(Y^\dagger+m) - (\mu+iM)^2] \times [(Y+m)(Y^\dagger+m) - (\mu-iM)^2]\Big]\}\Bigg] \equiv \int DY\, exp\,[-N\Omega(Y)] \quad , \tag{B.10}$$

where the trace has to be intended on the flavor and the Matsubara indexes. In the thermodynamic limit $N \to \infty$ this integral can be written through the *saddle point* approximation. The saddle point equation is:

$$-Y + \Big[[(Y+m)(Y^\dagger+m) - (\mu-iM)^2] + [(Y+m)(Y^\dagger+m) - (\mu+iM)^2]\Big] \times \Big[[(Y+m)(Y^\dagger+m) - (\mu+iM)^2][(Y+m)(Y^\dagger+m) - (\mu-iM)^2]\Big]^{-1} = 0 \tag{B.11}$$

We can try for the saddle point equation to use the same ansatz of Ref.[48], that is $Y = y_n \delta_{mn} \phi \delta^{fg} \equiv y_n \delta_{mn} \delta^{fg}$, where $y_n \in \mathbb{R}$. With this substitution we have now to solve:

$$y_n = \frac{(m+y_n)\left((m+y_n)^2 + \omega_n^2 - \mu^2\right)}{\left((m+y_n)^2 + \omega_n^2 - \mu^2\right)^2 + 4\mu^2\omega_n^2} \tag{B.12}$$

If we take $\mu = 0$ we obtain exactly the same result of Ref[48], whereas setting $n = 0$ we have the same result of Eq.(6.20) with only the lowest Matsubara mode. Therefore the effective potential can be written as:

$$\Omega(y, m, T, \mu) = \sum_{n=0}^{\infty} \left[y_n^2 - \frac{1}{2} log\Big[[(y_n+m)^2 - (\mu+i\omega_n)^2][[(y_n+m)^2 - (\mu-i\omega_n)^2]\Big]\right] \equiv \sum_{n=0}^{\infty} \Omega_n(y_n), \tag{B.13}$$

where

$$\Omega_n(x, m, T, \mu) = x^2 - \frac{1}{2} log\Big[[(x+m)^2 - (\mu+i\omega_n)^2][[(x+m)^2 - (\mu-i\omega_n)^2]\Big] \tag{B.14}$$

Hence the obtained effective potential can be expressed as a sum of *independent* potentials, each one related to a specific Matsubara mode. The chiral condensate

can be computed as:

$$\left\langle \bar{\psi}\psi \right\rangle = \frac{1}{N_f V}\frac{\partial log Z_{RM}}{\partial m}\bigg|_{m=0} = \frac{1}{N_f V}\left\langle \frac{N}{2} Tr\left[\begin{pmatrix} W+m & \mu+iM \\ \mu+iM & W^\dagger+m \end{pmatrix} \begin{pmatrix} W+m & \mu-iM \\ \mu-iM & W^\dagger+m \end{pmatrix} \right]^{-1} \times 2 \begin{pmatrix} W+m & \mu \\ \mu & W^\dagger+m \end{pmatrix} \right\rangle \bigg|_{m=0} \tag{B.15}$$

Substituting the previous ansatz we have the solution:

$$\left\langle \bar{\psi}\psi \right\rangle = \sum_{n=0}^{\infty} \frac{2N}{V} y_n \frac{(y_n^2+\omega_n^2-\mu^2)}{(y_n^2+\omega_n^2-\mu^2)^2+4\mu^2\omega_n^2} = \sum_{n=0}^{\infty} \frac{2N}{V} y_n, \tag{B.16}$$

where the last equality follows from Eq.(B.12). The last expression is exactly the same of Ref.[48] and of Ref.[30] for $n = 0$. It would be reasonable to expect that the presence of more Matsubara frequencies can affect in some way the phase boundary of the chiral phase transition, due to a different vanishing of the order parameter with respect to the $n = 0$ case. In the following section we will see that this is not the case: the phase boundary it is not modified including an arbitrary large number of Matsubara modes.

Appendix C

Different Random Matrix Models of QCD

In this appendix we briefly summarize the advantages and the limits of *some* other Random Matrix models of QCD, to allow a comparison with the model used in this thesis and to give the reader some useful references to deepen.

C.1 The Akemann Model

Akemann [2] defined a model for the eigenvalues of the Dirac operator in terms of complex eigenvalues, that can be considered as an extension of the usual gaussian unitary ensemble. The partition function in the sector ν and N_f flavors is given by:

$$Z_N^{(N_f,\nu)}(\tau) \equiv \int \prod_{j=1}^{N} dz_j dz_j^* w^{(N_f+\nu)} |\Delta(z_1^2, \ldots, z_N^2)|^2 \tag{C.1}$$

with the weight function:

$$w^{(N_f+\nu)}(z) = |z|^{2(N_f+\nu)+1} exp\left\{-\frac{N}{1-\tau^2}\left[|z|^2 - \frac{\tau}{2}(z+z^{*2})\right]\right\} \tag{C.2}$$

and $\Delta(z_1, \ldots, z_N) = \prod_{k>l}^{N}(z_k - z_l)$ is the Vandermonde determinant. $\tau \in [0,1]$ is a non-Hermiticity parameter that can be related to the chemical potential through as $4\mu^2 = 1 - \tau^2$. With respect to Stephanov's one, this model is always in the broken phase of the chiral symmetry. The advantage of this model is that the eigenvalue representation allows explicit calculations of correlation function inside the microscopic range. However it can be expressed only in terms of the eigenvalues and not through a matrix formulation based on the symmetries of the Dirac operator of QCD. It was shown, comparing the spectral densities, that in the microscopic limit the partition function of Eq.(C.1) agrees with Stephanov's one, but only for *small* chemical potentials.

C.2 The Wettig-Shafer model

The Wettig-Shafer [60] model is a slight modification of the Jackson model [31] at $\mu = 0$ and it considers a more general temperature dependence of the RM partition

function:

$$Z(T,\mu=0)=\int D\Phi \exp\left[-NTr(\Phi\Phi^{\dagger})\right]\prod_{k=1}^{m} det\begin{pmatrix}\Phi+M & iC_k\\ iC_k & \Phi^{\dagger}+M\end{pmatrix} \tag{C.3}$$

where they make interesting considerations about the possible form of C_k based on temperature correlations between instanton/anti-instanton pairs in the instanton liquid model (from which this RM model is inspired.)
At the end they suppose for C to have a diagonal form with $\alpha \in [0,1]$ elements equal to a value c and the remaining are zero. Varying the parameters α and c they study the behavior of the chiral condensate and show the possibility for the system to have in the massless case a transition of the first order, in addition to the known second order one. Maybe this could be useful in the description of the $N_f = 3$ case, which admits a first order transition at $\mu = 0$.

C.3 The Vanderheyden-Jackson model

The Vanderheyden-Jackson [55] model is an attempt to construct a Random Matrix model suitable for the exploration of diquark condensation as well the chiral symmetry breaking. For this purposes they introduced the color degree of freedom but they lost in such way the analogies with the instanton model. They considered a partition function at nonzero μ, T of the form:

$$\begin{aligned}Z(\mu,T)=\int DH D\psi_1^{\dagger}D\psi_1 D\psi_2^{T}D\psi_2^{*} exp\Bigg[i\begin{pmatrix}\psi_1^{\dagger}\\ \psi_2^{T}\end{pmatrix}^{T}\\ \times\begin{pmatrix}H+(\pi T+i\mu)\gamma_0+im & \eta P_{\Delta}\\ -\eta^{*}P_{\Delta} & -H^{T}+(\pi T-i\mu)\gamma_0^{T}-im\end{pmatrix}\begin{pmatrix}\psi_1\\ \psi_2^{*}\end{pmatrix}\Bigg].\end{aligned} \tag{C.4}$$

Here H is a random matrix of dimension $4\times N_c\times N$ which represents the interaction of a single quark with a gluon background. The parameters m and η are the *magnetic field* variables for the chiral symmetry breaking and the color symmetry breaking, respectively. $P_{\Delta}=iC\gamma_5\lambda_2$ where λ_2 is the Gell-Mann matrix and C is the charge conjugation operator. The interaction H is intended to reproduce the effects of gluon fields. If we consider only the effects of a *single gluon exchange* (sge), H has the following block-structure:

$$H_{sge}=\begin{pmatrix}0 & X_{sge}\\ X_{sge}^{\dagger} & 0\end{pmatrix} \qquad \text{with} \qquad X_{sge}=\sum_{\mu=1}^{4}\sum_{a=1}^{8}\sigma_{\mu}\otimes\lambda^{a}\otimes A^{\mu a}. \tag{C.5}$$

Here $\sigma_{\mu}=(1,i\vec{\sigma})_{\mu}$ are the 2×2 spin matrices, and λ_a are the $N_c\times N_c$ Gell-Mann matrices. The $A^{\mu a}$ are real $N\times N$ matrices which represent the gluon fields.
This model has the goal to study the interplay between chiral and color symmetries. The model can be expressed in terms of an effective potential $\Omega(\sigma,\Delta)$ which depends on two couplings A and B that can be tuned to increase/decrease the weight of the

chiral and color symmetries. It is interesting to study the phase diagram in the (T, μ) plane, where one can tune properly the A and B variables to distinguish four types of solution in the *saddle-point*-minimization of the effective potential $\Omega(\sigma, \Delta)$:

- the 0-phase, the trivial phase in which both σ and Δ vanishes,
- the χ-phase, in which the chiral symmetry is spontaneously broken but $\Delta = 0$,
- the Δ-phase,in which the color symmetry is spontaneously broken but $\sigma = 0$,
- the $\chi\Delta$ phase, a mixed phase in which both fields are non vanishing, $\sigma \neq 0$, $\Delta \neq 0$.

The chiral phase is the same as the obtained in Stephanov's model because in this limit the color dependence is factorized and becomes trivial.

C.4 Osborn Model

The Osborn model [38] is one of the first *two matrices* models, where the "chemical potential terms" are not chosen to be constant as in Stephanov's model. Instead he considers another basis where the μ terms are modeled with random matrices as:

$$D_2 = \begin{pmatrix} 0 & iA + \mu B \\ iA^\dagger + \mu B^\dagger & 0 \end{pmatrix}, \tag{C.6}$$

and the partition function is given by:

$$Z(T, \mu) = \int dA\, dB\, w_G(A) w_G(B) \prod_{f=1}^{N_f} det(D_2 + m_f) \tag{C.7}$$

where $w_G(Y) = exp(-\alpha N Tr(Y^\dagger Y))$ are the gaussian weights. One can then modify the partition function in two steps:

- diagonalize the matrix with the substitutions $C = iA + \mu B$ and $D = iA^\dagger + \mu B^\dagger$
- parametrize $C = U(X + R)V$ and $D = V^\dagger(Y + S)U^\dagger$ where U and V are unitary matrices, X, Y are complex diagonal matrices and R, S are complex triangular matrices.

After these transformations it is possible to show that the partition function becomes a function of the elements $z_k = -x_k y_k$. This model can be related to the Akemann one for $2\mu^2 \ll \alpha N(1 + \mu^2)|z_{min}|^2$.
It is interesting to notice that with a μ dependent choice of α (i.e. $\alpha = (1 - \mu^2)\alpha_0$) and a proper renormalization constant one can obtain a μ independent partition function. This would mean that all the thermodynamic quantities would remain at the same $\mu = 0$ values according to the expected independence below a critical value, that is $\mu_c = 1$. At $\mu = \mu_c$ and $T = 0$ this model shows a first order line, but is not able to describe the chirally restored phase at $\mu_c > 1$.

Bibliography

[1] M.M Aggarwal and et al. "An experimental Exploration of the QCD Phase Diagram: The Search for the Critical Point and the Onset De-confinement". In: (2010).

[2] G Akemann. "Microscopic Correlation Functions for the QCD Dirac Operator with Chemical Potential". In: *Phys.Rev.Lett.* 89 (2002).

[3] G. Akemann, J. Baik, and P. Di Francesco. *The Oxford Handbook of Random Matrix Theory*. Ed. by Oxford Handbooks. 2011.

[4] M. Alford. "Color superconductivity in ultra-dense quark matter". In: *Proceedings of science* 001 (2006).

[5] Y. Aoki et al. "The order of the quantum chromodynamics transition predicted by the standard model of particle physics". In: *Nature* 443 (2006), pp. 675–678.

[6] Giovanni Balduzzi. "A better approach to localize the QCD critical point". ETH Zurich, 2015.

[7] T. Banks and Casher. A. "Chiral symmetry breaking in confining theories". In: *Nuclear Physics B* 169 (1980). Ed. by North-Holland Publishing Company, pp. 103–125.

[8] Claudio Bonati et al. "Chiral phase transition in two-flavor QCD from an imaginary chemical potential". In: *Phys. Rev.* D90.7 (2014), p. 074030. DOI: 10.1103/PhysRevD.90.074030. arXiv: 1408.5086 [hep-lat].

[9] E. Brezin et al. *Applications of Random Matrices in Physics*. Ed. by Springer. 2006.

[10] F. Bruckmann. "A random matrix-like model for the Polyakov loop and center symmetry". In: (). URL: http://arxiv.org/pdf/1007.4052.pdf.

[11] P. Chomaz. "The nuclear liquid gas phase transition and phase coexistence: a review". In: *International Nuclear Physics Conference INPC 2001*. Vol. 610. AIP Conference Proceedings 610. Berkeley, United States: American Institute of Physics, July 2001, pp. 167–181. URL: http://hal.in2p3.fr/in2p3-00019902.

[12] P.H Damgaard et al. "The microscopic spectral density of the QCD Dirac operator". In: *Nuclear Physics B* 547 (1999). Ed. by Elsevier Science, pp. 305–328.

[13] M. D'Elia and F. Sanfilippo. "The order of the Roberge-Weiss endpoin (finite size transition) in QCD". In: *Phys.Rev.* D80 (2009).

[14] C. Domb and M.F Sykes. "On the susceptibility of a ferromagnet above the Curie point". In: *Proc.Roy.Soc* A240 (1957), pp. 214–228.

[15] F.J. Dyson. "A Brownian-Motion Model for the Eigenvalues of a Random Matrix". In: *J.Math.Phys* 3 (1962).

[16] F.J. Dyson. "The Threefold Way. Algebraic Structure of Symmetry Groups and Ensembles in Quantum Mechanics". In: *J.Math.Phys* 3 (1962).

[17] Gergely Endrődi. "QCD phase diagram: overview of recent lattice results". In: *J. Phys. Conf. Ser.* 503 (2014), p. 012009. DOI: 10.1088/1742-6596/503/1/012009. arXiv: 1311.0648 [hep-lat].

[18] J. Feinberg and A. Zee. "Non-Hermitean Random Matrix Theory: method of hermitization". In: *Nuclear Physics B* 504 (1997), pp. 579–608.

[19] Ph. de Forcrand and O. Philipsen. "The QCD phase diagram for small densities from imaginary chemical potential". In: *Nucl. Phys.* B642 (2002), pp. 290–306. DOI: 10.1016/S0550-3213(02)00626-0. arXiv: hep-lat/0205016 [hep-lat].

[20] Michael Fromm et al. "The QCD deconfinement transition for heavy quarks and all baryon chemical potentials". In: *Journal of High Energy Physics* 2012.1 (2012), pp. 1–25.

[21] M. Fukugita, M. Okawa, and A. Ukawa. "Finite size scaling study of the deconfining phase transition in pure SU(3) lattige gauge theory". In: *Nucl.Phys.* B337 (1990), p. 181.

[22] K. Fukushima and T. Hatsuda. "The phase diagram of dense QCD". In: *Rept.Prog.Phys* 74 (2010).

[23] J. Gasser and H Leutwyler. "Thermodynamics of chiral symmetry". In: *Physics Letters B* 188 (1997), pp. 477–481.

[24] C. Gattringer and C.B. Lang. *Quantum Chromodynamics on the Lattice - An introductory Presentation*. Ed. by Springer. 2010.

[25] R. V. Gavai and Sourendu Gupta. "The Critical end point of QCD". In: *Phys. Rev.* D71 (2005), p. 114014. DOI: 10.1103/PhysRevD.71.114014. arXiv: hep-lat/0412035 [hep-lat].

[26] E. Guadagnini. *Lezioni di Fisica Statistica*. 2015. URL: http://www.df.unipi.it/~guada/.

[27] A.J Guttmann. "Asymptotic Analysis of Power-Series Expansion". In: C Domb and J Lebowitz. *Phase Transitions and Critical Phenomena Vol.13*. Ed. by Academic Press. 1989.

[28] M.A Halasz. "An improved random matrix model for the chiral phase transition in QCD at finite temperature". In: *arXiv:hep-lat/0011086v2* (2000).

[29] M.A Halasz and A.D.and J.J.M Verbaarschot Jackson. "Yang-Lee zeros of a random matrix model for QCD at finite density". In: *Physics Letters B* 395 (1997). Ed. by Elsevier, pp. 293–297.

[30] M.A Halasz et al. "Phase diagram of QCD". In: *Physical Review D* 58 (1998).

[31] A.D. Jackson and J.J.M Verbaarschot. "A random matrix model for chiral symmetry breaking". In: *Physical Review D* 53 (1996).

[32] J.B Kogut, M.A. Stephanov, and D. Toublan. "On two-color QCD with baryon chemical potential". In: *Phys.Lett.* B 464 (1999).

[33] H Leutwyler and A. Smilga. "Spectrum of Dirac operator and role of winding number in QCD". In: *Phys. Rev. D* 46 (1992).

[34] M. L. Mehta. *Random Matrices*. Ed. by Elsevier. Amsterdam, 2004.

[35] A. Monnai. *Relativistic Dissipative Hydrodynamic Description of the Quark-Gluon-Plasma*. Ed. by Springer Japan. 2014.

[36] K Morita and A Nakamura. "Stable Yang-Lee zeros in truncated fugacity series from net-baryon number multiplicity distribution". In: *Physical Review D* 92 (2015).

[37] T. Muta. *Foundation of Quantum Chromodynamics*. Ed. by World Scientific Lecture Notes in Physics. 2010.

[38] J.C. Osborn. "Universal results from an alternate random matrix model for QCD with a baryon chemical potential". In: *Phys. Rev. Lett.* 93 (2004).

[39] J.C. Osborn, K. Splittorff, and J.J.M Verbaarschot. "Chiral symmetry breaking and the Dirac spectrum at nonzero chemical potential". In: *Physical Review Letters* 94 (2008).

[40] A. Pelissetto and E. Vicari. "Relevance of the axial anomaly at the finite-temperature chiral transition in QCD". In: *Phys. Rev.* D88 (2013).

[41] R.D. Pisarski and F. Wilczek. "Remarks on the chiral phase transition in chromodynamics". In: *Phys. Rev* D29 (1984).

[42] A. Roberge and N. Weiss. "Gauge theories with imaginary chemical potential and the phases of QCD". In: *Nucl.Phys.* B275 (1981).

[43] H.J Rothe. *Lattice Gauge Theories - An introduction*. Ed. by Worlds Scientific Printers. 2005.

[44] C. Sasaki, B. Friman, and K. Redlich. "Density fluctuations in the presence of spinodal instabilities". In: *Physical Review Letters* 99 (2008).

[45] T. Schafer and E.V Shuryak. "Instantons in QCD". In: *Rev.Mod.Phys* (1997).

[46] C. Schmidt. "Lattice QCD at finite density". In: *Proceedings of Science* 021 (2006).

[47] E.V Shuryak and J.J.M Verbaarschot. "Random matrix theory and spectral sum rules for the Dirac operator in QCD". In: *Nuclear Physics A* 560 (1993). Ed. by North-Holland Publishing Company, pp. 306–320.

[48] M.A Stephanov. "Chiral symmetry at finite T, the phase of the Polyakov loop and the spectrum of the Dirac operator". In: *Physics Letters B* 375 (1996).

[49] M.A Stephanov. "QCD critical point and complex chemical potential singularities". In: *Physical Review D* 75 (2006).

[50] M.A Stephanov. "QCD phase diagram: an overview". In: *PoS LAT2006* 024 (2006).

[51] M.A Stephanov. "Random Matrix Model of QCD at Finite Density and the Nature of the Quenched Limit". In: *Physical Review Letters* 76 (1996).

[52] Gerard 't Hooft. "A two-dimensional model for Mesons". In: *Nuclear Physics B* 75 (1974). Ed. by North-Holland Publishing Company, pp. 461–470.

[53] Heinz. U.W. and G. Kestin. "Joszo's Legacy: Chemical and Kinetic Freeze-out in Heavy-Ion Collisions". In: *Eur. Phys. J.ST* 155 (2007), pp. 75–87.

[54] C. Vafa and E Witten. "Restrictions on symmetry breaking in vector-like gauge theories". In: *Nuclear Physics B* 234 (1984). Ed. by North Holland Publishing Company, pp. 173–188.

[55] B. Vanderheyden and A.D. Jackson. "Random matrix model for chiral symmetry breaking and color superconductivity in QCD at finite density". In: *Phys. Rev.* D62s (2000).

[56] J. Verbaarschot. "Spectrum of the QCD Dirac operator and Chiral Random Matrix Theory". In: *Phys. Rev. Lett.* (1994).

[57] J.J.M Verbaarschot. "QCD, Chiral Matrix Theory and Integrability". In: E. Brezin et al. *Applications of Random Matrices in Physics*. Ed. by Springer. 2006.

[58] J.J.M Verbaarschot and I. Zahed. "Spectral density of the QCD Dirac operator near zero virtuality". In: *Phys.Rev.Lett.* 70 (1993).

[59] J.M Verbaarschot. "Universal behavior in Dirac spectra". In: *Cambridge 1997, Confinement, duality and nonperturbative aspects of QCD* (1997), pp. 343–378.

[60] T. Wettig, A. Schafer, and H.A Weidenmuller. "The chiral phase transition in a random matrix model with molecular correlations". In: *Physics Letters B* 376 (1997), pp. 28–34.

[61] T. Wettig and J. Verbaarschot. "Random Matrix Theory and Chiral Symmetry in QCD". In: *Ann.Rev.Nucl.Part.Sci.* 50 (2000), pp. 343–410.

[62] E.P. Wigner. "Random Matrices in Physics". In: *SIAM Rev.* (1967).

[63] C.N Yang and T.D Lee. "Statistical Theory of Equations od State and Phase Transitions. I. Theory of Condensation". In: *Physical Review* 87 (1952), p. 404.

[64] C.N Yang and T.D Lee. "Statistical Theory of Equations od State and Phase Transitions. II. Lattice Gas and Ising Model". In: *Physical Review* 87 (1952), p. 410.

[65] P. Zinn-Justin. "Random Hermitian matrices in an external field". In: *Nuclear Physics B* 497 (1997), pp. 725–732.